**Universidade de Aveiro** Secção Autónoma de Ciências da Saúde
**2013**

**Ana Catarina Dinis de Pinho**

# Desvendando o papel da PPA na migração celular

# Unveiling the APP role in cell migration

**Universidade de Aveiro** Secção Autónoma de Ciências da Saúde
**2013**

**Ana Catarina Dinis de Pinho**

# Desvendando o papel da PPA na migração celular

# Unveiling the APP role in cell migration

Dissertação apresentada à Universidade de Aveiro para cumprimento dos requisitos necessários à obtenção do grau de Mestre em Biomedicina Molecular, realizada sob a orientação científica da Professora Doutora Sandra Vieira, Professora Auxiliar Convidada da Secção Autónoma de Ciências da Saúde da Universidade de Aveiro.

Este trabalho contou com o apoio do Centro de Biologia Celular (CBC) da Universidade de Aveiro, e é financiado por fundos FEDER através do Programa Operacional Factores de Competitividade – COMPETE e por Fundos nacionais da FCT – Fundação para a Ciência e a Tecnologia no âmbito dos projectos PTDC/QUI-BIQ/101317/2008, PTDC/SAL-NMC/111980/2009 e PEst-OE/SAU/UI0482/2011.

Dedicada à minha avó, Maria da Glória da Costa Duarte Dinis

**o júri**

presidente

Professora Doutora Odete Abreu Beirão da Cruz e Silva
Prof. Auxiliar com Agregação, Secção Autónoma de Ciências da Saúde, Universidade de Aveiro

Professora Doutora Sandra Isabel Moreira Pinto Vieira
Prof. Auxiliar Convidada, Secção Autónoma de Ciências da Saúde, Universidade de Aveiro

Doutora Maria João Lopes Gonçalves de Brito Amorim
Investigadora, Instituto Gulbenkian de Ciência

**agradecimentos**

À minha orientadora, Sandra Vieira, pela motivação, empenho, disponibilidade e pelo saber transmitido ao longo da realização deste trabalho.

À professora Odete da Cruz e Silva, pela oportunidade de realizar este trabalho no laboratório de Neurociências do Centro de Biologia Celular.

À Doutora María Lázaro, pela disponibilidade em colaborar na análise por FRAP e atenção dispensada.

Aos meus pais e ao meu irmão, pelo apoio incondicional, incentivo, confiança, compreensão e momentos de conforto, que foram imprescindíveis para a concretização desta etapa.

A toda a família, desde os graúdos, pela experiência de vida transmitida, aos mais miúdos, pela alegria constante.

Ao Paulo, pelo ânimo, presença, compreensão e apoio inigualável durante todo o percurso.

À Luísa, pelo companheirismo e por todos os momentos de entusiasmo e desalento partilhados; e à Susana, pelo convívio diário e fraternidade.

Aos meus colegas e amigos de Ciências Biomédicas, aos que estiveram presentes lado-a-lado no laboratório, Patrícia, Sónia, Ana Maria, João, Marta, Juliana, Emanuel e Luís, pela boa amizade diariamente vivida; e também aos que me acompanharam inicialmente neste percurso, em especial à Rafaela, Rita C., Rita R., Inês e Cindy, que a distância não fez esquecer.

À Joana Rocha, ao Roberto e à Regina, a quem agradeço especialmente, pelo auxílio, dedicação e disponibilidade únicos.

A todos os meus colegas do laboratório de Neurociências, pelo convívio diário em ambiente de aprendizagem e boa disposição. Em especial à Regina, à Lili e à Pati, pelos momentos de descontração e diversão e pelo encorajamento.

Às minhas amigas de longa data, à Andreia, Joana Lima, Joana Raquel, Joana Correia, Ana Cláudia e Beatriz, pela amizade resistente ao tempo e à distância, e aos meus amigos João e Joana pela companhia e momentos de lazer indispensáveis.

A todos os meus colegas do CBC, que de uma forma ou de outra me ajudaram neste percurso.

**palavras-chave**

Proteína precursora de amilóide de Alzheimer (PPA); PPA secretada (sPPA); migração celular; migração neuronal; células SH-SY5Y; citoesqueleto de actina; pequena GTPase cdc42

**resumo**

A proteína precursora de amilóide de Alzheimer (PPA) é uma glicoproteína transmembranar com propriedades de adesão, descrita como reguladora positiva de migração celular. Embora ubíqua, a isoforma 695 da PPA está enriquecida no cérebro e pode funcionar na migração neuronal de novos neurónios que emergem de nichos neurogénicos existentes no cérebro adulto.

No presente trabalho, objetivámos desvendar o papel da PPA e do seu fragmento secretado (sPPA) na migração celular, particularmente na migração de células do tipo neuronal, e os mecanismos moleculares subjacentes. Realizaram-se estudos de biologia celular em células SH-SY5Y humanas do tipo neuronal transfectadas com o cDNA de fusão PPA-GFP ou o vector EGFP, e sujeitas ao ensaio de '*Scratch Wound Healing*' na presença ou ausência de sPPA. A eficiência de migração das células SH-SY5Y foi monitorizada a cada hora através de imagens de microscopia. O número de células migratórias recrutadas, e a distância e velocidade de migração da margem foram os parâmetros monitorizados nas células não transfectadas, para analisar o papel parácrino do sPPA. A coordenação, distância e velocidade de migração celular, e a distância migrada "fora-da-trajectória", foram determinadas por análise da trajectória de cada célula transfectada, para estudar o papel autócrino da PPA transmembranar. A influência da PPA no fenótipo migratório e na distribuição da F-actina foram analisadas em células SH-SY5Y fixadas, e em condições '*in vivo*' em células HeLa fluorescentes co-expressando PPA-GFP e um marcador fluorescente de F-actina (LifeAct-RFP). Estas células migratórias foram ainda sujeitas a análise por FRAP para estudar os efeitos da PPA na dinâmica do citoesqueleto de F-actina. Foi também avaliado o efeito da PPA na activação da Cdc42, um membro da família das Rho GTPases que regula a polarização celular e a formação de filopodia, influenciando assim o direcionamento da migração.

Os nossos resultados mostram que o sPPA aumenta o número de células migratórias em períodos mais tardios, diminui a velocidade migratória da margem e aumenta a distância migrada "fora-da-trajectória". A PPA transmembranar foi observada como tendo um papel na coordenação e persistência direcional da migração celular, numa forma dependente da desfosforilação do seu resíduo S655. Adicionalmente, análises morfológicas mostraram que a PPA ajuda as células a adquirir a distribuição de F-actina assimétrica polarizada característica de células migratórias. Os dados de FRAP sugerem que a PPA aumenta a estabilidade da F-actina quer na frente quer na traseira das células migratórias, aumentando a eficiência da migração celular uma vez que a adesão célula-substrato pode orientar a direccionalidade da migração. Finalmente, observámos que a PPA liga à Cdc42 e aumenta a sua ativação, outro mecanismo pelo qual a PPA pode determinar a migração direcionada. Estes resultados ajudam a desvendar os mecanismos moleculares subjacentes ao papel da PPA na migração celular, com potenciais aplicações no estudo da migração neuronal na neurogénese adulta.

**keywords**

Alzheimer's amyloid precursor protein (APP); secreted APP (sAPP); cell migration; neuronal migration; SH-SY5Y cells; actin cytoskeleton; small GTPase cdc42

**abstract**

The Alzheimer's amyloid precursor protein (APP) is a transmembranar glycoprotein with adhesive properties, reported to positively regulate cell migration. Although ubiquitous, the APP 695 isoform is brain enriched and may function in neuronal migration of newly born neurons arising from adult brain neurogenic niches.

In the present work we aimed to unveil the roles of APP and its secreted fragment (sAPP) in cell migration, particularly in neuronal-like migration, and the underlying molecular mechanisms. Cell biology studies were first performed in neuronal-like human SH-SY5Y neuroblastoma cells transfected with an APP-GFP fusion construct or the EGFP vector, and subjected to the well-established 'Scratch Wound Healing' assay in the presence or absence of sAPP. The efficiency of SH-SY5Y cells migration was monitored every hour by microscopy imaging. The number of recruited migrating cells, and the leading-edge migration distance and velocity were the parameters monitored in non-transfected cells, to analyze the sAPP paracrine role. Cell coordination, migration distance and velocity, and "out-of-track" distance during cell migration, were determined by single-cell track analysis of transfected cells to study the autocrine role of full length APP. The influence of APP in the migratory phenotype and in F-actin distribution were analyzed in SH-SY5Y fixed cells, and in fluorescing HeLa cells co-expressing APP-GFP and a live F-actin red fluorescent marker (LifeAct-RFP), by live cell imaging. These migrating cells were further subjected to FRAP analysis to study the APP effects on F-actin cytoskeleton dynamics. Finally, we also evaluated the effects of APP on the activation of Cdc42, a Rho GTPase family member that main regulates cell polarization and filopodia generation, influencing directional migration.

Our results show that sAPP is capable to increase the number of cells recruited to migrate at later periods, but decreases the migratory velocity of the leading edge and increases the "out-of-track" migrated distance. Full-length APP was observed to have a role in the coordination and directional persistence of cells migration, in a S655-dephosphorylation dependent manner. Additionally, the morphological analyses showed that APP helps SH-SY5Y cells to acquire the polarized asymmetric F-actin distribution characteristic of migrating cells. FRAP data suggest that APP increases the stability of both front and rear F-actin of migrating cells, which may increase cell migration efficiency, as cell-substrate adhesion can guide the directionality of migration. Finally, we observed that APP binds to and enhances Cdc42 activation, another mechanism by which it can determine directional migration. These results help to unveil the molecular mechanisms underlying APP role in cell migration, with potential applications in the field of neuronal migration in adult neurogenesis.

# Index

# Abbreviations

| | |
|---|---|
| AICD | APP intracellular domain |
| APP | Alzheimer's amyloid precursor protein |
| Aβ | Amyloid β-peptide |
| Cdc42 | Cell division cycle 42 |
| cDNA | Complementary deoxyribonucleic acid |
| CNS | Central nervous system |
| Dab1 | Disabled-1 |
| DISC1 | Disrupted in schizophrenia-1 |
| ECM | Extracellular matrix |
| EGF | Epidermal growth factor |
| EGFP | Enhanced green fluorescent protein |
| FAK | Focal adhesion kinase |
| FBS | Fetal bovine serum |
| flAPP | Full-length APP |
| FN | Fibronectin |
| FRAP | Fluorescence recovery after photobleaching |
| F-actin | Filamentous actin |
| G-actin | Globular actin |
| GFP | Green fluorescent protein |
| ICC | Immunocytochemistry |
| NPC | Neural progenitor cell |
| OB | Olfactory bulb |
| PAK | p21-activated protein kinase |
| Rac1 | Ras-related C3 botulinum toxin substrate 1 |

| | |
|---|---|
| RFP | Red fluorescent protein |
| Rho | Ras homolog |
| RMS | Rostral migratory stream |
| ROI | Region of interest |
| sAPP | Secreted APP |
| SGZ | Subgranular zone |
| SVZ | Subventricular zone |
| SWH | Scratch wound healing |
| S655A APP | Constitutively dephosphorylated S655 APP mutant |
| S655E APP | Constitutively phosphorylated S655 APP mutant |
| TBS | Tris-Buffered Saline |
| TBS-T | Tris-Buffered Saline Tween |
| TGN | Trans-Golgi network |
| WB | Western Blot |
| Wt | Wild-type |

# 1. Introduction

## 1.1. The Alzheimer's Amyloid Precursor Protein (APP)

The Alzheimer's Amyloid Precursor Protein (APP), an ubiquitously expressed protein, is the precursor of amyloid β-peptide (Aβ), the main component of the brain senile plaques that characterize Alzheimer's disease (AD).

The evolutionary conservation of APP and the presence of APP isoforms lacking Aβ sequence indicates that amyloidogenesis is unlikely the main function of this protein family. Accumulative evidences have demonstrated that APP has physiological roles in cell adhesion, neuron generation, migration and differentiation, neurite outgrowth and synapse formation. Taken together, these findings corroborate a potential crucial role for APP as part of a complex mechanism involved in a wide variety of neuronal functions, including normal neural development or response to traumatic brain injuries [1]. The first studies to draw a correlation between APP and neurogenesis showed that embryonic expression of APP peaked during the height of neuronal differentiation and neurite outgrowth [1].

### 1.1.1. APP gene family and molecular structure

The APP family is a group of ubiquitously expressed and evolutionarily conserved type I transmembrane glycoproteins, whose functions have yet to be fully elucidated [2].

In mammals, this gene family includes *APP* and the homologs *amyloid precursor-like proteins 1 and 2* (*APLP-1 and APLP-2*). APLP's show strong sequence homology to APP, particularly in the C-terminal domain, but only APP contains the Aβ sequence, encoded by part of exons 16 and 17 [1,3,4].

The human APP gene is located on the chromosome 21q21 and contains 19 exons, of which exons 7, 8 and 15 can be alternatively spliced [5,6]. Several isoforms of APP that arise from alternative splicing were identified, with all these transcripts encoding multidomain proteins with a single membrane-spanning region. The most abundant isoforms are $APP_{770}$, $APP_{751}$, and the predominantly neuronal $APP_{695}$ [2,7,8]. These differ in the size of their extracellular sequence and by the absence ($APP_{695}$) or presence ($APP_{751}$ and $APP_{770}$) of a Kunitz serine proteinase inhibitor (KPI) domain [1,8].

The APP molecule contains three main domains: a large extracellular amino-terminal domain, a single membrane-spanning domain and a short intracellular cytoplasmic domain (Figure 1) [9].

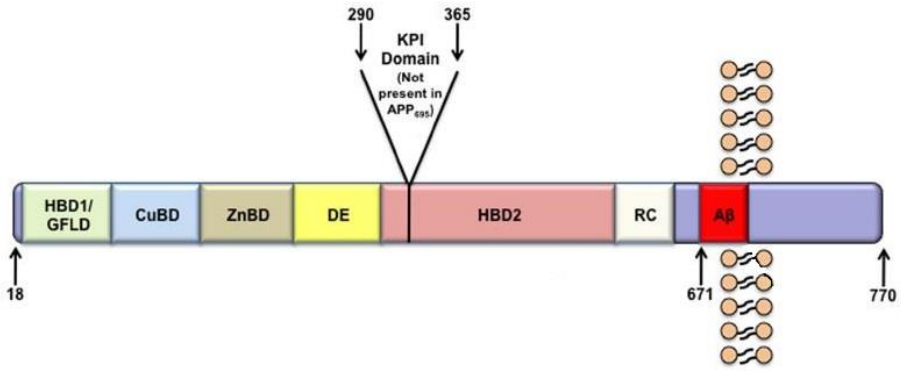


**Figure 1. APP functional domains.** From the N-terminal region, APP functional domains include a signal peptide (SP), a heparin-binding and growth-factor-like domain (HBD1/GFLD), a copper-binding domain (CuBD), a zinc-binding domain (ZnBD), an acidic region (DE), a Kunitz-type protease inhibitor domain (KPI; not present in $APP_{695}$), a second heparin-binding domain (HBD2), a random coiled region (RC), and the amyloid beta domain (Aβ), that extends from the ectodomain into the transmembrane domain. The remaining region consists of the cytoplasmic tail of APP, including the APP intracellular domain (AICD). Reproduced from reference [2].

The extracellular region contains multiple distinct functional domains, including a cysteine-rich domain and an acidic domain. The cysteine-rich domain contains a heparin-binding/growth-factor-like domain 1 (HPBD1), a copper-binding domain (CuBD), a zinc-binding domain (ZnBD), and a second heparin-binding domain 2 (HPBD2) [2,5,10]. Ion-metal binding to APP was shown to modify the protein conformation and to interfere with APP binding to constituents of the extracellular matrix. Isoforms 770 and 751 contain a 56-amino acid KPI domain that inhibits proteases, and isoform 770 contains an additional 19-amino acid OX-2 domain, homolog to the MRC OX-2 antigen, found on the surface of neurons and thymocytes. Relatively in the middle of the extracellular domain lies a putative growth-promoting motif named "RERMS" (residues 403-407 of $APP_{770}$), followed by a gelateinase A inhibitor (residues 407-417 of $APP_{770}$), a collagen binding site (residues 523-540 of $APP_{770}$), and the Aβ sequence. The Aβ domain comprises the 28 residues just outside the membrane plus the first 12-14 residues of the transmembrane domain (amino acids 700-723 of $APP_{770}$). The Aβ sequence contains additionally zinc, cooper and heparin binding sites, and a RHDS motif (amino acids 5-8 of Aβ) that appears to promote cell adhesion [8,11,12]. The C-terminal cytoplasmic region contains a $^{653}$YTSI$^{656}$ sorting motif and a $^{681}$YENPTY$^{687}$ internalization signal for membrane proteins (human $APP_{695}$ isoform numbering), which regulate APP trafficking. The cytoplasmic portion also mediates interactions with several proteins suggesting a role in signal transduction [5,10]. For example, the APP cytoplasmic domain has been shown to bind to the Fe65 protein and G proteins that serve as signal transducers of various cell surface receptors [13].

### 1.1.2. APP intracellular trafficking

APP is a single transmembrane protein that is synthesized on membrane-bound ribosomes and co-translationally inserted into the endoplasmic reticulum (ER) membrane via its signal peptide [8,14]. During its transport from the ER to the plasma membrane (PM), nascent APP is post-translationally modified through the secretory pathway, being N-glycosylated in the ER and further O-glycosylated (maturation) in the Golgi, followed by its ectodomain and cytoplasmic phosphorylation, and tyrosine sulphation [15,16]. The acquisition of N- and O-linked sugars occurs rapidly after biosynthesis, and APP half-life is relatively brief (around 1h). Both during and after the trafficking through the secretory pathway, full length APP can undergo a variety of proteolytic cleavages to release secreted derivatives into vesicle lumens and to the extracellular space [8,15]. In the trans-Golgi network (TGN), APP can be packaged into secretory vesicles and delivered to the PM [15]. However, only a small fraction of nascent APP molecules reach the PM (estimated at ≈10%), whereas the majority of APP at steady-state localizes to the Golgi apparatus and TGN [16].

At the cell surface, APP can be proteolytic cleaved or undergo re-internalization within minutes of arrival at the cell surface, via its "YENPTY" internalization motif near the carboxyl terminus, being delivered into the endocytic pathway [15,16]. From the late endosomes, APP is either transported to lysosomes, where it suffers complete degradation, or recycled by transport vesicles to the TGN and to the cell surface (Figure 2) [15–17].

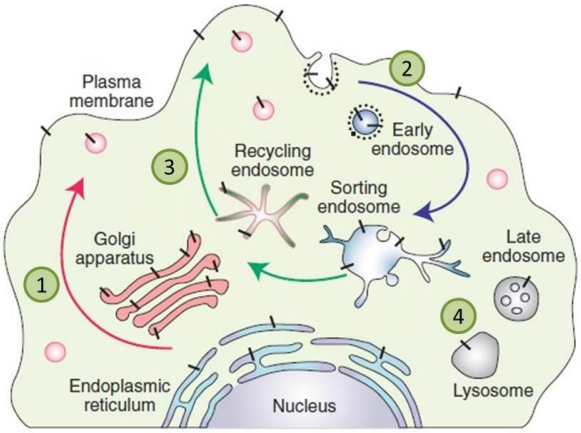


**Figure 2. Intracellular trafficking of APP: 1.** Nascent APP molecules (black bars) mature through the constitutive secretory pathway; **2.** Once APP reaches the cell surface, it is rapidly internalized and (**3**) subsequently trafficked through endocytic and recycling organelles to the TGN or the cell surface; **4.** A small fraction is also degraded in the lysosome. Reproduced from reference [16].

APP vesicular transport mainly occurs via clathrin coat complexes, which are involved in two main sorting paths: the endocytic pathway, from the reinternalization at the cell surface to

the endosome; and the transport pathway from the TGN to the endosome [18,19]. APP contains the NPXY amino acid motif (YENPTY), which regulates the targeting of proteins to these clathrin-coated vesicles and their transport [18,19]. Further, a growing number of clathrin adaptor proteins, like Fe65 and Dab1, have been found to bind APP's NPXY motif to clathrin coats, thus regulating APP intracellular trafficking [18].

Another complex implicated in the transport of APP is the retromer complex. It is a multi-subunit complex that mediates the endosomal-to-TGN retrograde transport of several transmembranar proteins [15]. This complex consists of two sorting nexin subunits and a cargo-recognition trimer consisting of vacuolar protein sorting (VPS) 26, VPS29, VPS35 [18]. VPS35, at the core of the retromer complex, binds to other retromer elements and to the cytoplasmic tail of the transmembrane protein cargo being sorted. sorLA (sorting protein-related receptor containing LDLR class A repeats), a type-1 transmembrane molecule, binds the retromer complex to cargo proteins such as APP, working as an adaptor protein [18].

The fusion of transport vesicles to the membrane of the targeted organelle completes the process of transmembrane protein sorting. This fusion step is governed by three main protein families: SNARE (soluble N-ethylmaleimide sensitive factor-attachment protein receptor) proteins, Rab proteins, and SM (Sec1/ Munc18) proteins. Membrane fusion and cargo delivery occur when SNAREs expressed in the membranes of the transport vesicle interact with a single SNARE protein expressed in the membrane of the targeted organelle, while the Rab and SM proteins play important roles in mediating this interaction [18].

### 1.1.3. APP proteolytic processing

APP can undergo amyloidogenic or non-amyloidogenic processing via cleavage by different secretases, leading to the production of a number of intra- and extracellular metabolites (Figure 3) [4,16].

In the non-amyloidogenic pathway, APP is cleaved by α-secretase in the Aβ region, liberating a large soluble extracellular N-terminal fragment, sAPPα (secreted APP). Several enzymes have been shown to have α-secretase activity including members of the ADAM ("a disintegrin and metalloproteinase") family, ADAM9, ADAM10 and ADAM17 and BACE2 (β-site APP cleaving enzyme 2). Recent studies suggest that ADAM10 is the major α-secretase in the brain both in development and in the adult. The APP carboxy-terminal fragment (APP-CTF) that remains tethered to the membrane, αAPP-CTF, undergoes a transmembrane cleavage by γ-secretase, producing a non-pathogenic P3 peptide and the cytoplasmic APP intracellular domain (AICD), which can translocate to the nucleus [4,16].

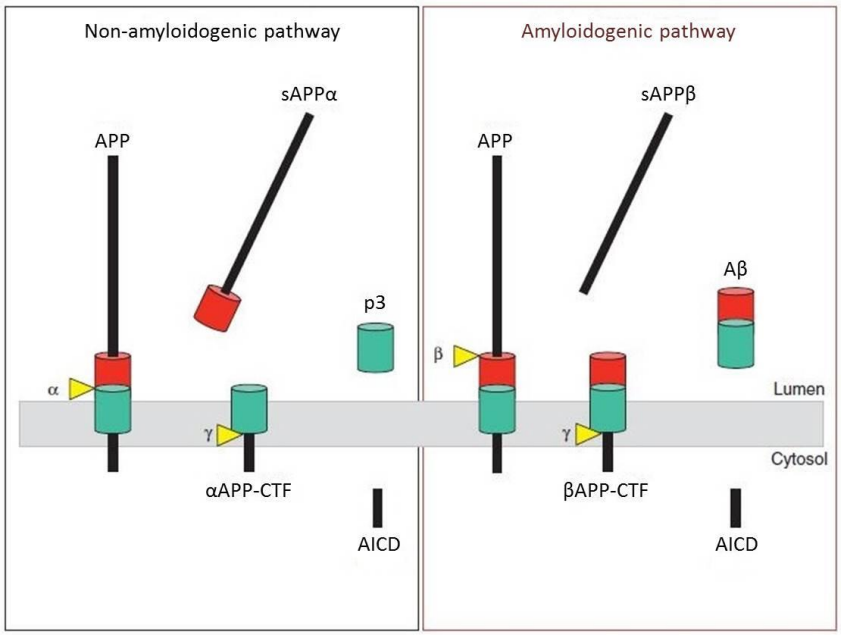


**Figure 3. APP proteolytic processing.** Cleavage by α-secretase enables the secretion of sAPPα and the preservation of the αAPP-CTF in the membrane, which can undergo cleavage by γ-secretase to release the p3 peptide and AICD. Alternatively, proteolytic cleavage by β-secretase results in the secretion of the slightly truncated sAPPβ and the preservation of the βAPP-CTF, which can also undergo cleavage by γ-secretase to release the Aβ peptide and AICD. Reproduced from reference [16].

In the alternative amyloidogenic cleavage pathway, APP is first cleaved by β-secretase to produce a long soluble secreted form of APP, the sAPPβ peptide, and the βAPP-CTF. This cleavage event is mediated by BACE1. Subsequent cleavage of βAPP-CTF by γ-secretase yields the AICD fragment as well as the Aβ peptide that can aggregate into amyloid or senile plaques, one of the pathophysiological hallmarks of AD [4,16].

The non-amyloidogenic processing mainly occurs at the cell surface where α-secretases are present, whereas the amyloidogenic processing involves transit through the endocytic organelles where APP encounters β- and γ-secretases [16].

### 1.1.4. APP phosphorylation

Direct phosphorylation of APP might be a significant mechanism in the regulation of APP binding, subcellular trafficking, processing and function. As a phosphoprotein, APP contains several phosphorylation sites on its intracellular and extracellular portions [20–22]. Two of these phosphorylatable residues, $Ser^{198}$ and $Ser^{206}$ (amino acid numbering according human $APP_{695}$ isoform), are localized in the APP ectodomain and its phosphorylation occurs in a post-Golgi secretory compartment and at the cell surface by ectoprotein kinases [22]. Additionally, eight potential phosphorylation sites, $Thr^{654}$, $Tyr^{653}$, $Ser^{655}$, $Thr^{668}$, $Ser^{675}$, $Tyr^{682}$, $Thr^{686}$ and $Tyr^{687}$

(amino acid numbering according human $APP_{695}$ isoform) are localized in the APP cytoplasmic domain, being mainly located at three functional motifs, $^{653}$YTSI$^{656}$, $^{667}$VTPEER$^{672}$, and $^{682}$YENPTY$^{687}$, shown to regulate the interaction of APP with some of its binding proteins [6,20,22].

Phosphorylation of Ser$^{655}$, located at the $^{653}$YTSI$^{656}$ basolateral sorting signal, has been reported to regulate APP trafficking, processing and interaction with other proteins. Noteworthy, phosphorylation of Ser$^{655}$ has been observed to occur both *in vitro* and *in vivo* and it is the only residue phosphorylated by the protein kinase C (PKC), particularly in mature APP molecules [20,22–24]. Besides PKC, Ser$^{655}$ was also reported to be phosphorylated by calmodulin-dependent protein kinase II (CaMKII) [23] and APP kinase I [6,21,24]. In previous works from our Neuroscience laboratory, using APP 655 phosphomutants, serine 655 to glutamate (S655E) and to alanine (S655A) to mimic phosphorylation and dephosphorylation at the Ser$^{655}$ residue, respectively, unraveled that APP phosphorylation at Ser$^{655}$ enhances APP secretory traffic, increasing its exit from the TGN to the cell surface, and also increases sAPPα production by the alpha-secretase pathway [25]. Further, Ser$^{655}$ phosphorylation enhances APP retrieval to the TGN via the retromer, by increasing APP binging to the retromer complex while decreasing its targeting to the lysosomal route, thus expanding mature APP half-life [15].

## 1.2. Neuronal migration during neurogenesis

### 1.2.1. Neural stem cells and neurogenesis

Stem cells are undifferentiated cells defined by their ability for self-renewing division and by their potential for generating multiple lineages of differentiated cell types [26,27]. Both embryonic stem (ES) cells and adult stem cells fit this definition, however, their stemness properties are largely different. ES cells are pluripotent, capable of differentiating into a large number of cell lineages of all three germ layer origins. Adult stem cells exist in many adult organs, being involved in tissue repair and regeneration, once they can differentiate in the major specialized cell types of that tissue. Among the best studied adult stem cells, neural stem cells (NSCs) can differentiate to neurons and glial cells in the nervous system [26].

Neurogenesis is defined as a process consisting on the proliferation of neural stem/ progenitor cells and their differentiation into new neurons that are able to integrate the existing neuronal circuitry [26,28]. It was traditionally believed to only occur during embryonic and perinatal stages, in the mammalian central nervous system (CNS) [27,28]. Only recently it has become generally accepted that new neurons are indeed added in discrete regions of the adult mammalian CNS [28].

The presence of neurogenesis throughout adult life has been demonstrated in many species including humans [26]. Altman's pioneered studies, in 1965, provided the first anatomical evidence for the presence of newly generated dentate granule cells in the postnatal rat hippocampus [27,29]. In 1984, functional integration of new neurons in the adult CNS was first shown in songbirds [27,30].

### 1.2.2. Neuronal migration during embryonic neurogenesis

In the developing brain, cell migration is, together with neuron production and differentiation, a crucial process for structural organization, being therefore highly regulated to allow the correct formation of complex networks, wiring neurons, and glia [31,32].

Most neurons are produced in the Ventricular Zone (VZ), in the center of the brain, and migrate radially from the VZ to the developing neocortex (Figure 4A and B). Very early in neocortical development, the distances that neurons must migrate are small. The earliest produced neurons use a mode of migration referred to as somal translocation. In this, the neuron extends a long basal process, which is an extension of the cell's body, just beyond the edge of the VZ into the outer region of the brain compartment (Figure 4A). The basal process attaches to the pial surface, which is the outer surface of the developing brain. The nucleus of the cell then moves through the cytoplasm of the basal process. As the nucleus moves up, the process becomes shorter and thicker, but remains attached to the pial surface. At the end of somal translocation, the nucleus of the cell has moved out of the VZ and into the embryonic cortex [31].

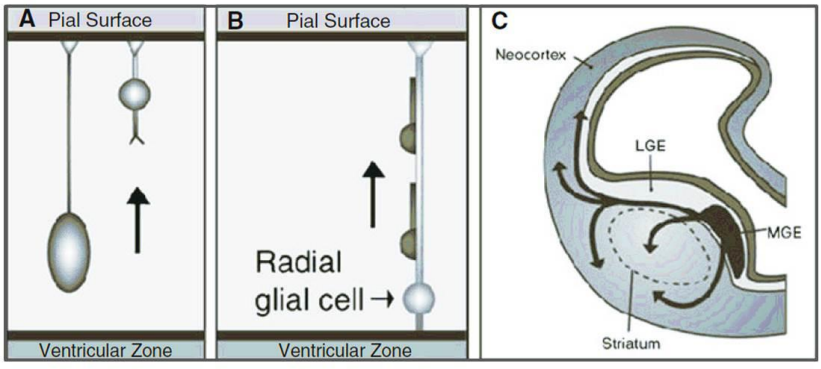


**Figure 4. Different modes of neuronal migration to the neocortex. A.** Neuron migration by somal translocation, where cell extends a cytoplasmic process and attaches to the outside of the brain compartment (pial surface), and then the nucleus moves up into the brain area. **B.** Neuron migration by a radial glial guide, where radial glial cells provide scaffold for neuron to migrate along. **C.** Neuron migration from second proliferative zone in ganglionic eminences, by tangential migration. Arrows indicate direction of migration for different neuron populations; LGE – Lateral Ganglionic eminence; MGE – Medial Ganglionic eminence. Reproduced from reference [31].

As development proceeds, the primary mode of neuronal migration from the VZ changes. Because of the greater distances, neurons require neural progenitor cells within the VZ, called “radial glial guides”, to support their migration [31]. Similar to neurons migrating via somal translocation, radial glial guides also extend a basal process that attaches to the pial surface of the cortex, however, the nucleus of the radial glial cells remains in the VZ and the basal process forms a kind of scaffolding along which immature neurons can migrate (Figure 4B). The migrating neurons attach themselves to the radial glial guide and move along the cellular scaffold out into the developing cortex [31,32]. Each glial scaffold can support the migration of many neurons. This type of migration is called “radial migration” because cells migrate perpendicular to the ventricular surface [32].

Recent studies have identified a second proliferative zone located in the region of the ventral telencephalon that will later develop into the basal ganglia (Figure 4C). During embryonic and fetal development three compartments in this region (the medial, lateral and caudal ganglionic eminences) are the source of an important class of inhibitory cortical interneurons [31,32]. Unlike neurons migrating from the VZ, these neurons migrate long distances using a mode of migration termed “tangential migration”, because the route of migration traverses the contour of the developing cortical mantle tangentially [31,32]. Tangential migration involves a variety of signaling pathways not seen in radial migration. Neurons use a number of guidance molecules produced in local regions along their migratory route to direct their movement into the cortex [31].

The migration of neurons into the developing neocortex results in the formation of an orderly 6-layered structure. With one exception, earlier migrating neurons form deepest layers of cortex and later migrating neurons form successively more superficial layers (Figure 5A) such that the order of migration has been described as ‘inside-out’. The exception to the inside-out rule is the very earliest set of migrating neurons. These first neurons to leave the proliferative zone initially form a primitive structure called the preplate (PP; Figure 5B, first panel). Once the preplate is complete, the next wave of migrating neurons splits the preplate into two separate regions, the marginal zone (MZ) and the subplate (SP). These neurons begin to form a new region between the MZ and SP that is the emerging cortical plate (CP; Figure 5B, second panel) [31]. The first neurons to arrive in the CP are the cells that will form cortical layer 6, the deepest layer of cortex; subsequently migrating cells will form progressively more superficial layers of cortex [31].

Both the MZ and the SP are transient brain layers that play a critical role in the development of the cortex, disappearing by the end of the fetal period (Figure 5B, third panel). The MZ contains an important class of cells, the Cajal-Retzius cells (CR), which control the

positioning of neurons into the correct layers of cortex. The CR cells produce a molecular signal, Reelin, that is part of the pathway that signals neurons when to stop migrating and take up their positions in cortex. Each new wave of migrating neurons bypasses the previous wave of neurons such that each new wave of migrating cells assumes the most superficial position within the developing cortex. As each new wave of neurons reaches the top of the cortical plate, it moves into the zone of Reelin signaling and receives the cue to stop. Finally, neurons in the subplate layer do not participate in the formation of cortical layers, but are essential for establishing the primary sensory inputs to the developing neocortex [31].

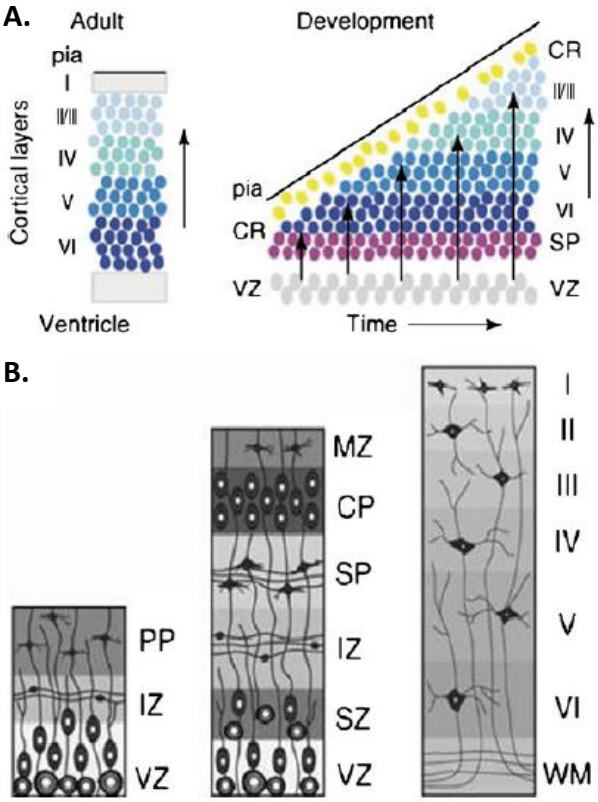


**Figure 5. Migration of neurons into the developing neocortex. A.** The earliest produced neurons migrate to the deepest cortical layers (dark blue). Subsequently migrating neurons migrate to successively more superficial layers (lighter blues) creating an inside out order of migration. **B.** The first neurons migrate from the ventricular zone (VZ) to form the preplate (PP) (first panel); the next neurons split the PP into the marginal zone (MZ) and the subplate (SP), both transient brain structures (second panel); the mature brain has six well developed cortical layers (I-VI), but none of the embryonic structures (MZ, SP, VZ) (third panel). The intermediate zone (IZ) has become a mature white matter layer (WM). Reproduced from reference [31].

### 1.2.3. Neuronal migration during adult neurogenesis

In the early postnatal brain, developmental processes such as the production and migration of astrocyte and oligodendrocyte progenitors still occur. Although the brain is completely formed and structured few weeks after birth, it maintains a degree of plasticity

throughout life, including axonal remodeling, synaptogenesis, but also neural cell birth, migration and integration [27,32].

Adult neurogenesis is spatially restricted under normal conditions to two main neurogenic niches in the adult brain, the subventricular zone (SVZ) of the lateral ventricles and the subgranular zone (SGZ) of the dentate gyrus (DG) in the hippocampus [26–28,32]. These neurogenic niches are micro-environments composed of stem cells, where the self-renewal and proliferation of NSC is constant [2,27,33]. NSCs reside in these structures and produce neural progenitors that migrate toward their final location [32]. These exceptional forms of neurogenesis appear to continue throughout adult life but produce only a small percentage of the neuronal population [31]. In contrast, proliferation and migration of glial progenitors continue for a prolonged period as oligodendrocytes and astrocytes differentiate; in fact, glial progenitors (particularly oligodendrocyte progenitor cells) appear to persist indefinitely in the adult brain in a wide anatomical distribution, and can differentiate in response to injury [31].

Neurogenesis and cell migration in other adult CNS regions is generally believed to be very limited under normal physiological conditions, but could be induced after injury [27,28]. Recent findings indicate that white matter and discrete cortical areas could be sites of secondary neurogenesis. Indeed, the amygdala and the piriform cortex, which represents the major part of the olfactory cortex, receiving OB (olfactory bulb) projection axons, also display newly-generated neurons in the adult brain of several mammalian species, including rodents, rabbits and nonhuman primates [32].

It is yet not clear why newly added neurons are not born directly in the place they need to reside. This implies that cells need to be able to migrate from these discrete niches to their final destination [32]. There is an extensive neuronal migration, nerve growth, and axon/dendritic targeting in the adult CNS that otherwise is inhibitory for mature neurons [28].

Adult neurogenesis recapitulates many features of embryonic neurogenesis [27]. In the adult SVZ, newborn neurons go through extensive migration, first migrating tangentially along the wall of the lateral ventricle, then traveling anterior along the rostral migratory stream (RMS) to the OB and finally dispersing radially as individual cells into the outer cell layers in the bulb [28]. Proliferating radial glia-like cells give rise to transient amplifying cells, which in turn generate neuroblasts (Figure 6). In the RMS, neuroblasts form a chain and migrate closely associated with each other, in a tube-like structure formed by glial cells (astrocytes), towards the OB – “chain migration” [27,28]**.** Once reaching the core of the OB, immature neurons detach from the RMS and migrate radially towards glomeruli where they differentiate into different subtypes of interneurons [27,28,32]. The majority become GABAergic granule neurons, which lack axons and form dendro-dendritic synapses with mitral and tufted cells. A

minority become GABAergic periglomerular neurons, a small percentage of which are also dopaminergic [27,28].

The motility of chain migration is regulated by several factors, including netrin/DCC, GABAA receptor activation, PSA-NCAM, EphB2/ephrin-B2 and some integrins. The directionality of chain migration is influenced by netrin/DCC and Slits/Robos signaling. Once migrating neuroblasts reach the OB, Reelin acts as a detachment signal and tenascin-R initiates the detachment of the neuroblasts from the chains and directs radial migration to their target areas [28].

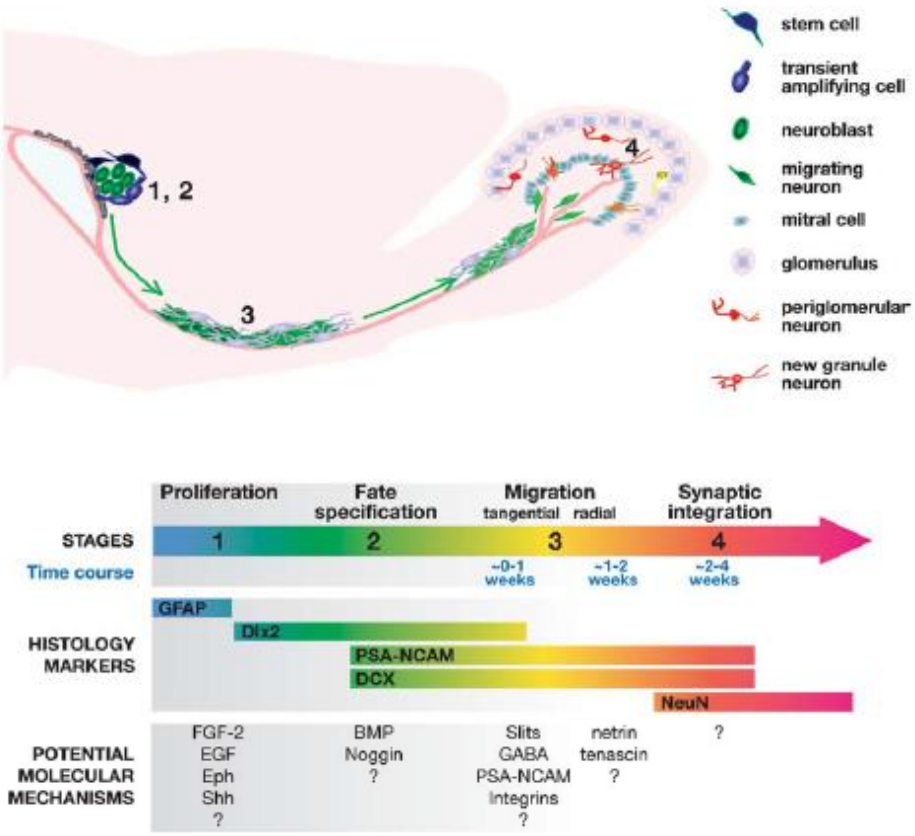


**Figure 6. Generation of new interneurons in the OB from neural stem cells in the SVZ.** Adult SVZ neurogenesis undergoes four developmental stages: **Stage 1**. Proliferation: stem cells (*blue*) in the SVZ of the lateral ventricles give rise to transient amplifying cells (*light blue*). **Stage 2**. Fate specification: transient amplifying cells differentiate into immature neurons (*green*). Adjacent ependymal cells (*gray*) of the lateral ventricle are essential for neuronal fate specification by providing inhibitors of gliogenesis. **Stage 3**. Migration: Immature neurons (*green*) migrate with each other in chains through the rostral migratory stream (RMS) to the olfactory bulb. The migrating neurons are ensheathed by astrocytes. Once reaching the bulb, new neurons then migrate radially to the outer cell layers. **Stage 4**. Synaptic integration: Immature neurons differentiate into either granule neurons (Gr, *orange*) or periglomerular neurons (PG, *red*). Reproduced from reference [28].

In the adult SGZ, newly generated neurons migrate only a short distance to the inner granule cell layer [28,32]. Proliferating radial and non-radial precursors give rise to intermediate progenitors, which in turn generate neuroblasts (Figure 7). Immature neurons migrate into the inner granular cell layer and differentiate into dentate granule cells in the

hippocampus [27]. These newborn neurons rapidly extend long axonal projects, through the hilus, along the mossy fiber pathway and reach their target CA3 pyramidal cell layer. The dendrites of these neurons grow in the opposite direction of the axons, maintaining growth to increase in complexity over months [2,28].

New neurons follow a stereotypic process for synaptic integration into the existing circuitry. Compared to mature granule cells, newborn neurons exhibit hyper-excitability and enhanced synaptic plasticity during specific developmental stages. After a prolonged maturation phase, adult-born neurons exhibit similar basic electrophysiological properties as mature neurons, such as firing behavior and the amplitude and kinetics of GABAergic and glutamatergic inputs [27].

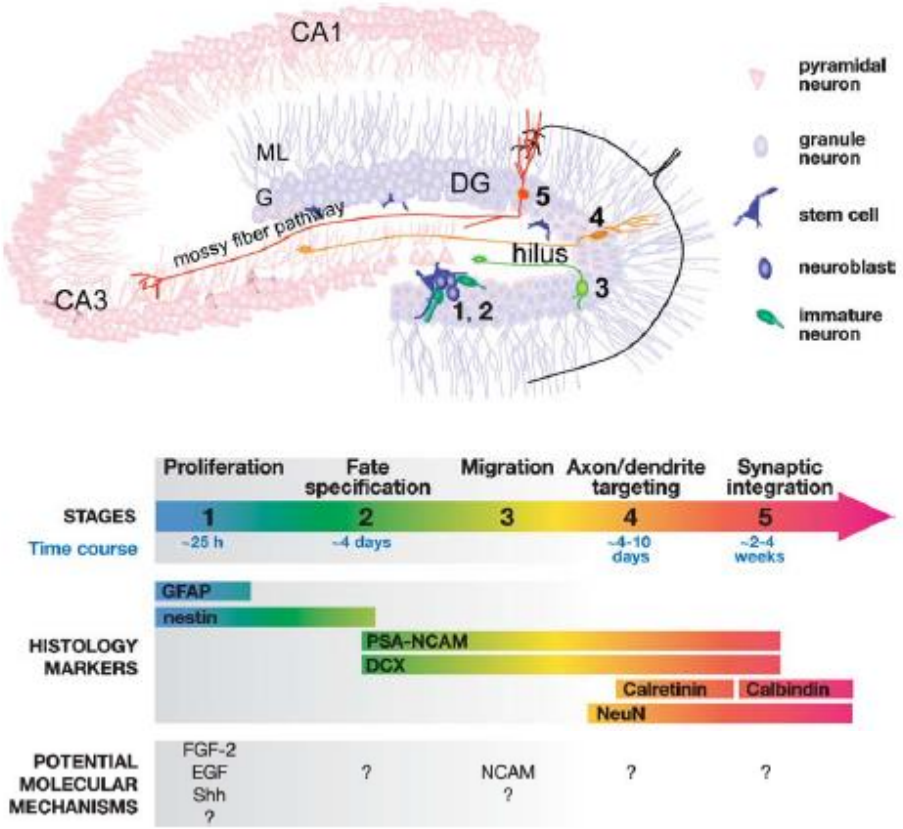


**Figure 7. Generation of new granular neurons in the dentate gyrus of the hippocampus from neural stem cells in the SGZ.** Adult SGZ neurogenesis undergoes five developmental stages: **Stage 1**. Proliferation: Stem cells (*blue*) with their cell bodies located within the subgranular zone in the dentate gyrus have radial processes that project through the granular cell layer and short tangential processes that extend along the border of the granule cell layer and hilus. These stem cells give rise to transient amplifying cells (*light blue*). **Stage 2**. Differentiation: transient amplifying cells differentiate into immature neurons (*green*). Proliferating progenitors in the SGZ are tightly associated with astrocytes and vascular structures. **Stage 3**. Migration: Immature neurons (*light green*) migrate a short distance into the granule cell layer. **Stage 4**. Axon/dendrite targeting: Immature neurons (*orange*) extend their axonal projections along mossy fiber pathways to the CA3 pyramidal cell layer. They send their dendrites in the opposite direction toward the molecular layer. **Stage 5**. Synaptic integration: New granule neurons (*red*) receive inputs from the entorhinal cortex and send outputs to the CA3 and hilus regions. DG, dentate gyrus region; ML, molecular cell layer; GL, granular cell layer. Reproduced from reference [28].

There are similarities between active adult neurogenesis in the two neurogenic regions, including niche composition, signaling pathways maintaining precursor pools, temporal sequence of new neuron integration, critical periods of survival and enhanced plasticity, and contributions to learning and memory [27,32].

#### 1.2.3.1. Regulation of progenitor cell migration in the adult brain

A fundamental issue concerning adult migration is to understand the intrinsic and extracellular cues that allow the persistence of migratory progenitors. Increasing evidence argues for the involvement of developmental signals that are maintained in restricted adult brain structures. In the adult, as in development, orientated neuronal migration requires the cooperative actions of attachment, repellant and guidance signals, and migrating cells need to be equipped with proteins conferring them with the intrinsic capacity to migrate [27,32].

Polysialylated neural cell adhesion molecule (PSA-NCAM) regulate cell-cell interactions and positively regulates cell migration in both neurogenic areas in the adult brain [32].

Doublecortin (DCX), a microtubule-associated protein, plays an important role regulating microtubule polymerization and stabilization during cell migration.

Concentration gradients of chemoattractant and chemorepulsive molecules participate in the directionally-orientated migration of neuronal progenitors in the postnatal RMS: Slit-1 and Slit-2 are known to induce repulsive effect; Prokineticin2, produced by the granular and periglomerular layers of the OB, was shown to orientate, *in vitro,* the migration of neuronal progenitors through the activation of a type G protein coupled receptor; two neurotrophic factors, glial cell line-derived neurotrophic factor (GDNF) and brain derived neurotrophic factor (BDNF), contribute to the maintenance of oriented neuronal migration toward the OB [32].

Three main detachment signals have been shown to participate in the switch from tangential to unicellular radial mode migration, undergone by migrating neuroblasts when they reach the OB: Reelin, Tenascin R and Prokineticin2. In the OB, Reelin acts as a detachment signal on chains of migrating neuroblasts [32]. The extracellular matrix glycoprotein Tenascin-R, expressed in the granular layer of the OB, acts as a detachment signal necessary and sufficient for the recruitment of neuroblasts from the RMS to the OB [32]. Prokineticin2, mentioned above as a chemoattractant molecule, seems to be also involved in the detachment of neuroblasts from the chains once arrived in the OB [32].

The extracellular matrix (ECM) molecules and tyrosine kinase receptors are two other important factors regulating neuronal migration during adult neurogenesis.

Migration in adult brain requires modification of the microenvironment surrounding the migrating cell. Numerous ECM molecules, such as tenascin-C, chondroitin sulfate

proteoglycans and laminin are present along the RMS. Matrix metalloproteases (MMPs) cleave ECM components and thereby modify the extracellular environment. MMPs are expressed along the SVZ-OB pathway, and one of them (MT5-MMP) is produced by the neuroblasts themselves. Interestingly, MMP inhibition reduces tangential migration in neonates, where migration in the RMS still proceeds individually, but not in adults where chain migration is functional. MMP inhibition also inhibits radial migration both in neonates and adults, suggesting that MMPs are also important for individual cell migration. Proteins containing a disintegrin and metalloprotease domain (ADAMs) are transmembrane proteins with metalloprotease, integrin-binding, intracellular signaling and cell adhesion activities. ADAM21 has been proposed as a potential player in neurogenesis and neuroblast migration, supported by its possible interaction with integrins [32]. Indeed, integrins constitute an important family of heterodimeric cell surface proteins that bind to ECM components and to counter-receptors on adjacent cells. Several subunits of integrins are present in the postnatal and adult SVZ, and blocking α6 or β1 integrins strongly perturbs migration and translocation. β1 integrins and its laminin ligands promote the formation of chains in the adult RMS and are required for the maintenance of glial tube integrity [32]. VLDLR, ApoER2 and Dab1 have also been identified as major components of the cellular machinery that supports the formation of the chains. These receptors and adaptor are usually implied in Reelin signaling, but in this case they seem to integrate a Reelin-independent process, with F-Spondin being here a potential ligand [32].

The Eph family of tyrosine kinase receptors and their transmembrane Ephrin ligands are also important factors regulating neuronal migration during adult neurogenesis expressed in the adult SVZ. During development, Eph/Ephrin interactions are involved in axon guidance, neural crest cell migration and formation of angiogenic capillary plexi. The lockade of Eph/Ephrin interactions in the adult brain results in highly increased SVZ astrocyte proliferation together with disrupted neuroblasts migration [32]. Another tyrosine kinase receptor of the family of the epidermal growth factor (EGF) receptors, the ErbB4 receptor, and its ligands neuregulins (NRG1 and NRG2), are involved in SVZ cell proliferation and in the chain migration process in the adult SVZ/RMS: in ErbB4 mutants, neuroblasts migrate as misorientated cell clusters or as individual cells probably as a result of altered cell adhesion. Similarly, EGF receptor activation induces both SVZ cell proliferation and progenitor cell migration. Cell surface proteins and secreted substances regulate the activity of cell surface receptors that control cell-cell and cell-environment interactions necessary for adapted cell migration [32].

Altogether, mechanisms involved in migration (repulsive, attractant, permissive, motogenic factors) are shared between developmental and adult stages, and underline that proper migration relies on the integration of all the environmental cues signaling in a cooperative manner [32].

## 1.3. The potential role of APP in neurogenesis

### 1.3.1. APP interaction with Dab1 and DISC1 in neuronal migration

The transmembrane APP glycoprotein is expressed throughout the developing and adult brain, and a role has been attributed to APP in neuronal precursor cells migration into the cortical plate, with both the extracellular and intracellular domains of APP being required for this function [34]. Dab1 (Disabled-1) and DISC1 (Disrupted in Schizophrenia-1), two cytosolic signaling proteins, were both found to interact with APP to regulate migration [34,35].

Dab1 is a key neuronal migration factor found to act downstream of APP in this process [34]. The interaction between APP and Dab1 is of particular interest, as the phosphorylation of Dab1 in response to Reelin signaling has been well established to play an essential role in migration. However, the pathway through which APP-Dab1 complexes help regulate migration is unknown [35].

Recently, it was reported that the intracellular domain of APP interacts with the N-terminal domain of DISC1, supporting a biochemical and functional interaction between APP and DISC1 in neuronal migration [35]. DISC1 acts downstream of APP and Dab1 to regulate cortical precursor cell migration. Specifically, overexpression of DISC1 rescues the migration defect caused by a loss of APP expression. Moreover, a loss of APP causes a subcellular redistribution of the DISC1 protein in primary cortical neurons. Based on these findings, it was proposed that the APP cytoplasmic region transiently interacts with DISC1 to help regulate the translocation of DISC1 to the centrosome, where it plays a key role in controlling neuronal migration during cortical development. These results suggest that a proper balance of APP expression is necessary for cortical migration during development [2,35].

### 1.3.2. Interaction of APP and Pancortins modulates cortical cell migration

Recent studies reported a novel biochemical and functional interaction between pancortins and APP [36]. Pancortins were identified as extracellular binding partners for APP, and it was confirmed that each of the pancortin isoforms (AMY, AMZ, BMY, and BMZ) binds either directly or indirectly to the APP ectodomain [36].

BMZ knock down or AMY overexpression phenocopies a loss of APP expression in the developing rodent brain, each showing a specific defect in the migration of neural precursor cells into the cortical plate. Authors proposed that BMZ binding to the extracellular domain of APP promotes proper migration into the cortical plate while binding of AMY to APP inhibits proper migration. Thus, losses of APP or BMZ, or AMY overexpression inhibit cortical plate entry. Interestingly, APP overexpression does not rescue the loss of BMZ, indicating that the migration-promoting effect of APP is dependent on BMZ expression [36].

Taken together, data suggests that pancortins functionally and biochemically interact with APP in cortical development. However, data showing that BMZ overexpression can partially rescue the phenotype observed in APP knock downs suggest that pancortins also may act through APP-independent mechanisms, perhaps through interaction with its APLP1 and APLP2 homologous, or through other type I transmembrane domain proteins [36].

### 1.3.3. APP metabolites in neurogenesis

The influence of APP in neurogenesis might be conferred differently via its two separate domains: the secreted sAPPα, shown to be neuroprotective and to promote neurogenesis, and the intracellular AICD domain, found to negatively modulate neurogenesis [1].

#### 1.3.3.1. sAPPα: a role in the positive regulation of neurogenesis

Under non-pathological circumstances, the non-amyloidogenic cleavage pathway of APP and release of the sAPPα metabolite is prevalent [2]. The physiological functions attributed to sAPPα include enhancement of synaptogenesis, neurite outgrowth, cell survival and cell adhesion. Other reports suggest that sAPPα exerts proliferative effects on neural progenitor cell (NPC) isolated from embryonic brains. The *in vivo* role of sAPPα in adult neurogenesis was reported, proposing that sAPPα binds prominently to cells of the SVZ [37]. These findings suggested that sAPPα participates in EGF-induced proliferation, although sAPPα alone fails to induce proliferation [37]. The growth-promoting properties of sAPP and its structural similarities with cysteine-rich growth factors support the hypothesis that sAPP may function as a growth factor *in vivo* [1].

Although it was suggested that these neurogenic sAPPα effect was limited to the SVZ, due to the absence of visible sAPPα-binding sites in the SGZ, there are evidence of increased proliferation and survival of NPCs in both the SVZ and the DG upon an enhancement of local sAPPα production [38].

Recent evidence suggests that sAPP may promote cell survival through the disruption of APP dimerization [2]. While the direct function of sAPP with relation to survival of newly generated neurons has not been fully determined, it is interesting to speculate that sAPP could regulate the physiological survival of NPC and newly generated neurons, as well as the survival of NPC under pathological conditions such as neurodegenerative diseases [2].

An important factor in the functional integration of newly generated neurons into the proper functional circuits is the migration of neuroblasts. Little is known about the effect of sAPP on the migration of neuroblasts, however, administration of nanomolar concentrations of sAPP to epithelial cells, thyrocytes and keratinocytes *in vitro* caused a marked increase not only in their proliferation but also on cells migration. Thus, sAPP might be a part of a long list of motogens, growth factors such as EGF regulating both cell proliferation and migration. In keratinocytes it was shown that this motogenic property was conferred through a chemo-attraction similar to, but distinct from, EGF [39]. Thus an upregulation of sAPP could suggest its utility as a chemoattractant, guiding NPC to the site of injury in an attempt at recovery [2].

#### 1.3.3.2. AICD: a role in the negative modulation of neurogenesis

Conversely to sAPPα function, AICD has been shown to be a negative regulator of NPC proliferation. This effect is mediated by AICD binding to FE65, since when AICD was co-transfected with a mutated FE65 binding site it lost its negative effect one NPC proliferation [2]. First, evidence suggests that AICD negatively regulates the transcription of the epidermal growth factor receptor (EGFR), a receptor that drives NPC proliferation [2]. Other study showed that the transient axonal glycoprotein-1 (TAG-1) extracellularly interacts with APP to increase AICD release [1,2].

Moreover, unlike sAPP, which has a cytoprotective role, the AICD has been shown to induce neuronal apoptosis. Studies overexpressing AICD display neuron specific apoptosis, suggesting that gene changes associated with AICD translocation are responsible for these apoptotic events.

On the other hand, it was recently shown that AICD expression activates genes associated with actin remodeling, including transgelin and tropomyosin 1, and that co-expression of AICD and Fe65 induced enhanced cytoskeletal dynamics, important in the maturation of neurons [40]. Thereby, the detailed mechanism by which AICD suppresses neurogenesis still remains to be fully elucidated [1].

## 1.4. Cell migration at a molecular level

Cell migration plays an essential role in a variety of physiological processes such as embryogenesis (neurogenesis), tissue regeneration, immune surveillance and wound healing [41,42]. All nucleated cell types, at a given time window of their development, execute cell migration. For most cells, migration phases are confined to morphogenesis and cease with terminal differentiation toward intact tissue. Each cell type exerts migration in different contexts using distinct molecular repertoires and extracellular guidance cues [43].

The migratory cycle is a complex process in which actin dynamics play a central role at every step. Actin assembly drives the extension of lamellipodia (flat membrane protrusions) and filopodia (finger-like protrusions) to push the membrane. To anchor the protrusion, the cell front interacts with the ECM by forming nascent adhesions (or focal complexes) that are connected to the intracellular lamellipodial actin network. Nascent adhesions can either disassemble or, in response to the actomyosin force, mature into larger structures called focal adhesions that assemble contractile actomyosin cables (stress fibers) (Figure 8). To complete this migratory cycle, the contraction of stress fibers retracts the trailing edge [42]. In this cycle, proteins from adhesion structures connect the ECM to the actin cytoskeleton, allowing the growing actin network to push the plasma membrane forward and the contractile stress fibers to pull the cell body and retract the tail [42,44].

In summary, cell locomotion can be described in five main phases: morphological polarization of the cell in the direction of movement, membrane extension (formation of a broad lamellipodium and filopodia), formation of cell substratum attachments, contractile force and traction, and release of attachments [45].

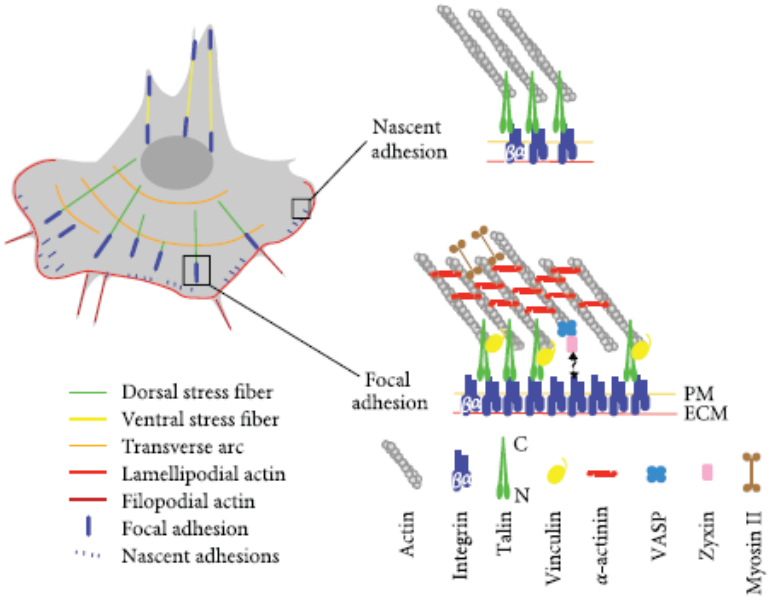


**Figure 8. Actin networks in cell migration and organization of nascent adhesions and focal adhesions**. Left, scheme of a migrating cell displaying characteristic actin structures: lamellipodial and filopodial actin networks and the three classes of stress fibers (transverse arcs, dorsal stress fibers, ventral stress fibers). Right, actin-binding proteins in focal complexes and focal adhesions. PM, plasma membrane; ECM, extracellular matrix. Reproduced from reference [42].

### 1.4.1. Morphological polarization

To migrate, cells must acquire a spatial asymmetry to turn intracellularly generated forces into net cell body translocation. One manifestation of this asymmetry is a polarized morphology, a clear distinction between cell front and rear. An early event in polarization is a change in filamentous actin (F-actin) distribution. Additional molecular rearrangements can succeed, leading to cellular spatial asymmetries involved in migration, such as forward redistribution of chemosensory signaling receptors, integrin adhesion receptors, and integrin cytoskeleton linkages [45]. Cell polarity is defined not only by actin-mediated protrusion and trailing edge retraction but also by positioning of the nucleus and reorientation of the Golgi apparatus and microtubule-organizing center (MTOC) towards the leading edge [46].

An important consequence of polarization is the extension of active membrane processes, including both lamellipodia and filopodia, that takes place primarily around the cell front, so that directional turning is generally accomplished gradually, with cell locomotion taking on a persistent random walk character. The overall rate of cell migration in the absence of stimulus gradients is thus dependent on two independent quantities: migration velocity and directional persistence time, i.e., the time period over which a cell continues to move roughly in the same direction [39,45].

### 1.4.2. Membrane extension

Lamellipodia are broad, flat, sheet-like structures, whereas filopodia are thin, cylindrical, needle-like projections. Cytoplasmic organelles are excluded from these structures, which abundantly contain actin and actin-associated proteins. Extension of both lamellipodia and filopodia in response to migratory stimuli is coupled with local actin polymerization [42,45,47].

An increase in the number of sites for actin polymerization is a first step, followed by addition of globular actin (G-actin) monomers to these filamentous actin (F-actin) growth sites near the membrane. New open barbed-end sites for actin polymerization may arise by a combination of mechanisms, including uncapping of already-existing filaments, their severing, or both, as well as *de novo* formation of new actin trimeric nucleation sites [42,47].

The gelsolin family regulates both severing and uncapping of actin filaments. At micromolar and greater concentrations of calcium, and in the presence of low levels of the chemoattractant-induced phosphoinositides, the severing activity of gelsolin becomes significant, shortening filaments and increasing their number but leaving them capped. At less than micromolar concentrations of calcium, gelsolin dissociates from actin filaments, opening barbed ends for new polymerization [42,45,47].

Uncapping of actin filament barbed ends would permit growth of existing filaments even in the absence of severing. Members of the calcium-independent capping protein family, such as capping protein β2, appear to be barbed-end regulators of predominant importance. New polymerization arising from uncapped F-actin barbed ends, however, results in an increase in the filament length distribution and not in its number. As with gelsolin, a positive correlation of cell migration rate with capping protein expression level may result from an effect on actin cytoskeleton, related to cell body translocation rather than membrane extension [42,45,47].

The regulation of local free G-actin levels may be a primary effector for membrane extension. Whatever the number of uncapped growth sites, the amount of F-actin could potentially be increased by raising the concentration of G-actin monomer, which exists in two pools: free G-actin and G-actin bound to a monomer-binding protein. Three major families of cytoplasmic proteins that bind G-actin appear to have a distinct role in controlling F-actin levels: β-thymosins as a G-actin source, profilins as a filament elongation promotor, and actin depolymerizing factor (ADF)/cofilins as a filament cutter (Figure 9) [45]. While profilin can bind to different actin nucleators, thymosin β4 cannot, and thus is regarded as a G-actin reservoir that can shuttle G-actin to profilin to promote actin filament growth [42,46,47].

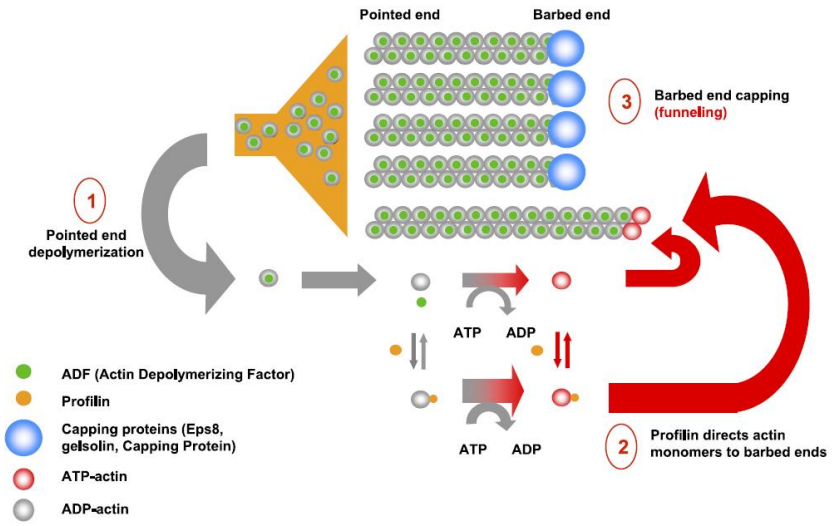


**Figure 9. Regulation of F-actin treadmilling. 1.** ADF binds to the side of ADP-actin filaments and induces pointed-end depolymerization to increase the concentration of monomeric actin at steady state. **2.** Profilin enhances the exchange of ADP for ATP to recycle actin monomers. The profilin-actin complex assembles exclusively at the barbed end. **3.** By blocking the majority of actin filament barbed ends, capping proteins increase the concentration of monomeric actin at steady state and funnel the flux of actin monomers to the uncapped filaments, which individually grow faster. Reproduced from reference [47].

The local actin polymerization is in itself an adequate energy source for extension, against the mechanical resistance provided by the cell membrane. A constant rate of new actin polymerization can lead to a constant rate of membrane extension. The ability of actin polymerization to drive membrane extension requires that actin filaments possess or acquire appropriate mechanical properties. In filopodia, actin filaments are grouped into rope-like bundles, while in lamellipodia they are cross-linked into lattice-like meshwork. Filament bundling and cross-linking both serve to increase the rigidity of the actin polymer network against the load of a membrane resisting deformation as a filopod or lamellipod attempts to extend. Both types of processes (lamellipodia and filopodia) can be observed growing simultaneously in a single cell at the same location, but they exhibit different distributions of actin-binding proteins yielding different spatial structures [45–47].

#### 1.4.2.1. Regulation of actin polymerization

Actin polymerization controls protrusion of the cell in the current paradigm for cell migration. There are two main types of nucleators of actin polymerization (actin-nucleating factors): the Arp2/3 complex and the formins mDia1 and mDia2 (Figure 10) [46].

Actin-Related Proteins ARP2 and ARP3 (Arp2/3) binds to the sides of existing actin filaments and promotes the extension of a new actin filament from its pointed end, forming a 70° angle with the pre-existing filament. Arp2/3 regulation is controlled by WAVE (WASP-

family verprolin-homologous protein)/Scar, WASP (Wiskott-Aldrich syndrome protein) and N-WASP (Neural Wiskott-Aldrich syndrome protein). WAVE/Scar is part of a multimeric complex, including Abi, Nap125, Sra-1 and HSPC-300 (hematopoietic stem cell protein 300), under the control of the small GTPase Rac, which induces the dissociation of Abi, Nap125 and Sra-1 from WAVE, thus mediating its activation. WASP and N-WASP are regulated by Cdc42 (cell division cycle 42). These proteins are also regulated by phosphorylation, phosphoinositides and other molecules, such as WIP (WASP-interacting protein) and TOCA (transducer of cdc42-dependent actin assembly), which also negatively regulate WIP [42,46,48].

Distinct to Arp2/3 complex, formins bind to the barbed end of actin filaments and promote actin growth in a linear fashion. Formins are regulated by small GTPases (RhoA and Cdc42 for mDia1 and mDia2, respectively) and require interaction with G-actin-bound profilin to promote actin polymerization [46].

Actomyosin-based contraction is controlled by the small Rho GTPases Cdc42, Rac and RhoA. Regulation by these GTPases is antagonistic. RhoA activates Rho-kinase, also called ROCK (Rho-associated protein kinase), which in turn phosphorylates and inactivates the phosphatase that dephosphorylates myosin light chain (MLC), resulting in increased contractility. Cdc42 has a similar mechanism, acting through MRCK (myotonic-dystrophy-kinase-related CDC42-binding kinase). Conversely, Rac activates PAK (p21-activated protein kinase), which phosphorylates and inactivates MLC kinase, thus leading to decreased contractility and promoting spreading. However, PAK may also phosphorylate MLC directly, which would increase contractility. In addition, PAK also regulates cell polarity, through the activation of a PIX (PAK-interacting exchange factor)/PAK complex that is targeted to the leading edge during G-protein-coupled receptor dependent migration. Finally, PAK regulates microtubules through stathmin phosphorylation, which results in decreased microtubule catastrophe [42,46,48].

Capping proteins such as gelsolin block actin polymerization at the barbed end and are mainly regulated by phosphoinositides. Finally, cofilin splits actin filaments, and its activity is regulated by phosphorylation induced by LIMK, which is in turn regulated by PAK- or Rho-kinase-mediated Ser/Thr phosphorylation [42,46].

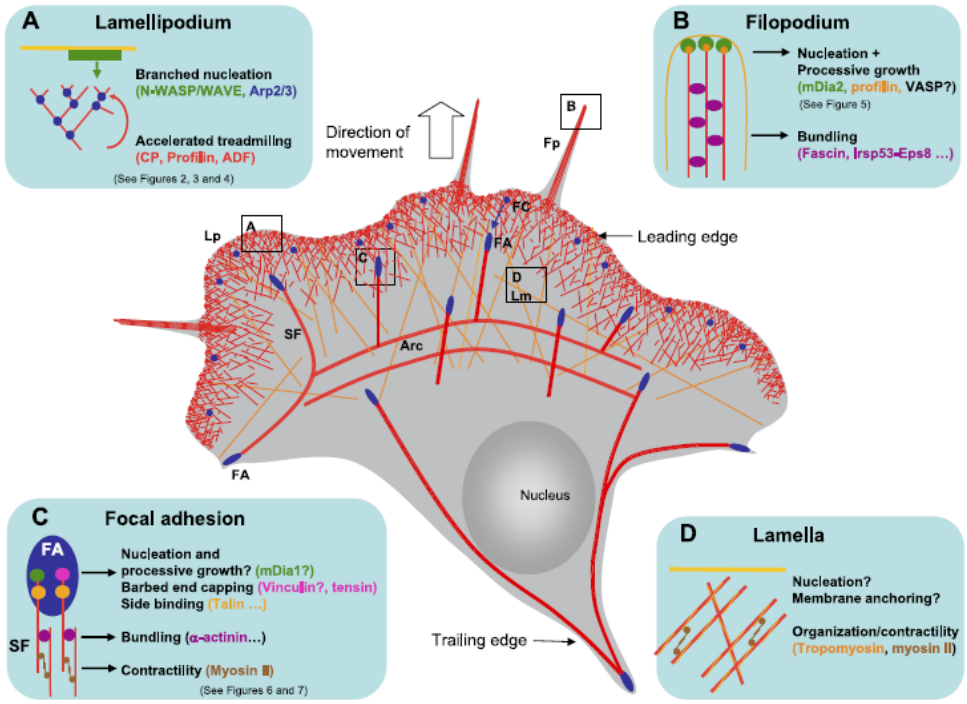


**Figure 10. The actin cytoskeleton in a migrating cell**. **A.** in lamellipodia, branched actin filaments are generated at the PM by the signal responsive WASP-Arp2/3 machinery and maintained in fast treadmilling by a set of regulatory proteins (ADF, capping proteins, profilin). **B.** during cell migration, cells extend fingerlike protrusions called filopodia beyond the leading edge of protruding lamellipodia to sense the environment. At the tip of filopodia, formins like mDia2 catalyze the processive assembly of profilin-actin. The resulting nonbranched actin filaments are tightly bundled by several proteins including fascin and the Irsp53-Eps8 complex. **C.** slow moving cells form focal adhesions in response to RhoA signaling. Focal adhesions connect the extracellular matrix to contractile bundles made of actin filaments, myosin II, and bundling proteins including α-actinin. Focal adhesions contain a variety of actin binding proteins including side binding proteins, capping proteins, and nucleators. **D.** the lamella is characterized by a slow actin turnover and contains the signature proteins tropomyosin and myosin II. The mechanisms by which actin filaments are nucleated and anchored at the plasma membrane are not known. Lp, lamellipodium; Fp, filopodium; Lm, lamella; SF, stress fiber; FA, focal adhesion; FC, focal complex. Reproduced from reference [47].

### 1.4.3. Formation and stabilization of attachments

Along with a bias for membrane extension at the cell front, preferential attachment abilities occur at the leading edge. New focal adhesions form at the cell front and persist until they reach the cell rear. Nascent adhesions appear in temporal waves, initially as small aggregates that increase in size and intensity as the cell migrates over them, persisting and remaining fixed on the substratum until they reach the rear, or an edge, of the cell. Cell–substratum attachments at the leading edge, which subsequently remain fixed to the substratum as the cell moves forward, effectively serve to remove adhesion molecules from the leading lamella. This implies existence of mechanisms to replenish such components at the cell front. Membrane proteins, including integrins, are directed rapidly toward the cell

periphery, including the leading edge, where they tend to remain. In addition to this directed surface movement of adhesion receptors, vesicle trafficking of adhesive components to the leading edge continues [42,45,48].

Upon adhesion to a substratum or the extension of a filopodium, a group of cytoskeletal associated proteins are phosphorylated on tyrosine. Focal adhesion kinase (FAK), paxillin, and tensin are among these phosphoproteins that comprise adhesive complexes. Tyrosine phosphorylation of paxillin, tensin, and FAK creates recognition sites for proteins containing src-homology 2 (SH2) domains that, along with other binding sites, play key roles in the assembly of adhesive complexes. Indeed, FAK has binding sites via its SH2-binding domain for src-related tyrosine kinases, including fyn, csk, and src; it has also binding sites for structural proteins such as paxillin, talin, and integrin. In addition to its binding properties, FAK exhibits tyrosine kinase activity and phosphorylates cytoskeletal-associated substrates such as src and paxillin, which in turn can initiate further recruitment of structural and signaling components. Likewise, paxillin has numerous SH2-binding domains, an SH3-binding domain, and LIM domains. It binds structural components such as vinculin as well as signaling molecules, including src, csk, FAK, and crk. Finally, tensin binds to src and paxillin through its SH2 domain, while through other domains it binds to actin and SH2 domain–containing proteins [42,45].

There is convincing evidence that Cdc42, Rac, and Rho play a major role in regulating the formation of adhesions. These regulatory proteins comprise a hierarchical cascade that initiates the formation of filopodia, lamellipodia, focal adhesions and stress fibers. Formation of filopodia is regulated by Cdc42, while formation of lamellipodia is regulated by Rac, whose activation stimulates membrane ruffling. Finally, formation of focal adhesions, highly organized adhesive complexes containing termini of actin stress fibers, is regulated by Rho. The activation of Cdc42 is the process that initiates this cascade [45]. Since filopodia, lamellipodia, and focal adhesions each involve distinct organizations of F-actin, the actions of this GTP-binding subfamily could be proximal to the regulation of actin-binding proteins. Candidates for intermediary actors are tyrosine kinases, including FAK; lipid kinases, including PIP (phosphatidylinositol phosphate) 5-kinase and PI (phosphatidylinositol) 3-kinase; and phospholipase Cγ (PLCγ). Each of these is implicated in migration in a characteristic way: FAK is thought to initiate formation of adhesions; PIP5K produces $PIP_2$, implicated in the assembly of actin filaments; and PI3K is implicated in chemotactic responses and modulation of integrin affinity. PLCγ is required for PDGF (platelet-derived growth factor)-, IGF-1-, and EGF-induced migration, presumably via hydrolysis of $PIP_2$ and mobilization of actin-binding proteins [42,45].

### 1.4.4. Contractile forces and traction

At least two distinct types of force must be generated independently by a migrating cell: the protrusive force needed to extend membrane processes (lamellipodia or filopodia), provided by actin polymerization and structural organization, independently of myosin motor activity; the contractile force needed to move the cell body forward, dependent on active myosin-based motors, involving separate mechanisms of force generation within the anterior and posterior regions of the cell. The process of extension and contraction can occur independently of one another and may use different mechanisms to generate their respective appropriate forces (Figure 11). The traction exerted by a cell on its substratum is directly related, but not identical, to the intracellularly generated contractile force, because this can be dissipated by deformation of the cell and by disruption of cell–substratum attachments. In turn, the substratum locally exerts an equal and opposite traction force on the cell via the same attachments, with magnitude depending on the susceptibility of the attachments to disruption. Hence, the magnitude of cell-generated contractile forces does not by itself determine cell migration speed. Maximal cell migration speed tends to correlate inversely with contractile force [45,46].

The resistance that contractile forces must overcome in order to complete cell body translocation is primarily due to adhesive interactions. The effective contractile force must essentially be in balance with the traction force provided by dynamic cell–substratum attachments in order to move the cell body. Moreover, this balance must incorporate an asymmetry in traction between the cell front and rear, allowing forward attachments to remain while rearward attachments are released. The degree of this asymmetry is predicted to be a key determinant of the range of substratum ligand concentrations permitting locomotion. This dependence of cell locomotion speed on overall cell-substratum adhesive strength and the degree of spatial asymmetry in adhesive strength suggests one means by which the various molecules regulating adhesive complexes can effectively control migration [45]. A major function of myosin II–based contraction in migrating cells is to help to break adhesive interactions by direct application of physical stress. Either myosin II or myosin I could serve to pull the cell body forward by contractile forces acting between the back edge of the leading lamella and the nucleus, while myosin II contraction at the cell rear reduces the resistive cell–substratum traction [45,46].

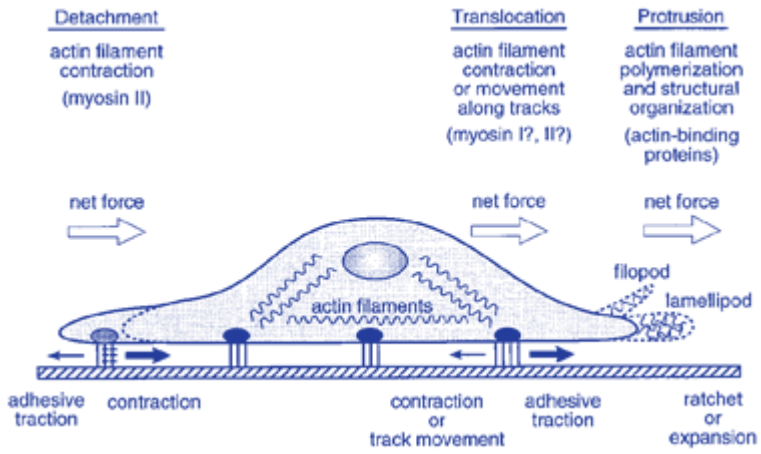


**Figure 11. The different forces involved in cell migration.** Protrusion of membrane lamellipodia or filopodia requires force generated by actin polymerization. Translocation of the cell body forward, once the membrane protrusion has become adherent to the substratum, may occur by myosin interactions with actin filaments. Detachment of the cell rear involves disruption of cell–substratum attachments, perhaps accelerated by myosin-mediated actin filament contraction pulling on adhesion complexes. Here, the magnitude of traction is less than the contraction force. Reproduced from reference [45].

### 1.4.5. Rear release and trailing edge retraction

For cells to translocate forward, adhesions at the rear must disassemble and the trailing edge retract, otherwise tension would rip the cell apart [46]. Rapid migration requires efficient mechanisms to release adhesions at the rear of the cell. In theory, rates of lamellipodal protrusion and rear release both contribute to the migration rate, however, in some cells the rate of rear release is the main determinant of the overall migration rate [45,46].

The major fraction of integrins is left on the substratum as the cell releases and moves forward. Integrins remaining on the cell surface undergo two fates: a regulated release in which they disperse on the cell surface, or endocytosis into vesicles that accumulate in the cell body. Integrin regulated release happens mainly in the cell edge at the cell rear, and once there, they either release and disperse to be used for new adhesions toward the cell front or, alternatively, remain aggregated, move forward along the cell edge, and form a new adhesion. Another fraction of the integrins from rear adhesions appear in endocytic vesicles that accumulate in the perinuclear region. Integrins endocytosis constitutes a possible route by which integrins accumulated in the rear might be supplied to the cell front (Figure 12) [45].

In accordance with observations that adhesions tend to release at the rear, the cell rear is a region where integrin–cytoskeletal linkages tend not to form and the membrane is less well-supported by the cytoskeleton. This contrasts with the cell front, where integrin–cytoskeletal linkages do form, and the membrane is well-supported. The cell rear is further distinguished from the cell front by its tendency to have unsupported membrane resulting in

the formation of membrane tethers, i.e., regions of membrane depleted of cytoskeletal components that can be pulled out from the cell [45,46].

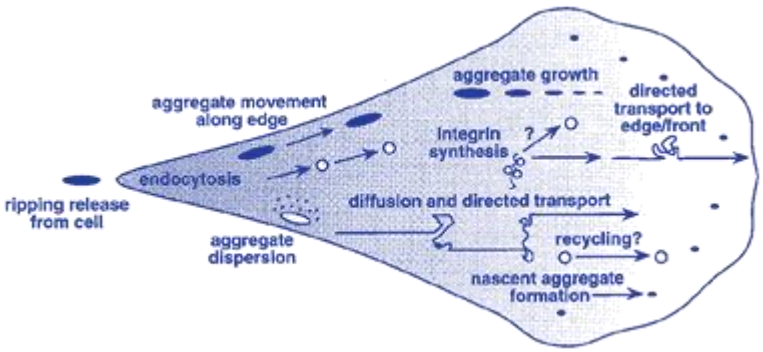


**Figure 12. Integrin Adhesion Receptor Dynamics in Cell Migration.** Newly synthesized or recycled integrins may be inserted into the plasma membrane behind the leading lamella, then transported to the edge by diffusion and directed transport. Once there, adhesion bonds are formed with substratum ligands, followed by nascent aggregates—adhesion complexes—that grow as the cell moves forward. At the rear of the cell, these adhesions are released as the trailing edge detaches from the substratum. Their integrin contents may be extracted from the membrane and left behind on the substratum, or dispersed by diffusion on the membrane surface, or internalized. The aggregates may also move along the edge of the migrating cell for a while before being eventually disrupted. Reproduced from reference [45].

The mechanisms that promote disassembly include microtubule-dependent targeting of dynamin and subsequent endocytosis of some adhesion components; myosin-mediated contractility which contributes through regulation of MLC phosphorylation by RhoA and Rac acting through Rho kinase and PAK; and finally the dissolution of the adhesive contacts at the rear edge is also achieved through affinity downregulation by dephosphorylation (e.g. by phosphatases as calcineurin), or simply by proteolysis of molecules such as talin by proteases, such as calpain. Calcium is a key modulator in rear edge retraction, probably acting through its regulation of calpain and calcineurin [42,45,46].

### 1.4.6. Adhesion dynamics in cell migration

Adhesions, points of molecular interaction between the cell and the substrate, can assemble and disassemble in response to extracellular cues, and regulate cell motility. During migration, adhesions assemble at the leading edge and disassemble at the trailing edge. However, adhesions also disassemble at the front during protrusion and feed components to nascent adhesions at the leading edge in a process called adhesion turnover. Thus, in protruding regions of cells, as new adhesions form, they can dissemble (adhesion turnover) or stabilize and grow into more mature, larger adhesions [46,47].

The molecular components of stable and nascent adhesions are similar, although there are molecules present in one type that are absent in the other. Among other molecules, talin

directly links integrins to actin and also activates signaling from integrins to the actin cytoskeleton. The molecular mechanisms underlying the 'decision' of an adhesion to mature or turnover are unclear. Rho GTPases are critical effectors in this process. They in turn are controlled by signals emanating from adhesion-related signaling modules, such as the multiprotein complex comprising FAK, Src, paxillin, Crk, CAS (cellular apoptosis susceptibility), PAK and GIT. Cleavage of adhesion components by proteases, such as calpain, also regulates disassembly at the front, although its role has been established more clearly in rear adhesions during detachment. Finally, relaxation signals emanating from the tips of microtubules that target adhesions, probably involving dynamin, are also implicated in adhesion disassembly [46,47].

### 1.4.7. Directionally persistent cell migration

Directional migration is an important component of cell motility. Although the basic mechanisms of random cell movement are well characterized, no single model explains the complex regulation of directional migration. Cells analyze an array of guidance information (e. g. constituents of the matrix, distribution of soluble or substrate-bound guidance cues) to select a direction of migration, and achieve directionally persistent migration by forming and stabilizing actin-rich protrusions or lamellipodia that maintain the orientation of the leading edge. Multiple factors can influence this process, including the topography of the ECM, cell polarity and cell adhesion. While the mechanism by which these factors are integrated to regulate directional migration remains unknown, it is clear that intracellular signaling, often mediated at the leading edge by the Rho family of small GTPases, operates at each step of the cell motility cycle to promote directional migration by regulating leading edge formation [41,49].

In a morphological point of view, if the protrusions and subsequent new adhesions formed by a polarized cell are themselves directionally persistent, the cell will move in a directionally persistent manner.

**Stable protrusions guide migration:**

The orientation of cell migration is determined by the frequency and direction of local lamellipodial protrusions extending laterally from the main longitudinal axis of the cell. Intracellular signaling pathways at the leading edge that regulate actin cytoskeleton remodeling or adhesion formation to create or stabilize local protrusions therefore likely contribute to directional migration [41].

Cells can differ in their intrinsic levels of directionally persistent cell migration. New protrusions are characteristically generated from the pre-existing leading edge, rather than in different directions around the cell. This process restricting lateral protrusions was shown to underlie directional migration in cells such as fibroblasts and leukocytes [41,49].

Local signaling within a protrusion in response to an external guidance cue can direct the formation of a new protrusion *in vitro* and *in vivo*. For example, the leading edge of neurons migrating within the CNS consists of multiple extending and retracting branches, and the direction of migration is determined by the orientation of the most stable branch, which is regulated by external guidance cues and internal signaling [41].

**Cell adhesion guides migration:**

Cell adhesion to the underlying substratum can guide the directionality of migration since it stabilizes lamellipodial protrusions. The topography of the ECM can provide important regulation of cell motility through physical cues that geometrically constrain adhesion sites to guide directional migration. When cells probe their physical surroundings, they acquire mechanical information or signals that help determine the direction of migration [41].

**Polarity and directional migration:**

Cells contain polarity signaling machinery that can influence directional cell motility. This polarization influences the formation of the leading and trailing cell edges. The Par complex, consisting of Par3, Par6 and aPKC (atypical protein kinase C), connects Rho GTPase signaling, centrosome reorientation, microtubule stabilization and membrane trafficking to the regulation of directional persistence. Par activation polarizes a broad spectrum of cellular processes, including the formation of the front–rear axis in moving cells. The stability of this front–rear axis correlates with the extent of persistent directional cell movement [41].

The Rho GTPase family member Cdc42 is a main regulator of cell polarization that influences directional migration. The Cdc42-dependent activation of the Par complex triggers polarized protrusions and directionally persistent cell migration. Cdc42 was shown to promote directional cell motility in fibroblast scratch-wound healing assays [41,50].

**ECM receptors, trafficking and motility:**

Integrin trafficking and co-receptors contribute to integrin function and adhesion formation during cell migration. Integrin trafficking may contribute to directional migration by facilitating the formation of new adhesions at the leading edge. Recent work shows that integrin trafficking and the co-receptor syndecan-4 can contribute to directional migration, in part, by modulating Rho GTPase signaling to control protrusion formation [41].

**Steering from the back:**

The trailing edge of a migrating cell contributes to the maintenance of directional migration by generating contraction forces to pull the cell rear forward and limiting the formation of protrusions to maintain the orientation of migration [41].

### 1.4.8. Cell coordination on collective cell migration

Compared with individual migration, collective cell migration is less understood. Recently, it was established that Rab11 is required for spatial control of Rac activity through the control of cell-cell communication during collective movements. Rab11 acts through the control of Moesin activity, cooperating to transfer forces from cell to cell in order to insure coordinated collective cell migration [51].

In collective migration, endocytosis has been shown to restrict RTK (receptor tyrosine kinase) signaling at the leading edge, either by controlling lateral diffusion of signaling molecules or by recycling RTKs to active regions of the plasma membrane at the leading edge. The small GTPase Rac, a key regulator of actin dynamics, is an important target of endocytosis during collective cell migration [51].

Cell-cell communication is required for proper restriction of Rac in the leading cell and this is a key process for directionality of the cluster migration. The mechanism by which cells are able to sense the relative level of Rac activity in neighboring cells remains unclear. Both Rab11 and Moesin are major regulators of this process. Moesin plays a critical role in organizing the epithelial architecture and in the regulation of membrane tension through regulation of the acto-myosin cytoskeleton. Plasma membrane tension is generated by the formation of protrusions at the leading edge, and this tension is subsequently transmitted to the cell body to inhibit formation of other leading edges [51].

Moreover, photo-activation of Rac has been shown to induce formation of protrusions in the photo-activated cell and inhibit formation of protrusions in the other cells of the group. Formation of protrusions in the leading cell might thus increase plasma membrane tension that is subsequently transmitted around the cluster to inhibit Rac signaling in other cells. Conversely, photoactivation of the dominant negative form of Rac in the leading cell leads to retraction of the protrusions and apparition of protrusions in other cells of the cluster suggesting that relaxing tension at the leading edge allows formation of protrusions in the other cells. Rab11 and Moesin could regulate this mechanical effect, but it remains challenging to understand the molecular mechanism that controls the transmission of tension from one cell to a group of migrating cells [51].

## 1.5. The potential role of APP and sAPP on cell migration

### 1.5.1. APP and FE65 regulate cell movement

There are compelling evidences that APP is involved in cell motility and that this function is modulated by binding to FE65, since APP-dependent increase in the rate of cell migration was enhanced upon FE65 overexpression [52]. In a MDCK (Madin Darby Canine Kidney) cell wound–healing assay, both APP and FE65 accelerated wound closure by increasing the rate of migration of cells at the wound edge, with the effects of either protein being greatly enhanced by additional overexpression of the other. Nonetheless, authors couldn't distinguish if APP-FE65 enhanced the rate of movement due to altered adhesion, altered actin dynamics, or both [52]. FE65 binds to APP through the YENPTY motif in the cytoplasmic domain of APP [52]. FE65 enhances the effect of APP on cell movement by probably regulating the amount of APP at the cell surface. Overexpression of FE65 increases the proteolytic processing of APP [53] and the translocation of APP to the cell surface, suggesting that binding of FE65 to the YENPTY motif regulate the role of APP in cell movement by targeting APP to the cell surface.

APP and FE65 colocalize with actin and Mena in lamellipodia. Mena is an Abl associated signaling protein thought to regulate actin dynamics, which binds to FE65. Mena is genetically linked to the Abl tyrosine phosphorylation signaling cascade and is required for normal neural development. It localizes to cell-substrate adhesion sites and sites of dynamic actin assembly and disassembly. Interestingly, Mena also binds to profilin, placing it in a position to regulate actin dynamics. Based on data, authors hypothesized that APP and FE65 regulate lamellipodial motility as part of a larger Mena-containing macromolecular complex (Figure 13) [52]. It was proposed that, at least some of the effects of this APP and FE65-containing macromolecular complex on cell movement are mediated by Mena and that lamellipodial Mena regulates cell motility in fibroblasts [54]. In contrast to the increase in cell movement caused by FE65 and APP, Mena decreases cell motility [54]. In addition, Ena (enabled), the *Drosophila* homologue of Mena, negatively regulates growth cone migration through an interaction with Robo, a transmembrane receptor that mediates repulsion of axons at the midline [55]. It is possible that Mena acts as a switch, either binding to Robo or to the FE65–APP complex: when Mena binds to Robo ("unstimulated" state Mena), motility is inhibited, but when conditions are shifted in response to some signal, Mena is alternatively recruited to the FE65–APP complex, the inhibition is released and motility increases [52].

The effects of FE65 and APP on cell migration might be due to changes in adhesion [52]. At the neuronal cell surface, APP colocalizes with patches of integrins, a family of heterodimeric cell adhesion receptors that mediate cell–matrix interactions required for cell

proliferation, differentiation, and migration. Integrins and Mena are both found in two types of cell substrate adhesion sites, known as focal adhesions and focal complexes. APP and FE65 localize with Mena in integrin-based focal complexes in mobile membrane compartments [52]. Further, it was shown that FE65 and APP specifically concentrate with β1-integrin in focal complexes, the dynamic adhesion sites typically found at a migrating cell's leading edge; but are not found in more stable and strong focal adhesions at the tips of actin stress fibers, found in relatively static regions of the cell. This is especially interesting since focal complexes can be precursors to focal adhesions, and until now there was no known difference in the biochemical composition of these two kinds of adhesion sites [52].

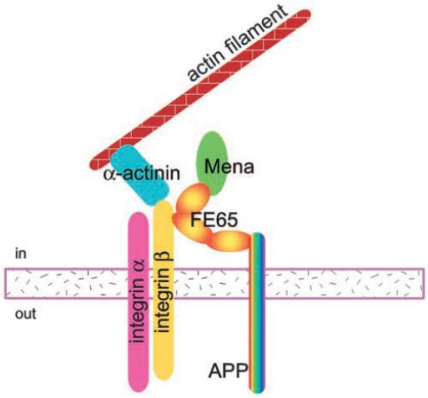


**Figure 13. Putative components and interactions of a APP/FE65-containing macromolecular complex:** FE65 might interact with APP through its C-terminal PID (phosphotyrosine interaction domain) and with Mena through its WW domain. Mena modulates actin polymerization, possibly through its interaction with profilin, whereas integrins are indirectly linked to actin through a variety of integrin- and actin-binding proteins, such as α-actinin. Regulation of the various interactions shown could connect environmental cues to actin dynamics at the lamellipodial focal complex. Reproduced from [52].

APP might function as a transmembrane molecule or as a secreted fragment and, notably, sAPP was shown to compete with APP for binding to integrins, decreasing the strength of an adhesion site and promoting motility [52].

### 1.5.2. sAPP as a motogen for keratinocytes

Cell migration is triggered by constituents of the ECM such as fibronectin (FN) and by soluble mediators commonly summarized as motogens. Many growth factors, such as EGF and the transforming growth factor alpha (TGF-α), in addition to induce cell proliferation and differentiation, have been shown to act as motogens on a variety of cell types. The motogenic effects include the ability to induce cell migration and to stimulate lamella dynamics, the latter manifested in more rapid and frequent protrusion and retraction of lamellipodial and filopodial membranar extensions [14,39].

Studies on the physiological role of APP identified sAPP as a keratinocyte growth factor [39]. The proteolytic release of sAPP from APP by α-secretase cleavage is similar to the processing of the growth factor TGF-α [39], and sAPP has growth factor-like domains. Further, sAPP was observed to also function as motogen and chemoattractant for human keratinocytes *in vitro*, suggesting sAPP as a major member of the factors involved in wound healing. Several effects of sAPP on keratinocytes migration were reported:

**sAPP-induced cell polarity:** Studies demonstrated that sAPP induced keratinocytes to switch from a non-polarized morphology, typical of non-motile cells towards a clear polarization characteristic of migrating cells. sAPP and FN seemed to act synergistically during polarization [39][14]. Under the stimulus of nanomolar concentrations of sAPP, is observed a tenfold increase in the number of cells acquiring a polarized morphology [14].

**Lamellipodia and ruffle dynamics:** During stimulation with sAPP, cells adopted a highly asymmetric and rapidly changing morphology characteristic of migrating cells. It was also verified a considerable increase (up to threefold) in lamella dynamics, with ruffles and lamellipodia being formed more frequently and running significantly faster [14,39].

**Proportion of migrating cells, their average velocity and their directional persistence:** sAPP was capable to recruit resting keratinocytes for migration (sAPP and FN appeared to act synergistically in this stimulation), increasing the proportion of migrating keratinocytes; the migration velocity was about twice the speed of nonstimulated keratinocytes; the directional persistence of cell migration was synergistically increased by sAPP and FN [39].

**Chemokinetic and chemotactic effects of sAPP:** sAPP triggers a directed, i.e., a chemotactic migration of keratinocytes towards a higher concentration of sAPP, and not a random migration [39].

As the motogenic effect of sAPP results in speeding up human keratinocyte migration about twofold, it even exceeds the effects of EGF, KGF (keratinocyte growth factor), and TGF-α on this cell type [14]. Like EGF, sAPP exerted its motogenic effect through the activation of Rac kinase, with data shown increased levels of activated Rac in sAPP-stimulated keratinocytes. However, the receptor for sAPP appears to be distinct from that of EGF, since inhibition of the EGF receptor kinase by tyrphostin has almost no effect on the motogenic stimulus exerted by sAPP [39]. Among the different sAPP forms sAPP751, which is expressed at high levels in the cells of the human epidermis, was the most potent motogen for human keratinocytes. In this context, the fact that keratinocyte migration is essential for the closure of epidermal wounds raises the question for a possible significance of sAPP on wound healing [14].

In synthesis, the APP role in cell motility and, in particular, in neuronal migration during neurogenesis, has been reported in the literature. However, further studies are necessary to better characterize the specific effects of APP on cell migration and to unravel the underlying molecular mechanisms.

# 2. Aims

In the present work we intended to unveil the roles of APP and it proteolytic fragment sAPP in cell migration, with its main aims being:

- To evaluate the paracrine role of sAPP in neuronal-like cells migration;
- To unveil the autocrine role of full length APP in neuronal-like cells migration, and the influence of APP S655 phosphorylation;
- To evaluate the influence of APP in determining a typical F-actin migratory phenotype;
- To study the APP effects on F-actin cytoskeleton dynamics of migrating cells.

# 3. Materials and Methods

## 3.1. Culture and maintenance of cell lines

### 3.1.1. Culture and maintenance of the SH-SY5Y cell line

SH-SY5Y neuroblastoma cells were used for studying neuronal-like migration since they retain a neuronal phenotype and possess full APP-processing and signaling pathways. SH-SY5Y cells are derived from the original cell line SK-N-SH, isolated from a bone marrow biopsy of a neuroblastoma patient. SH-SY5Y cells are maintained in 10% fetal bovine serum (FBS), 2 mM L-glutamine, 1% antibiotic/ antimycotic mix (Gibco) Minimal Essential Medium (MEM):F12 (1:1) (Gibco), in a 5% $CO_2$ humidified incubator at 37°C. Cells are split when 80-90% confluent.

### 3.1.2. Culture and maintenance of the HeLa cell line

HeLa cells are the most commonly used human cell line. This immortal cell line was derived from cervical cancer cells of a patient named Henrietta Lacks. The cell line is maintained in Dulbecco's Modified Eagle Medium (DMEM) with 1% non-essential amino acids (Gibco), 10% heat inactivated FBS (Gibco) and 1% antibiotic/antimycotic mix (Gibco), in a 5% $CO_2$ humidified incubator at 37°C. Cells are split when at 80-90% confluency.

## 3.2. Wt and S655 phosphomutants APP-GFP cDNAs

APP-GFP cDNAs were already available at the lab. APP isoform 695 ($APP_{695}$) cDNA was used as template to generate S655 cDNA point mutations, namely Serine 655 to Alanine (S655A) or to Glutamate (S655E), using site directed mutagenesis [15,25,56]. These two amino acids, due to their size and charge, mimic a constitutively dephosphorylated (S655A) and phosphorylated (S655E) S655 residue, respectively. Further, to engineer the $APP_{695}$-GFP cDNA constructs (APP-GFP), the stop codons of Wt and S655 phosphomutants $APP_{695}$ cDNAs were removed by PCR and the resultant APP cDNA fragments digested and subcloned into the GFP-encoding mammalian expression vector (pEGFP-N1, Clontech), encoding the Green Fluorescent Protein (GFP). The result was a fusion gene of APP with GFP in its C-terminal [25].

## 3.3. Amplification and purification of a pLifeAct-RFP cDNA

### 3.3.1. Bacterial transformation

*E. Coli* XL1-Blue competent cells were thawed on ice and 250 ng of pLifeAct-RFP cDNA were each added to a 100 µl aliquot of competent cells. Cells were incubated on ice for 30 min, further subjected to heat shock by incubation in a 42°C bath for 90 sec, and then rapidly transferred to ice for 2 min. 900 µl of SOC medium was added to the cells, followed by incubation at 37°C for 45 min. Finally, the cells were centrifuged at 14000 rpm for 30 sec, the supernatant discarded, and the pellet resuspended in the remaining volume (100 µL) to be plated onto LB/Ampicillin agar plates. Plates were incubated at 37°C during 16-18 h.

### 3.3.2. 'MegaPrep' DNA purification

In order to perform a Megaprep DNA Purification, one colony of LifeAct-RFP transformed bacteria was isolated and added to 3 mL of LB medium supplemented with (50 µg/ml Ampicillin and incubated with agitation during 16-18 h at 37°C. After bacterial growth, 1 mL of cells was transferred to 1 L of LB/Ampicillin medium and further incubated with agitation overnight (O/N) at 37°C.

The Megaprep procedure comprises two main phases: the preparation of cleared lysate and the plasmid DNA purification.

To prepare a cleared lysate, cells were centrifuged at 1500 x g for 20 min (Beckman Avanti J-25 I - Beckman Coulter), the supernatant was discarded and the pellet suspended in 30 mL of Cell Resuspension Solution. After resuspension, 30 mL of Cell Lysis Solution was added and inverted to mix. When the solution become clear and viscous, 30 mL of Neutralization Solution was added, mixed and centrifuged at 20000 x g for 15 min. The supernatant was filtered using filter paper, and the remaining volume measured. 1/2 volume of isopropanol was added and the mixture centrifuged at 14000 x g for 15 min. The supernatant was discarded and the pellet resuspended in 4 mL of sterile water.

For the second phase - plasmid DNA purification, 20 mL of Wizard® Megapreps DNA Purification Resin was added to the solution and mixed. The resin/DNA mixture was transferred to a Megacolumn, attached to a vacuum manifold port, and vacuum was applied to pull the resin/DNA mix into the Megacolumn. The column was then washed 2 times with 25 mL of Column Wash Solution containing Ethanol, also by applying vacuum. 10 mL of 80% ethanol was added to the column and vacuum applied for an additional minute after the liquid has passed through the Megacolumn. The column was subsequently transferred to a 50 mL

screw cap tube and centrifuged at 1300 x g for 5 min (Eppendorf Centrifuge 5810R). The liquid was discarded and the column placed again in the vacuum manifold and dried by applying 5 min of vacuum. The column was then removed, placed in a new 50 mL screw cap tube, and 3 mL of pre-heated (65-70°C) nuclease-free water was added to the column. After 1-2 min, the column was centrifuged at 1300 x g for 5 min to elute DNA, and the solution transferred to microcentrifuge tubes (400 µL per tube) and stored at -20°C. This procedure had been previously done in the laboratory for the APP-GFPs cDNAs.

### 3.3.3. Ethanol precipitation of plasmid DNA

Ethanol precipitation was also performed in order to increase DNA purification, which is essential for optimal transfections. 1/10 of sodium acetate was added to each microcentrifuge tube containing the DNA solution. 2,5 volumes of ethanol 100% was further added, mixed and incubated O/N at -20°C. Subsequently, the tubes were centrifuged (14000 x g, 15 min, 0°C), the supernatant was discarded and 750 µL of ethanol 70% (half of the tube capacity) was added, mixed and incubated O/N at -20°C. Following, the tubes were centrifuged (14000 x g, 5 min, 0°C), the supernatant was discarded and the pellet dried. Once the pellet was completely dry, with no traces of ethanol, the DNA was resuspended in 100 µL of sterile water and stored at -20°C.

## 3.4. Transient transfection of the cell lines with APP-GFP and LifeAct-RFP cDNAs

In order to study the role of APP and APP phosphorylation in cell migration, Wt, S655A and S655E $APP_{695}$-GFP cDNAs were used in single-transfections. For the analysis of cytoskeleton dynamics, the LifeAct-RFP cDNA, a red fluorescent marker of filamentous actin (F-actin), was used in co-transfections with Wt APP-GFP. The low affinity of LifeAct to F-actin reduces unwanted perturbations, with proved absence of effects on actin polymerization and depolymerization and lack of competition with major actin-binding proteins [57].

### 3.4.1. Transfection by the TurboFectTM reagent

Transient transfection of cells was accomplished using the TurboFectTM reagent (Thermo Scientific). Of note, a combination of TurboFectTM with CombiMagTM (OZ Biosciences) was also tested but with no satisfactory results.

Transfections were carried out according to the manufacter's instructions. For each 80-85% confluent monolayer of cells grown in 6-well plates, 2 µg of DNA were diluted in 100 µL of serum-free growth medium. After being briefly vortexed, 4 µL of TurboFect™ were added to the diluted DNA. Of note, the amounts of DNA and TurboFect™ used were previously optimized in a pilot assay. The mixture was vortexed and incubated for 15-20 min at room temperature (RT), during which the cells medium was replaced by fresh medium. After the incubation period, the mixture was added dropwise to each well, with gentle agitation of the plate to achieve even distribution. Cells were incubated at 37°C in a $CO_2$ incubator. After 6-8h, cell medium was again replaced, and cells incubated for a total of 24-48h.

## 3.5. Scratch Wound Healing (SWH) assays

After a broad review of the existing migration assays, the Scratch Wound Healing assay (SWH) was chosen as it is a widely used, simple and few expensive well-established assay, ideal for first experimental approaches to a scientific issue.

In order to perform the SWH assay, SH-SY5Y cells were previously transfected with either pEGFP-N1 or the APP-GFP cDNAs (Wt, S655A, S655E), and HeLa cells were previously co-transfected with Wt APP-GFP and LifeAct-RFP. Before cell seeding, two parallel vertical lines and two parallel horizontal lines were drawn with an acetate pen on the underside of each well to serve as a guidance axes.

Once the confluent monolayer was formed (approximately 95% confluent), the migration assay took place by gently scratch of the cells monolayer with a sterile P10 pipette tip, across the center of the well, creating a straight "wound" [58,59].

The medium was replaced by complete medium or by sAPP-enriched medium immediately after performing the wound. This conditioned medium was previously collected from an extra plate of Wt APP-GFP expressing cells transfected for 48h, with high cumulative sAPP amounts.

Fluorescent and phase contrast images of each wound were immediately captured to document the pre-migration stage (t0) of a selected cell-free area. The plate was maintained at 37ºC/5% $CO_2$ and the "healing" of the "wound gap" by cell migration towards the center of the gap was monitored by imaging both wound edges at every hour or 2h, during 8h (t0-t8), and in the following day (t24). Epifluorescence and phase contrast microphotographs of the wound were obtained using an Olympus IX-81 motorized inverted microscope equipped with a LCPlanFl 10x/0.30 objective lens.

### 3.5.1. Migration assay image analysis

The efficiency of SH-SY5Y cell migration (gap closure) was quantitatively evaluated through the analysis of the images acquired from t0 to t8, at each hour/2 hours, and at t24, using the ImageJ software, as follows.

In order to study the paracrine role of sAPP in cell migration, three different parameters were analyzed:

a) **Migrating cells score:** number of non-transfected cells observed at the wound area (wound borders determined at t0), at each time point. The Cell Counter plugin (ImageJ Software) was used to count the cells.
b) **Leading edge migrated distance:** average distance migrated by the leading edge of non-transfected cells along the time. Ten random cell coordinates of each leading edge (two per wound) were considered for the measurements.
c) **Leading edge migration velocity:** average velocity of migration of the non-transfected leading edge cells at each time period, determined on base of the migration distance data.

In order to study the role of full-length APP (flAPP) in SH-SY5Y cells migration, by the analysis of transfected cells migration, another methodology was used due to the low number of transfected cells in the wound region being monitored:

d) **Single-cell tracking:** based on the 2D coordinates of each transfected cell, a single-cell track graph of migration was obtained, from which it was possible to visually analyze the **cell coordination** on collective migration; based on the coordinates of each cell, the **migration distance and velocity** were also determined; the **directional persistence** was also analyzed by measuring the non-linear distance migrated by the cells, a parameter inversely proportional to an efficient persistence in the migration direction, named by us as the "out-of-track" percentage.

## 3.6. Wound effects on APP and sAPP levels

In order to evaluate the APP and sAPP levels in migrating and non-migrating Wt APP-GFP cells, HeLa cell monolayers grown in six-well plates were multiple wounded (8 wounds/plate) and cells left to migrate for 24h. Wounded and non-wounded cell monolayers, and respective conditioned medium, were collected and subjected to Western blot (WB) analysis for comparison of the APP and sAPP protein contents.

Cells conditioned medium (500 µl) was collected into a microtube containing 55 µl of 10% SDS, the remainder medium was removed with a Pasteur pipette, and cells collected with 250 µl of 1% SDS. Media and cell lysates were boiled for 10 min, cell lysates were further sonicated for 30 sec, and both stored at -20°C. Quantification of the protein content of the cell lysates was made using the BCA protein assay kit as described below.

### 3.6.1. Quantification of protein content

Quantification of the protein content of the cell lysates was made using the Pierce's bicinchoninic acid (BCA) protein assay kit (Thermo Scientific), and was performed in a 96-well plate. Standard samples were prepared using increasing known amounts of bovine serum albumin (BSA), as depicted in Table 1. Cell lysate aliquots (in duplicated) were prepared by mixing 5 µL of the cell lysate with 20 µL 1% SDS.

**Table 1.** Standards used in the BCA protein assay. BSA, Bovine Serum Albumin solution (2 mg/ml).

| Padrão | BSA (µl) | 1% SDS (µl) | Protein Mass (µg) |
|---|---|---|---|
| $P_0$ | 0 | 25 | 0 |
| $P_1$ | 1 | 24 | 2 |
| $P_2$ | 2 | 23 | 4 |
| $P_3$ | 5 | 20 | 10 |
| $P_4$ | 10 | 15 | 20 |
| $P_5$ | 20 | 5 | 40 |

The Working Reagent was prepared by mixing the BCA reagent A with the BCA reagent B in the proportion of 50:1, and 200 µL were added to each well. The microplate was incubated at 37$^{o}$C during 30 min, after which the absorbance at 562 nm was measured using a microplate reader (Infinite M200, Tecan), with 25 readings being performed for each well/sample to calculate an average sample O.D..

### 3.6.2. Western Blot procedures

Cell lysates were subjected to SDS-PAGE and to Ponceau Red staining (described below) previously to WB analysis, as follows. Samples were electrophoretically resolved on a 10% sodium dodecylsulfate polyacrylamide gel (SDS-PAGE) and then transferred to a nitrocellulose membrane. Membranes were first soaped in 1X TBS for 10 min. Further, the blockage of unspecific antibody binding sites was ensured by incubating the membrane for 1-2 h with 5% non-fat dry milk in 1X TBS-T solution. Membranes were further incubated O/N with a primary

antibody. The primary antibody used was the monoclonal 22C11 mouse antibody (1:250, Chemicon) directed against APP N-terminus, recognizing endogenous full-length APP (109 and 115 KDa), APP-GFP (139 and 145 KDa) and secreted APP (sAPP). After 3 washes with 1X TBS-T, membranes were incubated for 2 h with the secondary antibody (Horseradish peroxidase conjugated α-Mouse IgG, 1:5000, Amersham). Membranes were additionally washed 3X with TBS-T and submitted to signal development using Luminata™ Crescendo (Millipore) reagent, a substrate of the horseradish peroxidase enzyme to which the secondary antibody is labeled, producing a chemiluminescent signal. In a dark room, the membranes were incubated at RT for 5 min with Luminata™ Crescendo, and then an autoradiography film was placed on top of the membrane and placed inside a film cassette. After the exposure, the film was developed in developing solution (Sigma Aldrich), washed in water and fixed in fixing solution (Sigma Aldrich). The membrane was washed with 1X TBS-T and deionized water before drying.

### 3.6.3. Ponceau red staining of protein bands

Ponceau Red staining was applied as a loading control, alternatively to actin or β-tubulin immunoblotting. This type of staining has been described as a fast, inexpensive, and nontoxic method and its binding is fully reversible in a few minutes [60]. The nitrocellulose membrane was incubated in Ponceau S solution (Sigma Aldrich) for 7 min, followed by a brief rinse in deionized water so that the bands were clearly visible. The membrane was then scanned in a GS-800 calibrated imaging densitometer (Bio-rad). After that, the membrane was extensively washed with 1X TBS-T and deionized water to completely eliminate the staining and thus be further used in Western Blot assays.

## 3.7. Migratory cells morphological analysis

After a SWH assay of EGFP-N1 and Wt APP-GFP SH-SY5Y transfected cells migrating for 8 hours on coverslips, cells were fixed with a 4% paraformaldehyde/PBS solution for 30 minutes and permeabilized with a 0,2% TRITON in PBS solution for 10 minutes.

In order to visualize F-actin, a cytoskeleton protein mainly involved in migration, 1 µL of Alexa Fluor® 568 Phalloidin was diluted in 50 µL PBS 1% BSA and added to coverslips for 30 minutes, in the dark. Coverslips were further washed two times with PBS and one last time with deionized water, and subsequently mounted with DAPI-containing antifading reagent (Vectashield, Vector Laboratories) on microscope glass slides for fluorescence microscopy analysis. Epifluorescence microscopy was carried out using the Olympus IX-81 microscope equipped with LCPlanFl 20x/0.40 and 60x/0.70 objective lens.

The morphology of non-transfected and EGFP-N1 or Wt APP-GFP transfected cells mainly at the leading edge (and some few already at the wound area) were analyzed and classified as 'migratory' or not by imaging its shape and the cellular F-actin content and distribution. Cells were considered having a typical F-actin migratory phenotype when presenting a clear polarized and highly asymmetric morphology and visible lamellipodia (and filopodia) [39], as represented in Figure 14. The number of cells with a migratory phenotype at that given time (8h) was scored, and results presented as a percentage of the number of cells analyzed.

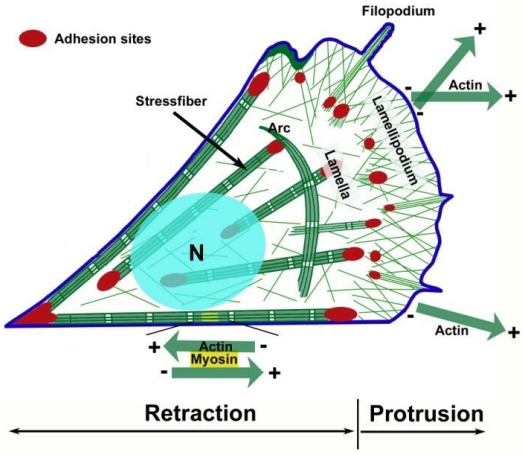


**Figure 14. Schematic representation of a migratory cell phenotype.** Relevant F-Actin structures are depicted, as lamellipodia, filopodia, stress fibers, adhesion sites (containing F-actin). Reproduced from reference [61].

## 3.8. Fluorescence Recovery After Photobleaching (FRAP)

In order to study the actin cytoskeleton dynamics in Wt APP-GFP migrating cells, HeLa cells co-expressing LifeAct-RFP and either EGFP-N1 or Wt APP-GFP were left to migrate for 20h in a SWH assay, and subjected to FRAP experiments by live-cell microscopy. The medium was replaced for phenol-red-free, high glucose DMEM after scratch the wound, to reduce nonspecific background intensity and improve the signal-to-noise ratio.

FRAP experiments were conducted on a Leica SP5 laser scanning inverted microscope equipped with a Plan-Apochromat x63/1.4 oil objective and an enclosed thermostatted stage that kept live cells at 37$^{o}$C and 5% $CO_2$.

Initially, four (at least) regions of interest (ROIs) with the same area were defined per cell: the cell front (for frontal lamellipodia analysis), the cell rear, a non-bleached area (negative control) and a background area. In some cells, more than one ROI was chosen to

represent the cell front and/or the cell rear, and data averaged. Magnification, laser power, and detector gains were identical across samples.

The F-actin red fluorescence was photobleached using the laser line at 561 nm at full power with a pixel dwell time of about 10 sec for EGFP-N1 cells and about 20 sec for Wt APP-GFP cells. Pre- and post-bleach images were monitored at low laser intensities. Images were taken at intervals of about 0,20 sec and until the recovered fluorescence intensity of the ROI reached a plateau.

In Figure 15 is depicted a schematic representation of a bleached ROI fluorescence intensities over time in a FRAP experiment.

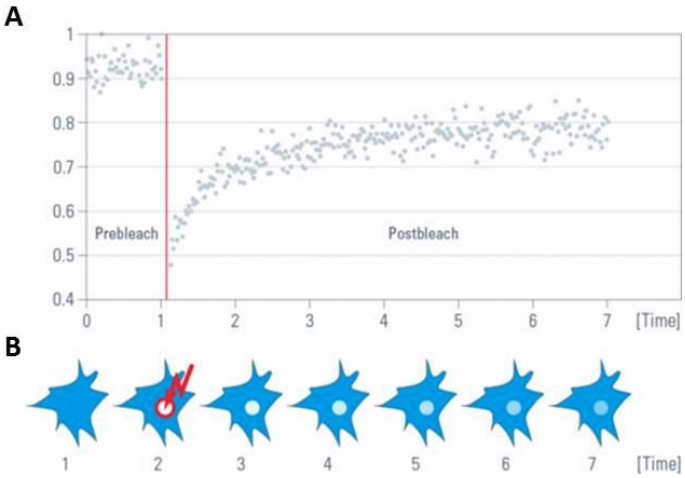


**Figure 15. Shematic representation of a FRAP experiment over the time.** A) Fluorescence intensities of the Bleach-ROI in a time series. Using a low laser power setting, several images are acquired to determine the initial fluorescence, creating reference values ("Prebleach"). Then, a high power laser is applied inside each ROI to bleach the fluorescence (the red line represents the bleach interval). Finally, another set of images using a laser power sufficiently low to prevent further bleaching is acquired to gain insight into the redistribution of molecules by the recovery of fluorescence ("Postbleach"). B) The same cell in a schematic drawing within a time series. At time point two, a region of interest (ROI) within a cell is bleached (red arrow). Non bleached molecules are moving into the ROI along the time. Reproduced from reference [62].

LAS AF software version 2.6.0.7266 was used for image acquisition and analysis. Fluorescence recoveries in the bleach region and overall photobleaching in the whole cell during the time series were quantified. No photobleaching of the cell or adjacent cells during fluorescence recovery was observed. The analysis of the relative fluorescence alterations was based on the following equation provided by the LAS AF software:

$$\frac{dF(t)}{F(0)} = k{:}\,1 \times \frac{F(t)-F(0)}{F(0)-F(b)},$$

where *F(t)* is the fluorescence intensity in the bleached ROI at time t (seconds), *F(0)* represents the fluorescence intensity of a non-bleached area serving as reference, and *F(b)* denotes the background fluorescence intensity. From this equation, the recovery chart is displayed, allowing the quantitative analysis of FRAP.

The percentage of recovery and the halftime of recovery were estimated. Percentage of recovery is the ratio between End and Initial intensities (representing the ratio between mobile and total – mobile+immobile – molecules). The average intensities of the prebleach and of the postbleach plateaus were determined to calculate this parameter. The Halftime of recovery is the time required for the bleached area to recover half of its end fluorescence intensity, and represents the speed of the molecules redistribution. This was calculated by identifying the first postbleach time point whose y value was equal or higher than half of the postbleach plateau intensity, and whose next five y values also respected this rule.

In Figure 16 is depicted a FRAP recovery curve illustrating the parameters that can be measured.

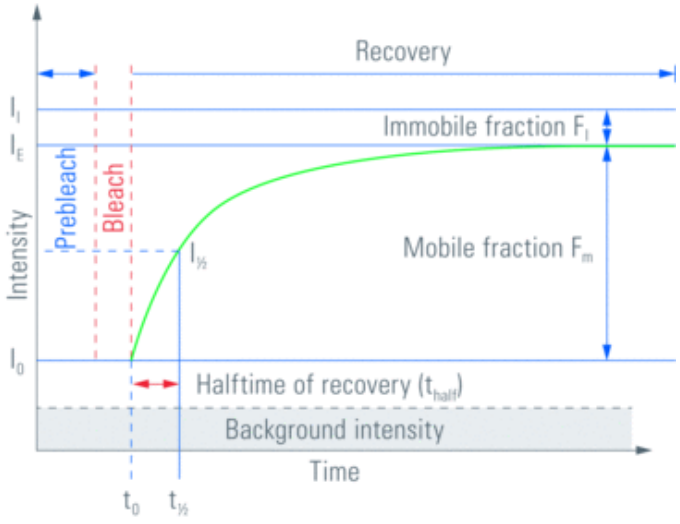


**Figure 16. Representation of the FRAP curve with the time course of the fluorescence intensity.** After bleaching the fluorescence in a region of interest, the intensity recovers to a new equilibrium. The halftime of recovery is extracted from the recovery kinetics and represents the time required for the bleached area to recover half of its end fluorescence intensity. The mobile fraction is the fraction of fluorescent molecules that contribute to the recovery. The immobile fraction is the fraction of molecules that cannot exchange between bleached and non-bleached regions, represented by the difference of the equilibrium intensities before and after the bleach pulse. $I_I$, initial (prebleach) fluorescence intensity; $I_0$, first postbleach fluorescence intensity; $I_E$, end value of the recovered fluorescence intensity. Reproduced from reference [63].

## 3.9. Immunocytochemistry analysis of β1-Integrin

After a 24h SWH Assay of HeLa cells transfected with EGFP-N1 and Wt APP-GFP cDNAs, performed on coverslips, cells were fixed with a 4% paraformaldehyde PBS solution for 30 min

and permeabilized with a 0,2% TRITON in PBS solution for 10 min. After three washes with PBS solution, cells were blocked with 50 µL PBS-3% BSA for 30 min. In order to visualize β1-integrin, cells were then incubated with anti-β1-integrin primary antibody (Millipore, 1:100 dilution) diluted in 3% BSA/1X PBS for 2 hours at RT. Coverslips were washed with PBS (three times, 10 min each), and incubated for 1-2h with TexasRed® secondary antibody (Goat Anti-Rabbit IgG, Life Technologies, 1:300 dilution) diluted in 3% BSA/1X PBS (dark, RT). After 3 washes with PBS and one last wash with deionized water, coverslips were mounted on microscope glass slides with DAPI-containing antifading reagent (Vectashield, Vector Laboratories) for further fluorescence microscopy analysis.

Fluorescence microphotographs of the entire wound area (leading edge and wound) were taken using an Olympus IX-81 microscope and a LSM 510 META confocal microscope (Zeiss). The fluorescence images obtained were quantitatively analyzed for β1-integrin intensity on transfected (GFP expressing) and non-transfected cells of the wound area using the ImageJ Software, specifically the LiveWire plugin for cell selection, followed by the intensity measurement tool. Intensity data presented are the mean intensity per pixel (*mean grey value*) that is corrected for the respective cell area.

## 3.10. Rac1/Cdc42 Activation Assay

The Rac1/Cdc42 Activation Assay uses PAK-PBD affinity beads to bind to the GTP-bound (active) form of Rac and Cdc42, two small G proteins of the Rho family. This is part of the 'RhoA/Rac1/Cdc42 Activation Assay Combo Biochem kit' (Cytoskeleton, Inc).

PAK (p21 activated kinase I) is an effector downstream active Rac and Cdc42, binding these proteins via its 'Cdc42/Rac Interactive Binding' (CRIB) region, also called 'p21 Binding Domain' (PBD). The CRIB/PBD protein motif has been shown to bind specifically to the GTP-bound form of Rac and/or Cdc42 proteins. The fact that the PBD region of PAK has a high affinity for both GTP-Rac and GTP-Cdc42 and that PAK binding results in a significantly reduced intrinsic and catalytic rate of hydrolysis of both Rac and Cdc42 make it an ideal tool for affinity purification of GTP-Rac and GTP-Cdc42 from cell lysates. The amount of activated Rac1/Cdc42 is determined by a Western blot using a Rac1/Cdc42 specific antibody.

### 3.10.1. Cellular stimulation assay

In order to investigate a potential influence of Wt APP-GFP in Rac1/Cdc42 activation, HeLa cells grown in 60mm culture plates were transfected with EGFP-N1 or Wt APP-GFP. Non-transfected cells were used as controls. 24h after transfection, the cells were submitted to

serum starvation to reduce the basal amount of active Rac1/Cdc42, and 50 µg/ml cycloheximide (CHX) were added to inhibit APP-GFP protein biosynthesis and establish a 'zero' time point of APP-induced stimulation [15]. After 5h in CHX serum free medium, the cells medium was change to complete medium and cells further incubated at 37ºC for 2h, after what cells were collected for being subject to the pull down experiment.

### 3.10.2. Cell collection

The culture plates were placed on ice, the media was aspirated, and cells washed with ice cold PBS. PBS was aspirated and plates were tilted on ice for an additional 1 min to remove all remnants of PBS. To lyse the cells, 250 µl of ice-cold Cell Lysis Buffer were added and the lysates were transferred into pre-labeled sample tubes on ice. Lysates were immediately clarified by centrifugation at 10000 x g, 4°C for 1 min. 50 µl of each lysate were saved for protein quantification and for quantification of the total specific small G-protein. The remaining cell lysates were snap frozen in liquid nitrogen and stored at -70°C for future use.

### 3.10.3. Control reactions

Control reactions were performed as an integral part of the kit. To perform positive and negative cellular protein controls, total cell lysates (225 ug) of non-transfected cells, subjected to the same procedures as samples (Section 3.10.1), were loaded with the non-hydrolysable GTP analog (GTP γS) and with GDP, respectively, and subjected to the PAK-PBD pull-down assay. Loading endogenous Rac1 and Cdc42 with GTP γS is an excellent substrate for PAK-PBD beads and should result in a strong positive signal pull-down assay. In the other hand, loading endogenous small G-proteins with GDP will inactivate them and these will bind very poorly to affinity beads. First, $1/15^{th}$ volume of Loading Buffer was added to the cell lysate. Then, $1/100^{th}$ volume of GTPγS was immediately added and the control samples incubated with gentle rotation at RT for 15 min. After this time period, the reaction was stopped by transferring the tube to 4°C and adding 1/10th volume of STOP Buffer. These control samples were immediately used in the pull-down assay as described below.

His-tagged small G-proteins were used as controls. 20 ng of each His-tagged control protein (His-Rac1 and His-Cdc42 control proteins) were run on the gel as another positive control and will allow for a quantitation estimate of endogenous small G-protein cellular content.

### 3.10.4. Pull-down assay

Frozen cell lysates were thawed in a RT water bath and immediately removed to ice upon thawing. 9 µl of PAK-PBD beads were added to equivalent protein amounts of lysate (225 µg). The samples were then incubated at 4°C on a rotator for 1 h. After this period, the samples were centrifuged at 4000 x g at 4°C for 1 min to pellet the beads, and ≈ 90% of the supernatant was very carefully removed (90 µl were saved for Western blot analysis). Following, the beads were washed with 500 µl of Wash Buffer and completely resuspended in less than 1 min. Samples were centrifuged at 4000 x g at 4°C for 3 min to pellet the beads, and the supernatants were carefully removed. 120 µl of LB were added to each tube and the beads thoroughly resuspended. Finally, the bead samples were boiled for 2 min and frozen at -20°C for further Western blot analysis.

### 3.10.5. Western Blot assay

The bead samples, controls and supernatants were subjected to WB in a 5-20% gradient SDS-PAGE. Incubation with the antibodies was performed O/N (primary) and for 2h (secondary), with the antibodies being diluted in 1X TBS-T solution according to the manufacturer indications (Table 2). Membranes were subjected to chemiluminescence-based protein bands detection, as above. The target proteins of this study were Cdc42 and Rac1, two members of the Rho family of GTPases but, unfortunately, until now, no signal was obtained with the Rac1 antibody.

**Table 2.** Antibodies used in the Western blot, respective target proteins and specific dilutions used. The secondary antibodies are from Amersham Pharmacia.

| Target Protein/Epitope | Size (kDa) | Primary Antibody | Secondary Antibody |
|---|---|---|---|
| **Cdc42** | 20-25 | Anti-Cdc42 (Cytoskeleton) Dilution: 1:500 | Horseradish Peroxidase conjugated α-Mouse IgG Dilution: 1:5000 |
| **Rac1** | 20-25 | Anti-Rac1 (Cytoskeleton) Dilution: 1:500 | Horseradish Peroxidase conjugated α-Mouse IgG Dilution: 1:5000 |

## 3.11. Western Blot data analysis

The autoradiography films resulting from immunoblot detection were scanned in a GS-800 calibrated imaging densitometer (Bio-Rad) and protein bands quantified using the Quantity One densitometry software (Bio-Rad).

## 3.12. Data analysis

Data is expressed as mean ± SEM (standard error of the mean) of at least three independent experiments. Statistical significance analysis was conducted by the unpaired t test or by one way analysis of variance (ANOVA) followed by the Tukey-Kramer multiple comparisons test, as indicated.

# 4. Results

## 4.1. Optimization of the Scratch Wound Healing Assay

With the aim to perform Scratch Wound Healing assays with SH-SY5Y cells, it became necessary to optimize certain conditions, such as the total time of the assay, the time intervals in which the microphotographs were taken, the FBS percentage of the cell medium, the cell confluence, the transfection efficiency and the ideal objective to take the microphotographs.

Initially, the *in vivo* assay was monitored for a total time of 8h. Nonetheless, when the wound scratch was further analyzed 24h after, this proved to be interesting to include since it represented a high state of wound closure. The wound healing was first monitored every 2 hours, but this was further altered to 1h intervals to better allow single-cell tracking. With the aim to minimize cell proliferation, cell medium was initially supplemented with only 2% FBS. Unfortunately, APP overexpression is known to partially induce cell apoptosis [64,65], with this occurring at a higher extent in serum deprivation conditions, as proved to be the case. To decrease transfected cells death rate the normal percentage (10%) of FBS was maintained. Cell confluence was optimized to 95-100%, to allow the creation of wound edges without gaps, after scratching the confluent cell monolayer. The transfection efficiency was optimized for cDNAs single- and co-transfection (APP-GFP and LifeAct-RFP co-transfection). The 20x and 10x objectives were tested and the second one chosen as the ideal objective to obtain microphotographs that included both wound edges and still allow some morphology analysis indispensable for the single-cell tracking. Figure 17 shows representative SWH phase contrast and epifluorescence microphotographs at times 0 and 24h (t0 and t24).

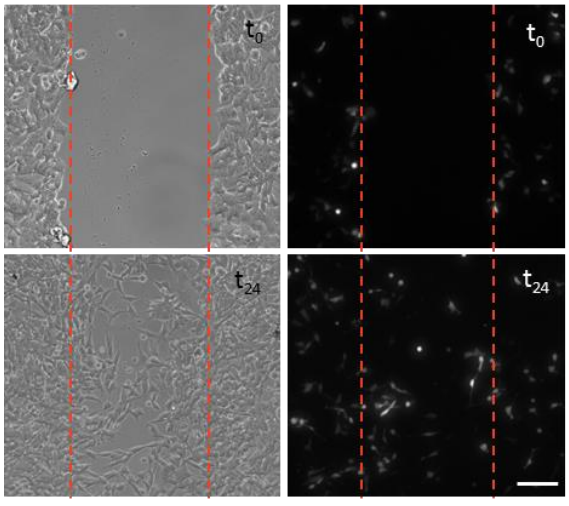


**Figure 17. Representative phase contrast and epifluorescence microphotographs of a scratch wound healing assay in SH-SY5Y cells.** Microphotographs taken immediately after the scratch was performed (t0), and 24h later (t24). Red parallel lines delimit the edges of the wound area, determined at t0. Bar, 100 µm.

## 4.2. Paracrine role of sAPP in cell migration

### 4.2.1. Migration of SH-SY5Y non-transfected cells in sAPP-enriched media

In order to study the paracrine role of sAPP in neuronal-like cells migration, SWH assays were performed in SH-SY5Y cells, and the migration of non-transfected cells (NTf) was monitored in three different experimental conditions: in the vicinity of either Wt APP-GFP or EGFP-N1 transfected cells, and in the vicinity of EGFP-N1 transfected cells upon exposure to sAPP-enriched medium (EGFP-N1+sAPP).

This conditioned medium was previously collected from an extra plate of Wt APP-GFP expressing cells transfected for 48h, with high cumulative sAPP amounts. Non-transfected cells in EGFP-N1+sAPP and in Wt APP-GFP conditions have an extra load of sAPP in their medium, when compared to cells in EGFP-N1 conditions. The sAPP levels are higher in EGFP-N1+sAPP condition, whose medium contains cumulative sAPP previously secreted for 48h by APP-GFP expressing cells, than in the Wt APP-GFP condition, where APP-GFP secreting cells gradually secrete sAPP into the medium for a 24h period (Figure 18).

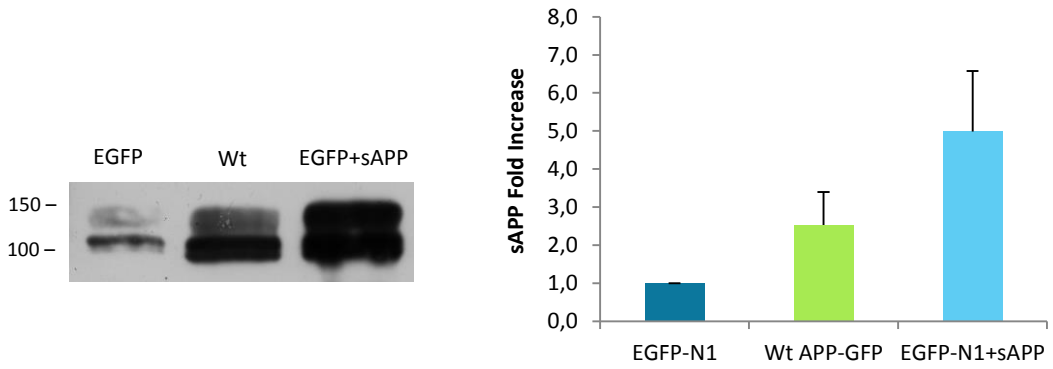


**Figure 18. Immunoblot analysis of sAPP levels secreted into the medium by SH-SY5Y cells expressing EGFP-N1 and Wt APP-GFP for 24h, compared to the sAPP levels of the EGFP-N1+sAPP condition.** Media was collected at the 24h end point of the migration assay. The sAPP-enriched medium used in the EGFP-N1+sAPP condition derived from conditioned medium of 48h APP-GFP expressing SH-SY5Y cells. sAPP was probed with the anti-APP N-terminal 22C11 antibody. Graphic: sAPP levels were quantified, corrected to Ponceau staining (loading control) and presented as fold increases over levels in EGFP-N1 condition.

The "healing" of the "wound gap" by cell migration towards the center of the gap was monitored by imaging both wound edges at every hour or 2h, during 8h (t0-t8), and in the following day (t24) as depicted in Figure 19.

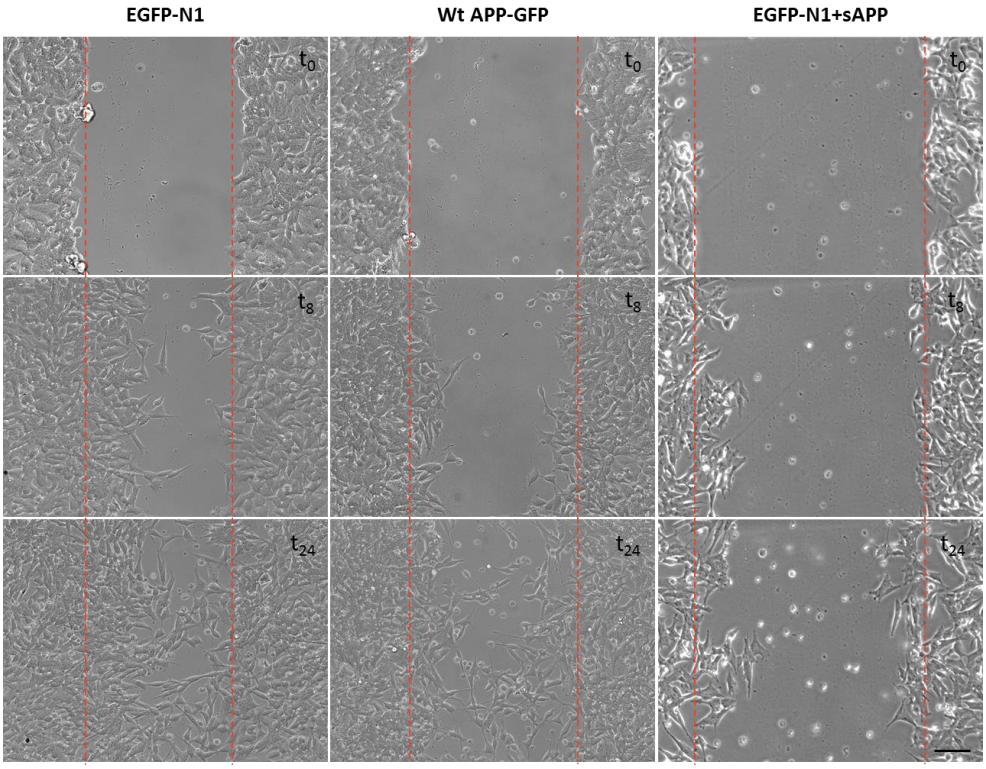


**Figure 19. Representative phase contrast microphotographs of a SWH assay in SH-SY5Y cells in EGFP-N1, Wt APPGFP and EGFP-N1+sAPP expression backgrounds.** Microphotographs taken immediately after scratching (t0), and 8h (t8) and 24h later (t24). Red parallel lines delimit the edges of the wound area, determined at t0. Bar, 100 µm.

The efficiency of SH-SY5Y cell migration was evaluated by analyzing three parameters at each time point of migration, as follows.

### a) Migrating Cells Score

The number of migrating cells of the non-transfected population observed at the wound area in each time point was scored. Figure 20A shows that in terms of absolute number, there was always more non-transfected cells at the wound in the control EGFP-N1 condition, with this number being followed closely by cells in Wt APP-GFP condition from 3h on. Unexpectedly, the number of non-transfected migrating cells in the EGFP-N1+sAPP condition was lower than in the other two conditions. This was particularly evident in the later migrating periods, at 8h of migration and upon 24h of migration, where it exhibited less than half of the number of migrating cells than in the other conditions.

In order to observe the patterns of migration recruitment and to minimize experimental errors arising from experimental variations in the number of cells initially at the wound edges, the fold increases in migrating cells were calculated for each time point, taking the number of migrating cells that have entered the wound area at t2 as 1.0 (Figure 20B).

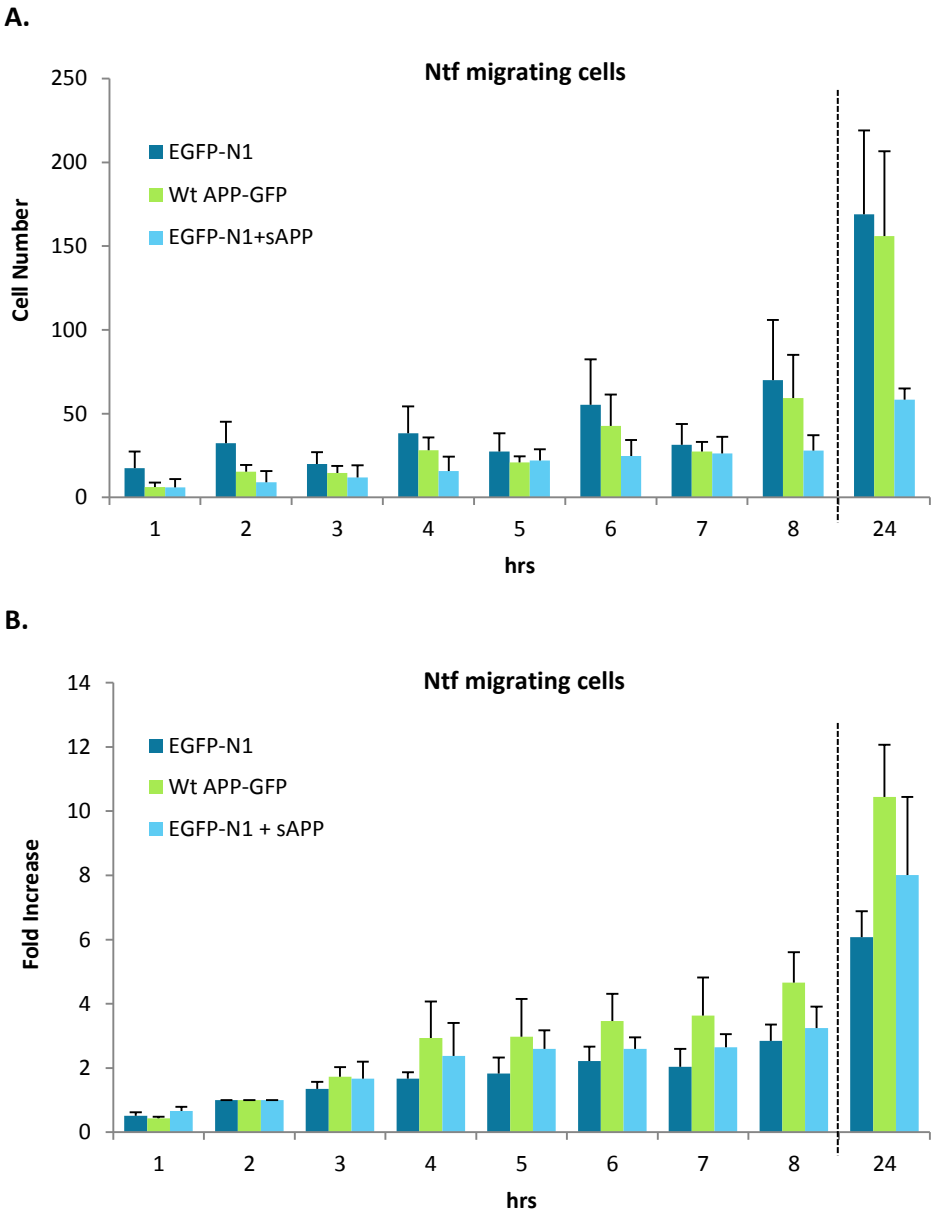


**Figure 20. Number of non-transfected migrating cells entering the wound area at the indicated time points in EGFP-N1, Wt APP-GFP, and EGFP-N1+sAPP expression backgrounds. A.** Absolute numbers. **B.** Fold increases over t2 (2h). The analysis was performed in microphotographs taken every hour until 8h of migration and upon 24h of migration. n=3-4. Ntf, non-transfected.

Figure 20B shows no variations in the fold increases of the number of migrating cells until 3h. Thereafter (from 4h on), a tendency for a higher recruitment of migrating cells in the Wt APP-GFP condition could be observed, although not yet significant. This was particularly evident in the later migrating periods (t8 and t24). Non-transfected cells in the EGFP-N1 condition presented the lower fold increases in their number overtime, and the fold increases of the EGFP-N1+sAPP condition were intermediate between EGFP-N1 and Wt APP-GFP conditions. At the t24 period, the final fold increases over t2 were of approximately 6.0, 10.5 and 8.0 for EGFP-N1, Wt APP-GFP and EGFP-N1+sAPP, respectively.

### b) Leading edge migrated distance

The leading edge migrated distance represents the average distance migrated by the leading edge of non-transfected cells with time. Ten random cell coordinates of the leading edges of each condition (EGFP-N1, Wt APP-GFP, and EGFP-N1+sAPP) and at each time point were considered for the measurements (Figure 21).

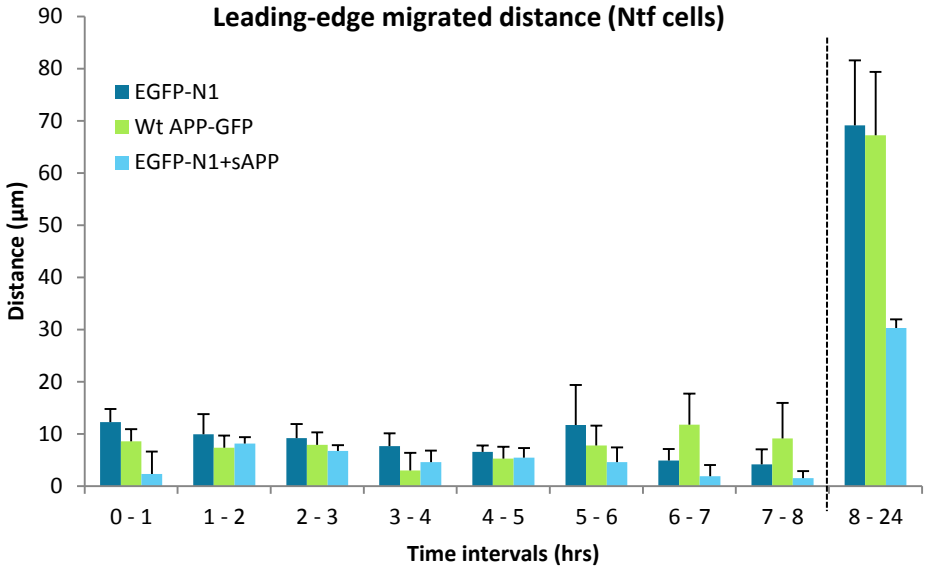


**Figure 21. Partial distances migrated hourly by non-transfected SH-SY5Y cells subjected to SWH assays in EGFP-N1, Wt APP-GFP and EGFP-N1+sAPP conditions.** From 0 to 8h, these represent the partial distances migrated at each hour by the leading edges, while the 8-24 distances represent the distance migrated by the leading edges in the last 16h interval. Ntf, non-transfected.

Results show that in the EGFP-N1 condition, with exception of the 5-6h interval, the distance migrated by the leading edge per hour slightly decreased overtime. For non-transfected cells in the Wt APP-GFP condition, a similar decreased occurred but only until 3-4h, increasing thereafter. Further, until 6h, cells in EGFP-N1 condition presented higher partial migrated distances compared to Wt APP-GFP; at t6 a switch occurred, and Wt APP-GFP migrated distances surpassed the EGFP-N1 ones. Relatively to the EGFP-N1+sAPP condition, migrated distances also generally decreased with time, from 1 to 8h, as for EGFP-N1. Further, these were the cells that always migrated lower distances, what was particularly evident in the later periods of migration. At the 24h period cells in EGFP-N1+sAPP have migrated less than half the distances migrated by non-transfected cells in the other two conditions.

### c) Leading edge migration velocity

Based on the total migration distance measured at the 24h period, the average velocity (µm/h) of the leading edge migration was determined for each condition (Figure 22).

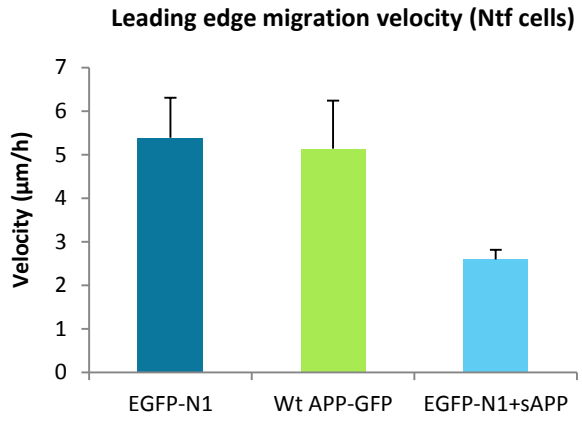


**Figure 22. Migration velocity of the non-transfected cells leading edge in EGFP-N1 and Wt APP-GFP conditions.** Velocity was calculated as the ratio between total leading edge migrated distance and the 24h period of migration. Ntf, non-transfected.

There were no visible differences between the average migration velocities of non-transfected cells in EGFP-N1 (5.38±0.92 µm/h) and Wt APP-GFP (5.14±1.10 µm/h) conditions, with cells migrating similar cumulative distances after 24h: 129.2±22.1 µm (EGFP-N1) and 123.3±26.5 µm (Wt APP-GFP). For cells in EGFP-N1+sAPP condition, however, cells migrated much less (62.3±5.3 µm), what is reflected in its lower average velocity (2.60±0.22 µm/h).

In order to address potential differences in the migration velocities in the first third of the migration assay (first 8h of the 24h period), these were calculate in an alternative manner, being derived from the graphic representation of the cumulative migrated distances with time of migration, where velocity is the slope of each linear regression (Figure 23).

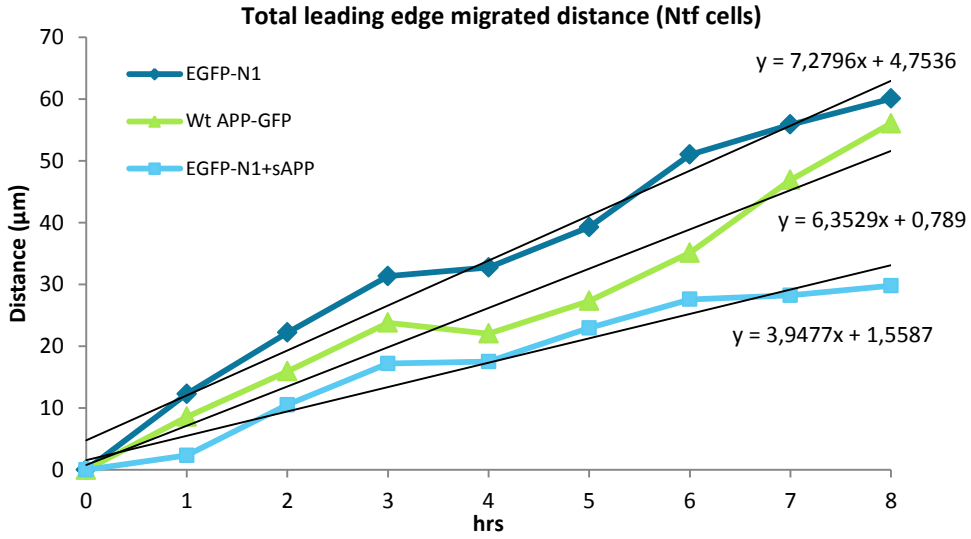


**Figure 23. Graphic representation of the variation of the total (cumulative) distance migrated by the leading edges of non-transfected cells with migration time, in EGFP-N1, Wt APP-GFP, and EGFP-N1+sAPP conditions**. The slopes of the respective linear regressions, showed in the graph, represent the average velocity of cells migrating for 8h. Ntf, non-transfected.

Leading edge migration showed similar migrating profiles in all the conditions, but performed these with different velocities, that decrease in the following order: EGFP-N1 (7.3 µm/h) > Wt APP-GFP (6.4 µm/h) > EGFP-N1+sAPP (3.9 µm/h). At the 8h time point, the leading edges of non-transfected cells in EGFP-N1 and Wt APP-GFP conditions migrated similar cumulative distances: 60.1±13.5 and 56.1±14.7 µm, respectively, while the EGFP-N1+sAPP leading edge migrated approximately half: 29.8±7.4 µm.

## 4.3. The role of full-length APP in cell migration

### 4.3.1. Single-cell tracking of APP-GFP transfected cells

The low Wt APP-GFP transfection rate together with its induced cell dead over time led to the absence of a clear leading edge of transfected cells. Therefore, in order to study the role of full-length APP (flAPP) in cell migration, single-cell tracking analysis of transfected cells migration was performed.

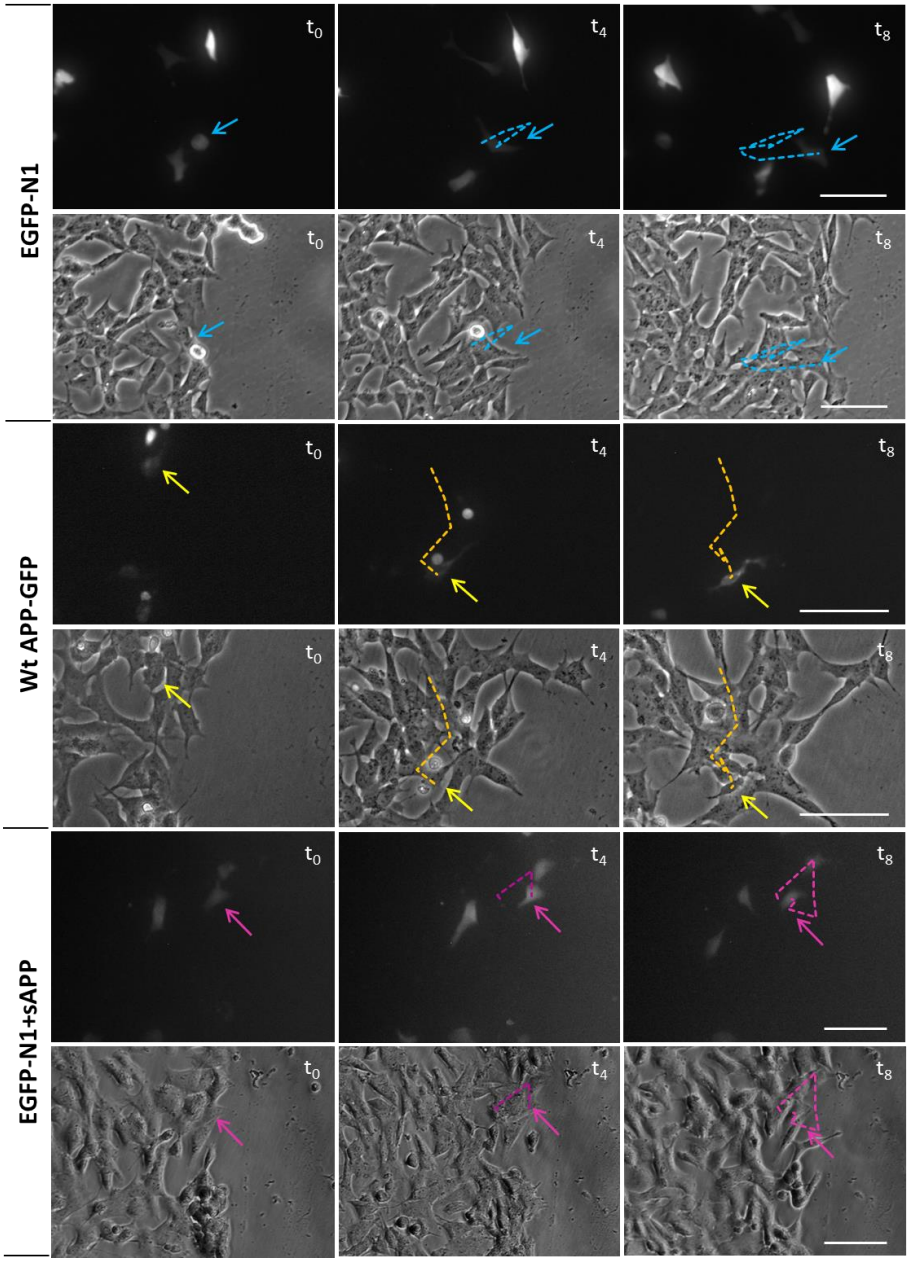


**Figure 24. Representation of single-cell track of migratory GFP expressing cells in EGFP-N1, Wt APP-GFP and EGFP-N1+sAPP conditions.** Epifluorescence and phase contrast microphotographs taken at t0, t4 and t8 periods of migration, with migratory tracks for each cell represented in different colors (arrows indicate cells being tracked). Migratory tracks were obtained based on hourly cells coordinates determined by the ImageJ software based on visual tracking. Bar, 100 µm.

Analysis of the migration assay microphotographs was different than the one used to assess the non-transfected cells migration, and as follows.

#### 4.3.1.1. Cell coordination

Cell coordination in migration is described as the collective migration of cells as part of a group in a highly coordinated manner, with individual cells organized in a coherent multicellular motile structure [51,66].

Various groups of transfected cells, either directly touching or in the vicinity were monitored for their migratory tracks. Based on the 2D coordinates of each transfected cell, determined as indicated in Figure 25D, a single-cell track graph of migration was obtained for various transfected cells in EGFP-N1, Wt APP-GFP and EGFP-N1+sAPP conditions, from which it was possible to visually analyze cell coordination on collective migration (Figure 25A-C).

From the Figure 25A graph, one can observe that EGFP-N1 expressing cells evidenced very different migratory tracks among the various cells, with these presenting completely unrelated patterns of migration. In opposition, Wt APP-GFP expressing cells exhibited coordinated migratory tracks within neighboring cells, with tracks varying similarly at each time point, creating very similar migratory patterns. EGFP-N1 expressing cells exposed to sAPP-enriched medium (EGFP-N1+sAPP) continued to evidence the observed EGFP-N1 unrelated tracks (unrelated to neighbor cells tracks), suggesting that cellular flAPP, and not medium sAPP, has a role in coordinated cell migration. These are promising results, but more cells are necessary to be analyzed to confirm the results.

Further, Wt APP-GFP expressing cells exhibited migration patterns with an apparent persistence in direction, what led us to also evaluate this parameter (in *c) Directional persistence*).

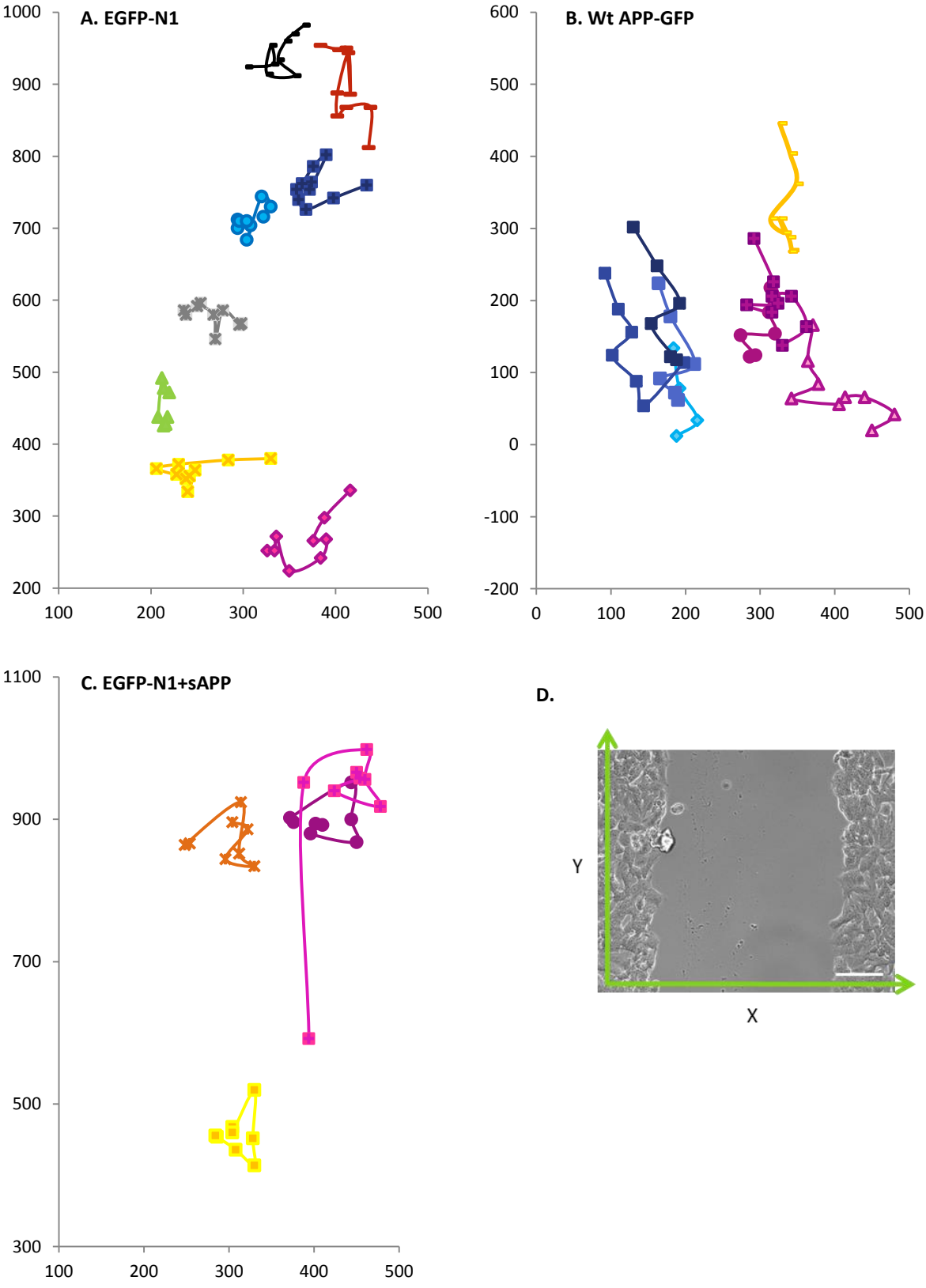


**Figure 25. Single-cell track of migratory GFP expressing cells in EGFP-N1 (A), Wt APP-GFP (B) and EGFP-N1+sAPP (C) conditions. A-C.** Migratory tracks of neighbor single cells are presented in different colors, and were obtained based on hourly cells coordinates determined by the ImageJ software based on visual tracking. **D.** Schematic representation of the axes considered for determining each migrating cell coordinates relatively to the wound edges.

#### 4.3.1.2. Migration Distance and Velocity

Based on the coordinates of each transfected cell in the various conditions (EGFP-N1, Wt APP-GFP and EGFP-N1+sAPP), the distance and velocity of these were also determined (Figure 26).

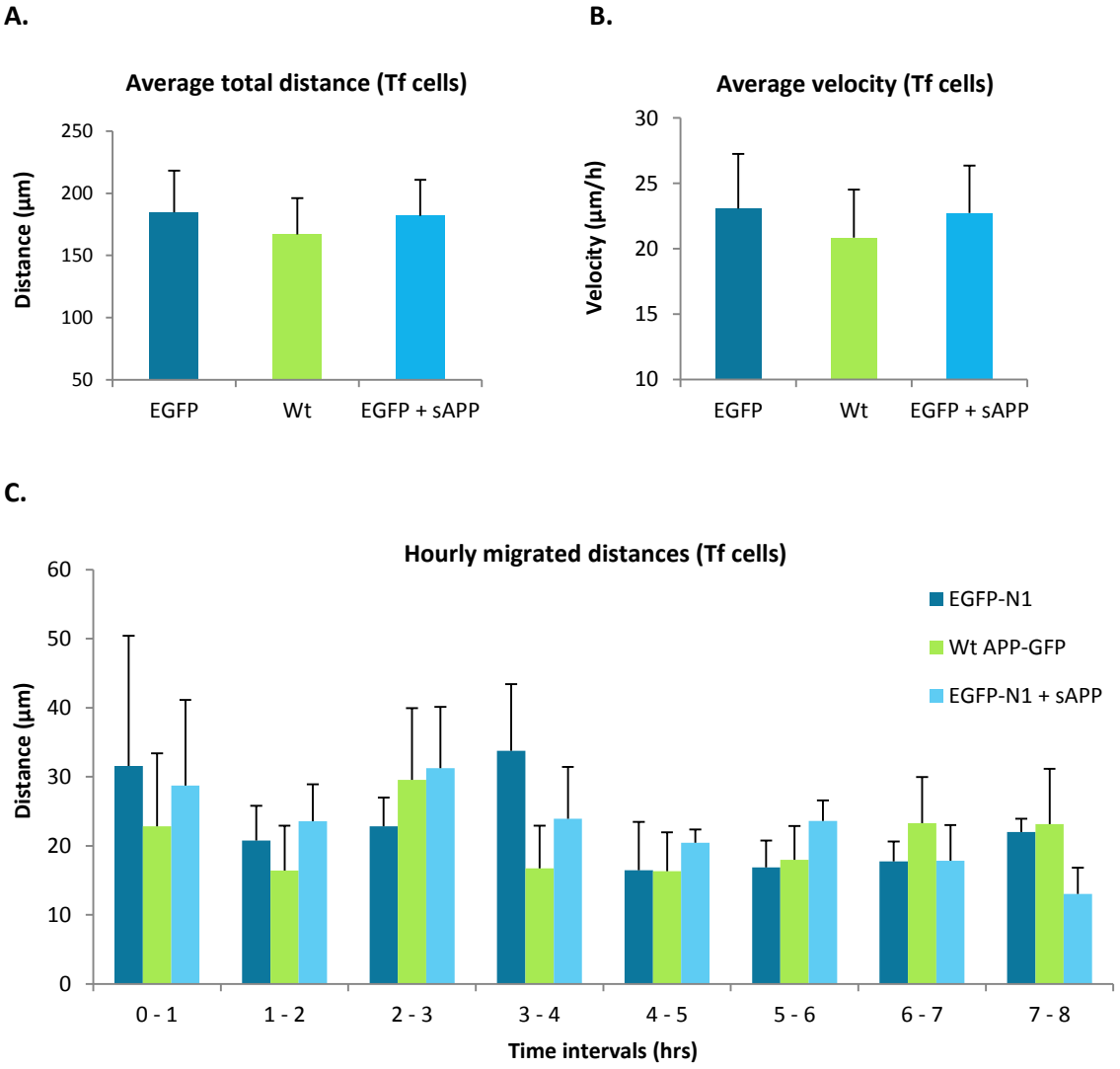


**Figure 26. Calculated total distance (A), average velocity (B), and partial hourly distances (C) of migratory GFP expressing cells in EGFP-N1, Wt APP-GFP and EGFP-N1+sAPP conditions.** The analyses were based on single fluorescent SH-SY5Y cell tracks in epifluorescence microphotographs of n=4 SWH assays, in a total of 25 (EGFP-N1), 16 (Wt APP-GFP), and 27 (EGFP-N1+sAPP). Tf, transfected.

The graphic analyses of total migrated distance (A) and average migration velocity (B) of transfected cells revealed no significant difference between the three conditions. When analyzing the partial distances hourly migrated by each cell, one can see a wave behavior with successive increases and decreases in the migrated distances. This was observed for all the conditions tested, although not totally synchronized. At t8, the cumulative distances migrated

by transfected cells were: 184.6±33.6 µm, 166.8±29.5 µm and 181.8±29.1 µm for EGFP-N1, Wt APP-GFP and EGFP-N1+sAPP, respectively. An apparent decrease in the cumulative distance was observed for Wt APP-GFP transfected cells, but more cells need to be analyzed to verify if there is a significant flAPP effect in the migration pattern and cumulative length.

To analyze if APP S655 phosphorylation could influence flAPP effects in migration, dephosphomimicking (S655A) and phosphomimicking (S655E) APP-GFP mutants were transfected in SH-SY5Y cells and their migration parameters evaluated (Figure 27).

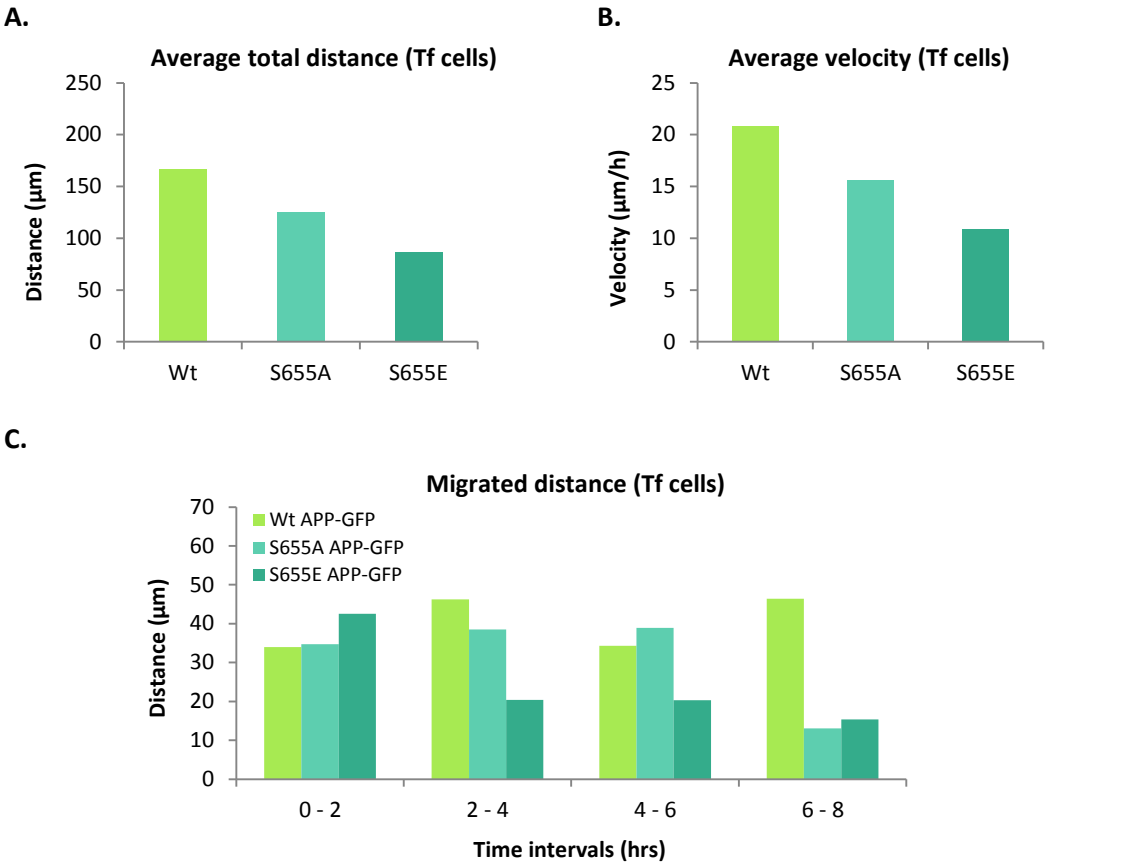


**Figure 27. Calculated total distance (A), average velocity (B), and partial hourly distances (C) of migratory Wt, S655A and S655E APP-GFP expressing cells.** The analyses were based on single fluorescent SH-SY5Y cell tracks in epifluorescence microphotographs of n=2 SWH 8h assays for the S655 mutants, in a total of 16 (Wt APP-GFP), 13 (S655A APP-GFP) and 10 (S655E APP-GFP) cells. Tf, transfected.

These preliminary results suggest that, in general, S655E APP-GFP expressing cells migrate lower distances than S655A APP-GFP cells, with this slow down occurring from t2 onwards. S655A behaves more similarly to Wt APP-GFP, although from 6-8h S655A APP-GFP expressing cells have slowed down unto S655E values (Figure 27C). Nonetheless, this experiment needs to be repeated to confirm the observed behaviors.

#### 4.3.1.3. Directional persistence ("out-of-track percentage")

The directional persistence was also analyzed and quantified by a method named "out-of-track" percentage. In this method, the linear distance between the end and initial points of migration was calculated as well as the totally migrated distance over time (sum of hourly migrated distances). The numerical difference between these, presented as percentage of the linear migration, reflects deviations to the linear track, a value inversely proportional to the migration efficiency. Results are presented in Figure 28.

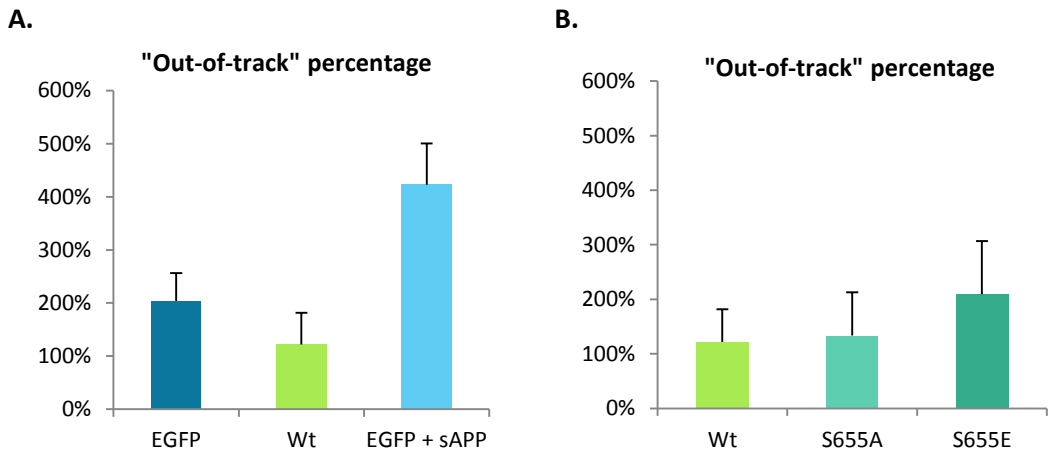


**Figure 28. Calculated "out of track" percentages for migratory. A. EGFP-N1, Wt APP-GFP and EGFP-N1+sAPP, and B. Wt, S655A and S655E APP-GFP transfected cells.** Data was calculated from single cell tracks of GFP fluorescent cells determined as in Figure 25. n=2-4 SWH assays.

The "out-of-track" percentages evidenced that Wt APP-GFP cells migrated in a more directionally persistent way, with fewer detours of the track, reflected in their best "out-of-track" percentage (122%). In contrast, the EGFP-N1 cells almost doubled this deviation ("out-of-track" of 204%), while EGFP-N1+sAPP cells presented an "out-of-track" percentage 3.5 times higher (423%) (Figure 28A). Regarding S655 phosphorylation, again the S655A mutant behaved as the Wt APP-GFP, with an "out-of-track" of 133%, while the S655E mutant behaved as the vector EGFP-N1 cells, with an "out-of-track" of 210% (Figure 28B).

Altogether, results of the SWH migratory parameters of SH-SY5Y transfected cells lead us to propose a S655-dephosphorylation dependent role for flAPP in the coordination and directional persistence of cells migration. These parameters have been reported to be related to the actin cytoskeleton, with this being further addressed.

## 4.4. Actin cytoskeleton dynamics of migrating cells

### 4.4.1. F-actin migratory phenotype in SH-SY5Y cells

After a SWH assay of 8 hours of EGFP-N1 and Wt APP-GFP SH-SY5Y cells, performed on coverslips, cells were fixed and the red fluorescent-labeled phalloidin was used to visualize F-actin. The percentage of cells presenting a typical F-actin migratory phenotype was scored for both EGFP-N1 and Wt APP-GFP conditions. Cells were considered with the typical F-actin migratory phenotype when presenting a clear polarization, highly asymmetric morphology and visible lamellipodia (Figure 29B). Since the analysis occurred post cells fixation, it comprised both edges of the entire wound, enhancing the number of transfected cells analyzed.

**A.**

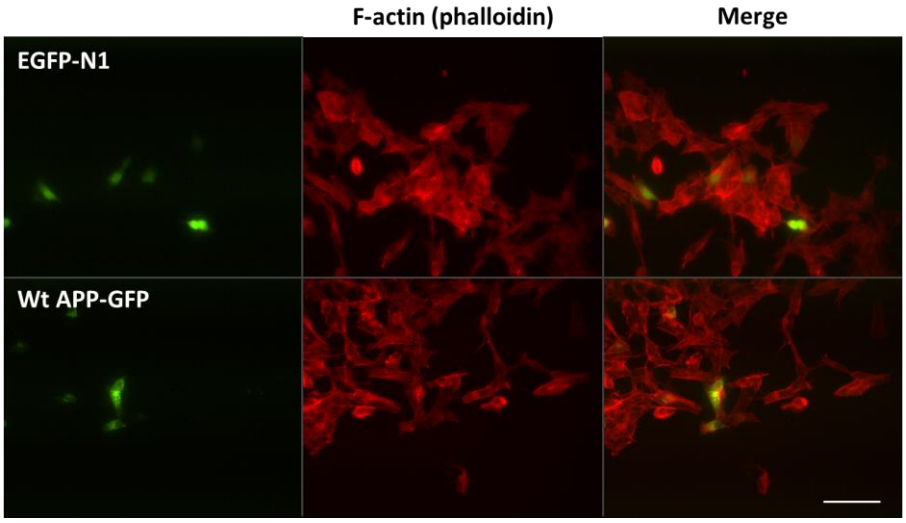


**B.**

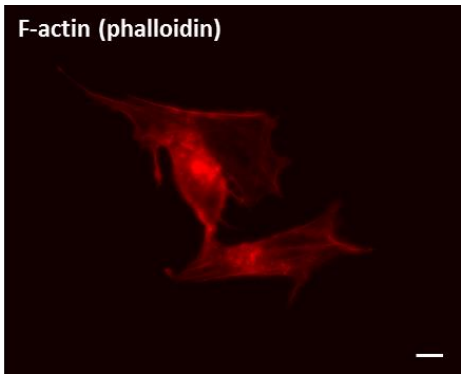


**C.**

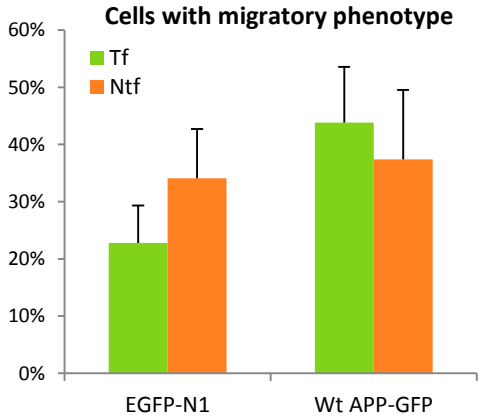


**Figure 29. SH-SY5Y cells presenting a migratory phenotype. A.** Epifluorescence microphotographs of representative EGFP-N1 and Wt APP-GFP expressing cells with migratory phenotypes. **B.** Representative non-transfected cells bearing the F-actin (red labeled phalloidin) migratory phenotype. **C**. Graphic analysis of the percentages of transfected (Tf) and non-transfected (Ntf) cells with migratory phenotypes in each condition tested. n=3, 20-35 APP-GFP transfected and 100 non-transfected cells per assay. Bars indicate 100 µm and 10 µm, in A. and B., respectively.

Results showed that the transfection *per se* difficults the acquisition of a migratory phenotype, with lesser cells presenting a clear migratory phenotype when transfected with EGFP-N1. Furthermore, Wt APP-GFP transfection enhanced the acquisition of a clear migratory phenotype (43.2%) relatively to EGFP-N1 transfection (24.3%), almost doubling it. Nonetheless, the number of independent experiments needs to be further increased to confirm significance. In parallel, similar analysis will be performed for the S655 phosphomutants. Noteworthy, although the assay is based on human discrimination, the similarity of the values obtained for non-transfected cells in between conditions strengthens it as an unbiased analysis.

These results suggest a role for APP in promoting cellular mechanism underlying the acquisition of a clear migratory phenotype. This may occur by APP-induced regulation of the actin polymerization dynamics, what was further addressed.

### 4.4.2. Characterization of APP effects on HeLa cells migration

With the aim to perform live cell imaging of fluorescing cells co-transfected with APP-GFP and a live F-actin red fluorescent marker (LifeAct-RFP), HeLa cells were used due to their easiness to co-transfect and human origin. Before proceeding using HeLa cells, their migration efficiency was tested and compared to SH-SY5Y cells efficiency. For this purpose, 8h SWH assays were performed in parallel, in SH-SY5Y and HeLa cells, for both EGFP-N1 and Wt APP-GFP conditions. At t0 and t8, three different wound areas of each condition were imaged by epifluorescence and phase contrast microscopy. The number of transfected and non-transfected cells observed at t8 in the wound area was determined, and the wound free area measured and compared to t0. The migration efficiency was therefore addressed by two different forms, by the number of cells that entered in the wound area and the decrease in the free area of the wound from t0 to t8. Results obtained for HeLa cells were similar to the ones of the SH-SY5Y cells (data not shown).

#### 4.4.2.1. HeLa cells: transfected cells gain in the wound area

The effect of Wt APP-GFP transfection in HeLa cells migration was assessed in detail at the 24h time point. With this aim, SWH assays for both EGFP-N1 and Wt APP-GFP conditions were performed for 24h on coverslips, and the entire wound area (all the wound and leading edges) analyzed post cells fixation (Figure 30A). The number of total and transfected cells that entered in the wound area was scored, determining the percentage of transfected cells in the wound area (Figure 30B). As EGFP-N1 has higher transfection efficiency than Wt APP-GFP, 3-6 images of outside the wound areas, per well, were also similarly analyzed for comparison.

**A.**

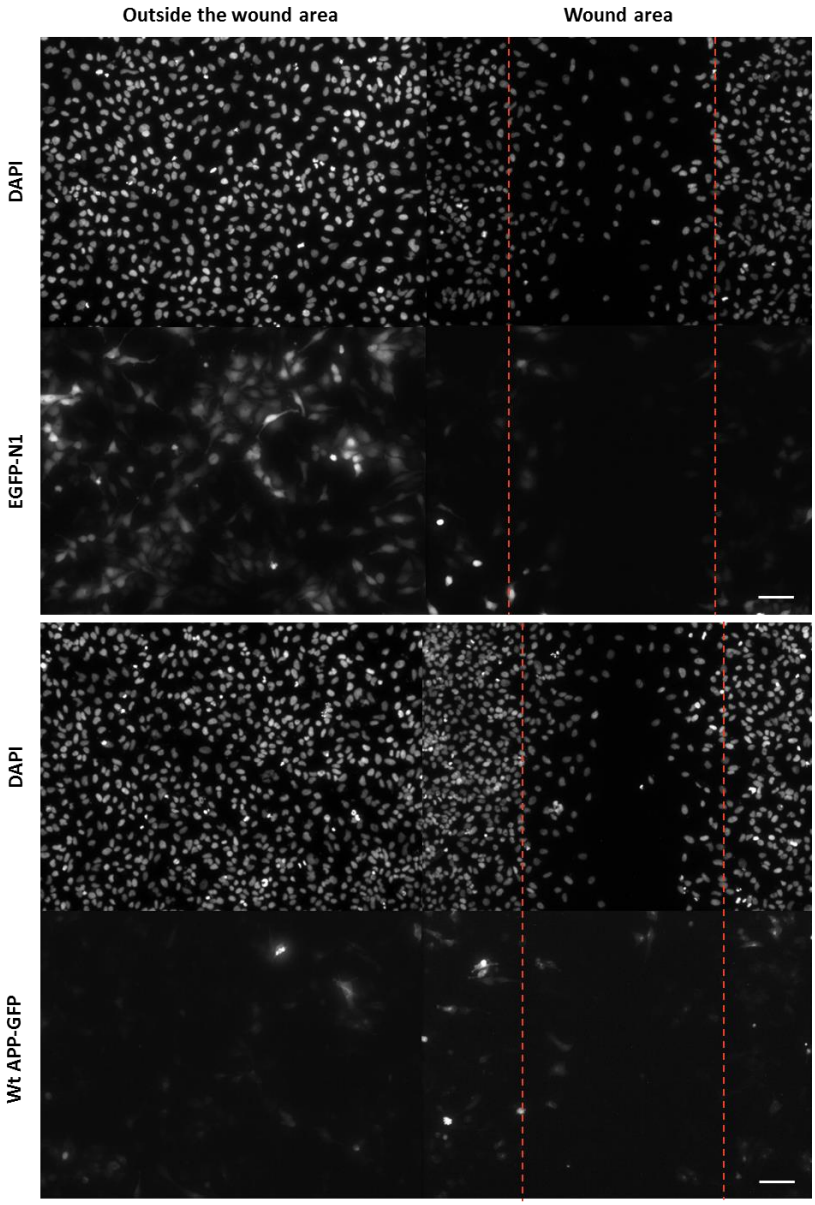


**B.**

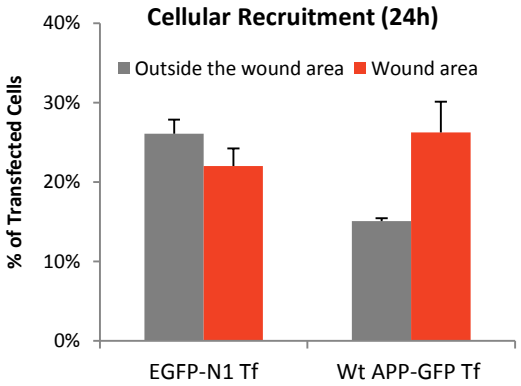


**Figure 30. SWH assays performed in Wt APP-GFP and EGFP-N1 expressing HeLa cells migrating for 24h. A.** Representative epifluorescence microphotographs of the wound area and an area outside this. **B.** Respective quantitative analysis of the gain in transfected (Tf) cells in the wound area. Bar, 100 µm.

In what concerns to the EGFP-N1 condition, there were no significant differences between the rate of transfected cells inside and outside the wound area. Indeed, no particular recruitment of EGFP transfected cells into the wound was visualized and even a small decrease seemed to occur (Figure 30). Regarding the Wt APP-GFP cells, there was a notorious gain in transfected cells in the wound area, relatively to outside non-wounded areas, indicating that Wt APP-GFP cells are more recruited through migration to the wound area than non-transfected cells.

#### 4.4.2.2. β1-integrin: EGFP-N1 vs. Wt APP-GFP wound cells

After a 24h SWH assay of Wt APP-GFP HeLa cells, performed on coverslips, cells were fixed and endogenous β1-integrin proteins were red fluorescent-labeled by ICC. The fluorescence images of the entire wound area were analyzed for β1-integrin intensity of Wt APP-GFP and EGFP-N1 transfected, and non-transfected cells (these in both conditions) at the leading edge and wound area (Figure 31).

**A.**

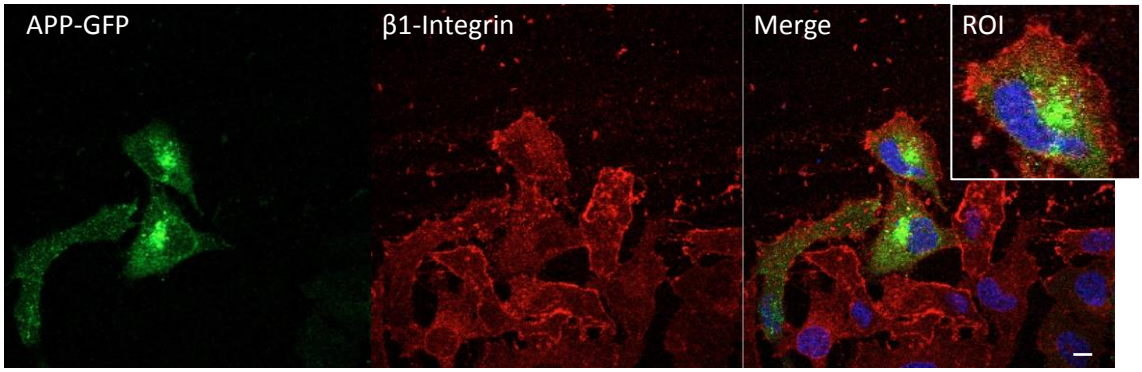


**B.**

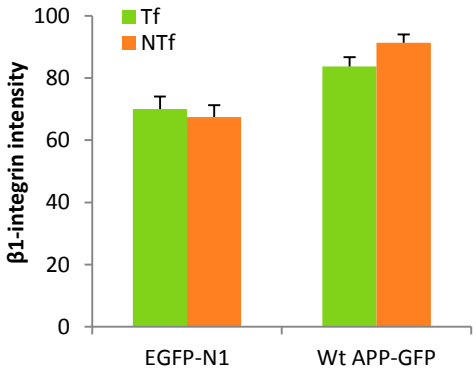


**Figure 31. β1-integrin intensity in Wt APP-GFP and EGFP-N1 HeLa cells of a scratch wound area (24h). A.** Representative confocal microphotographs of Wt APP-GFP migrating HeLa cells and neighbor cells, co-stained for beta1-integrin ROI, region of interest. **B.** Quantitative analysis of β1-integrin intensities in Wt APP-GFP versus EGFP-N1 HeLa migrating cells (data were cell area corrected). β1-integrin intensities in migrating non-transfected cells were also analyzed. Tf, transfected. Ntf, non-transfected. Bar, 10 µm.

In both the EGFP-N1 and the Wt APP-GFP conditions, no differences were detected between the β1-integrin integrated intensities in transfected and non-transfected cells (Figure 31B). Importantly, an increase in the integrated intensities of both types of cells in the Wt APP-GFP conditions seemed to occur, with APP-GFP expression potentially increasing β1-integrin intensity. This result was not statistically different and may result from technical variations in the ICC assay. Nonetheless, this increase was noticeable in various non-transfected cells in direct contact with APP-GFP expressing cells, and β1-integrin patches could be observed in transfected and non-transfected cells in Wt APP-GFP conditions, as denoted in the epifluorescence microphotographs (Figure 31A, ROI). Hence, further confirmation of this potential effect needs to arrive from more ICC experiments and, e.g., WB assays.

#### 4.4.2.3. Wounds effects on APP and sAPP levels

In order to evaluate the APP levels in migrating and non-migrating cells, Wt APP-GFP expressing HeLa cells were multiple wounded and left to migrate for 24h, after what cells and media were collected and subjected to WB analysis, together with non-wounded cell monolayers (Figure 32).

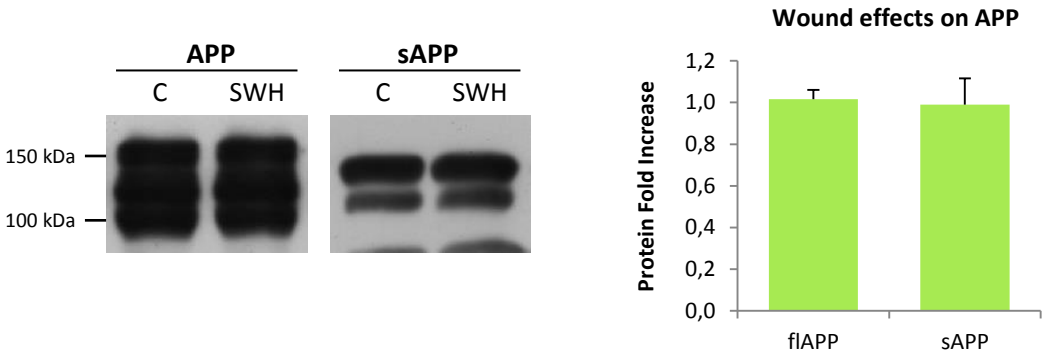


**Figure 32. Immunoblot analysis of cellular full-length APP (flAPP) and medium sAPP levels in HeLa migrating cells upon 24h of migration.** flAPP and sAPP were probed with the anti-APP N-terminus 22C11 antibody. Graphic: protein levels were quantified, corrected to Ponceau staining (loading control) and presented as fold increases of levels in migrating cells (SWH) over non-migrating controls (C).

Results showed no significant differences between the APP levels of wounded and non-wounded cells. Moreover, it was not verified any alteration in the rate of APP cleavage to sAPP.

### 4.4.3. Live Cell imaging of LifeAct-RFP and Wt APP-GFP co-transfected HeLa cells

In order to evaluate the effects of APP in F-actin dynamics, HeLa cells were co-transfected with Wt APP-GFP and LifeAct-RFP cDNAs, and subjected to a SWH assay. LifeAct-RFP is a red fluorescent small F-actin binder that allows for *in vivo* monitoring of F-actin dynamics. In the first two pilot SWH assays of HeLa cells grown on a culture dish appropriate for live imaging, we surprisingly noted a difficulty of cells to migrate. To solve this problem, we simultaneously performed 24h SWH assays of HeLa cells grown on plates with or without poly-L-ornithine coating. Since cells were much more capable to migrate when using poly-L-ornithine coating, this was used in live cell assays.

#### 4.4.3.1. F-actin phenotype of Wt APP-GFP HeLa cells

In order to evaluate the F-actin phenotype of Wt APP-GFP HeLa migrating cells at the wound, Wt APP-GFP and LifeAct-RFP co-transfected HeLa cells were left to migrate for 24h in a SWH assay. Cells were imaged by confocal live-cell microscopy afterwards (Figure 33).

Again, a high number of migrating cells presented the typical migratory phenotype, with this being especially evident for Wt APP-GFP expressing cells (Figure 33A). Noteworthy, various Wt APP-GFP expressing cells carried a higher number of and/or longer filopodia, with these F-actin processes also presenting APP-GFP fluorescence (Figure 33B). Of note, once the formation of filopodia is regulated by the Rho family member Cdc42, we further investigated a potential role of APP on the activation of Cdc42 (in Section 4.4.4.).

Further, Wt APP-GFP and F-actin co-localized in intracellular round structures, as depicted in ROI1 and ROI2 in Figure 33C.

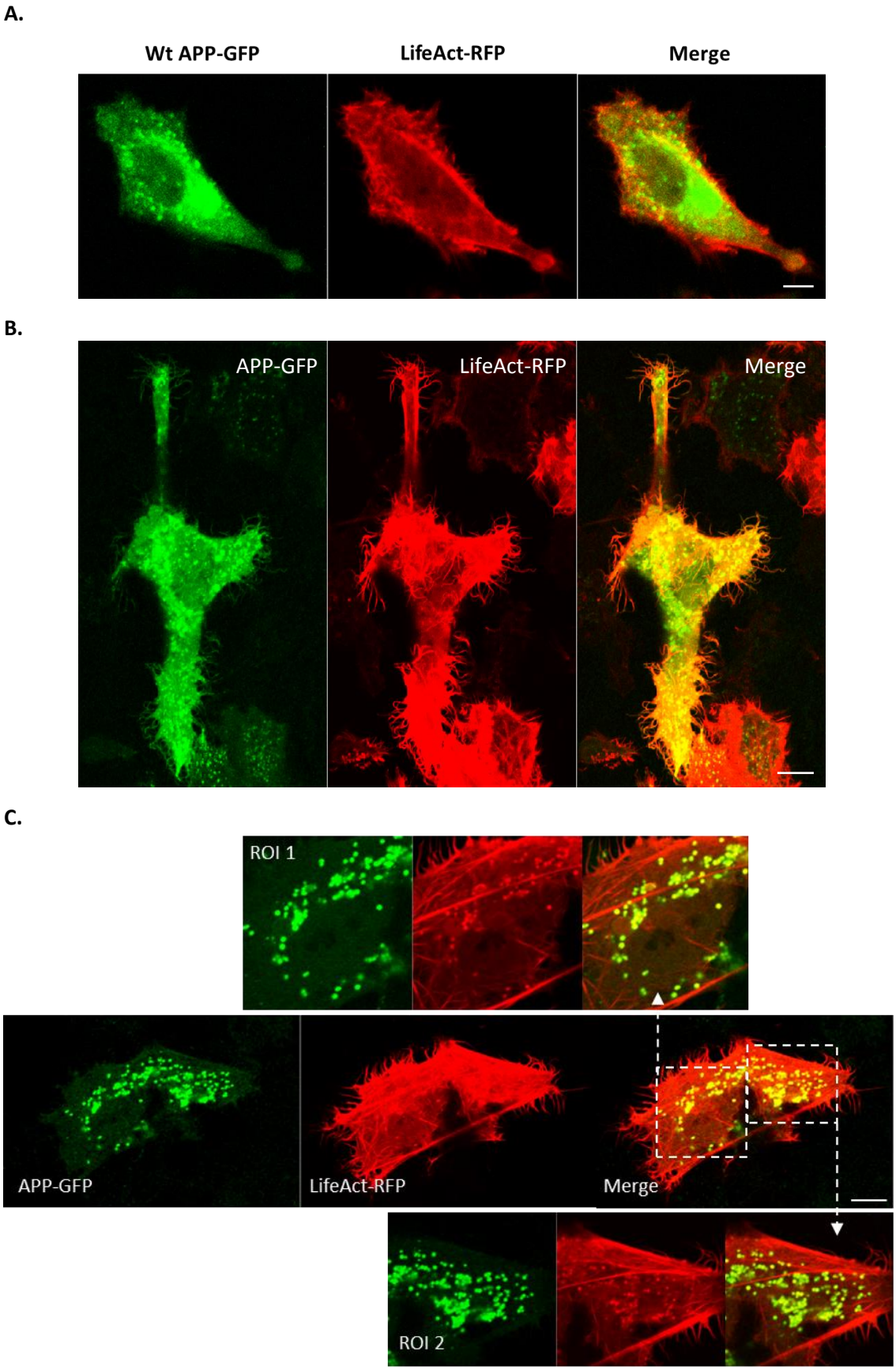


**Figure 33. Confocal microphotograph of HeLa cells co-expressing LifeAct-RFP and Wt APP-GFP.** A high number of cells in the wound of a SWH 20h assay presented the typical migratory phenotype (A). **B.** and **C.**, Cells outside the wound area. Co-transfected cells presented a high number of filipodia, where APP-GFP and Lifeact-RFP co-localized (B), as in rounded intracellular structures (C, ROI1 and 2). Scale bar,10 μm.

#### 4.4.3.2. FRAP assays: APP effects on F-actin dynamics

In order to study the F-actin cytoskeleton dynamics of Wt APP-GFP migrating cells, HeLa cells co-expressing either EGFP-N1 and LifeAct-RFP or Wt APP-GFP and LifeAct-RFP were left to migrate for 20h after a SWH Assay, and subjected to FRAP experiments in live-cell microscopy. At least four regions of interest (ROIs) were defined per cell: the cell front (lamellipodia enriched), the cell rear (focal adhesion enriched), a non-bleached area (negative control) and a background area. The F-actin red fluorescence was photobleached at the front and rear of migrating cells, and a set of images of the ROIs acquired during the pre-bleach, photobleach and postbleach phases gave rise to FRAP curves with the fluorescence intensity time courses. Figure 34A illustrates one set of images acquired at the different phases of the FRAP experiment, while Figure 34B depicts FRAP recovery curves obtained for each condition.

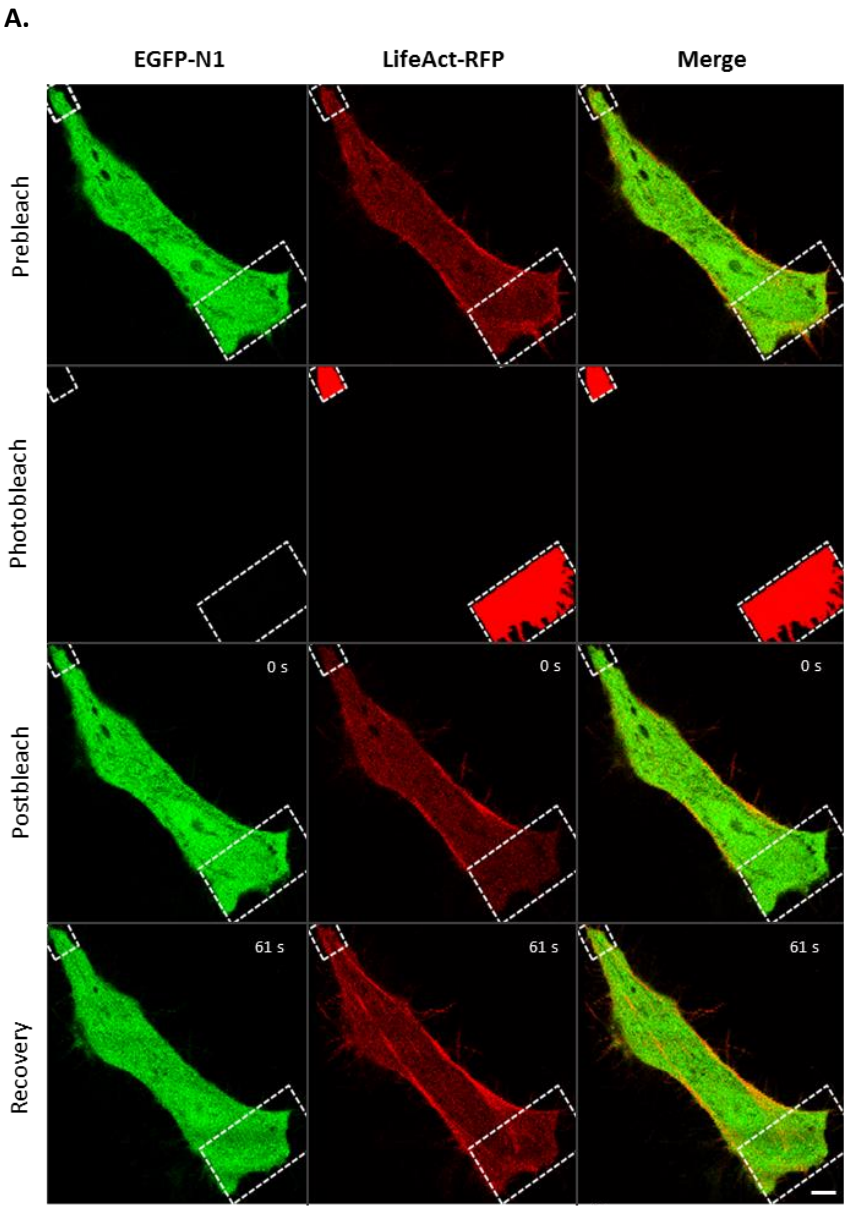

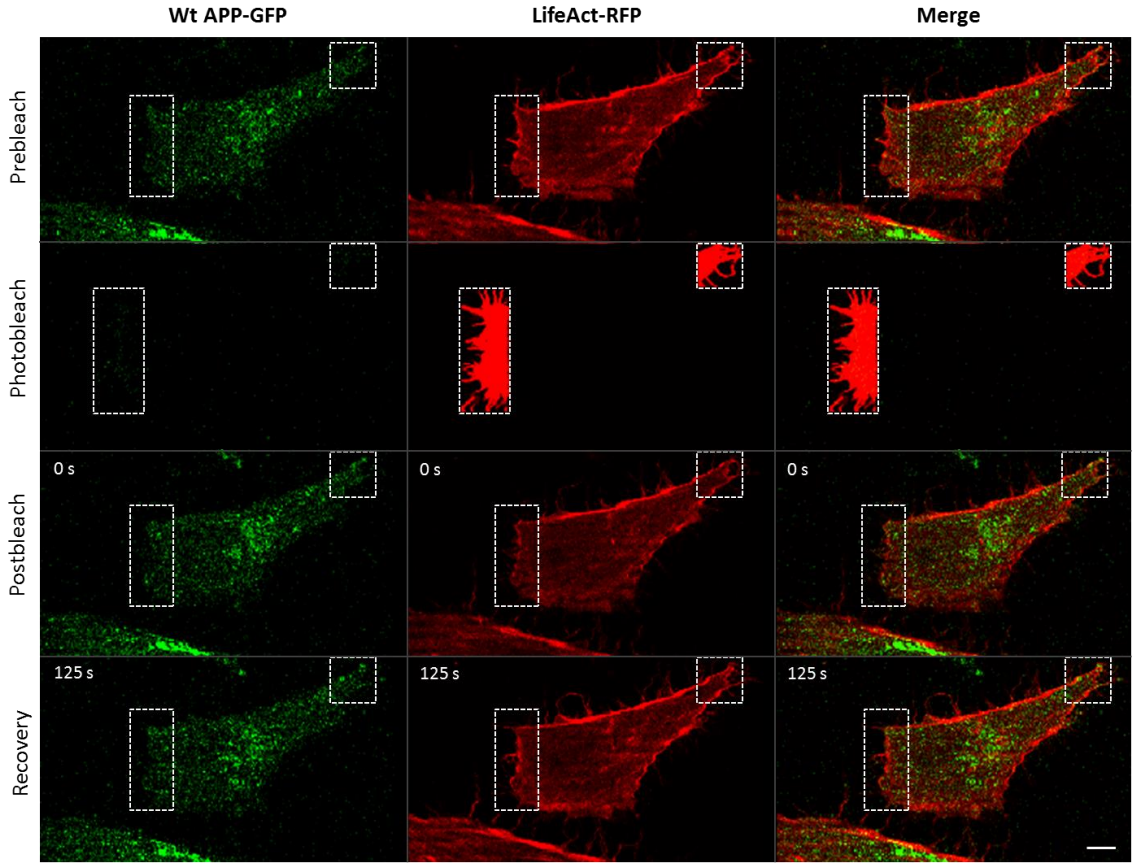


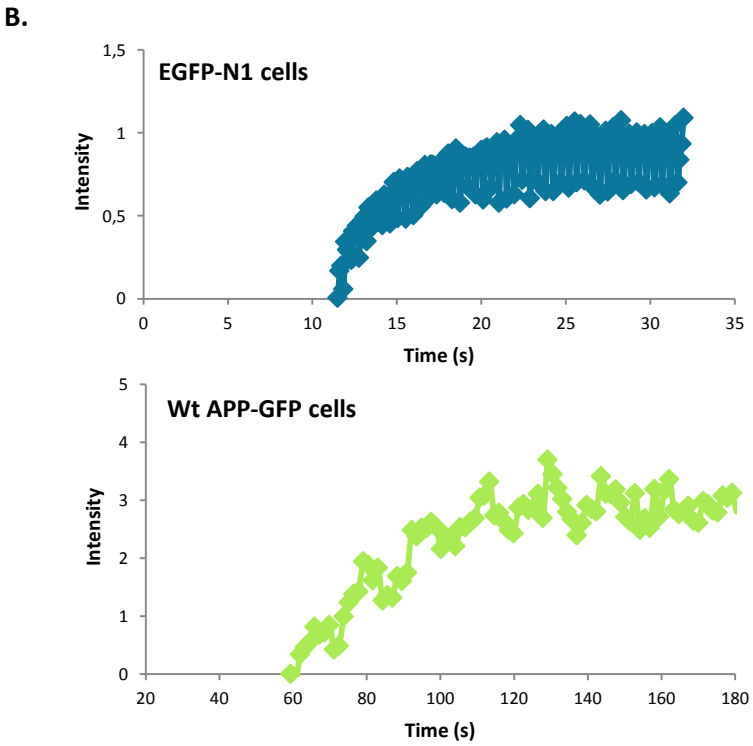


**Figure 34. F-actin treadmilling in Wt APP-GFP expressing cells, monitored by FRAP analysis. A.** Representative microphotographs of F-actin intensities in the prebleach, bleach and two postbleach phases (immediately after bleaching and at the recovery plateau) of a FRAP analyses of HeLa cells co-transfected for 20h with LifeAct-RFP and Wt APP-GFP or the control EGFP-N1. ROIs depict the cell front and rear. **B.** Respective FRAP curves are obtained by the imaging software (as in Materials and Methods). Bar, 10 µm.

Based on FRAP data, the parameters Percentage of Recovery and the Halftime of Recovery for F-actin were determined for each condition (Figure 35).

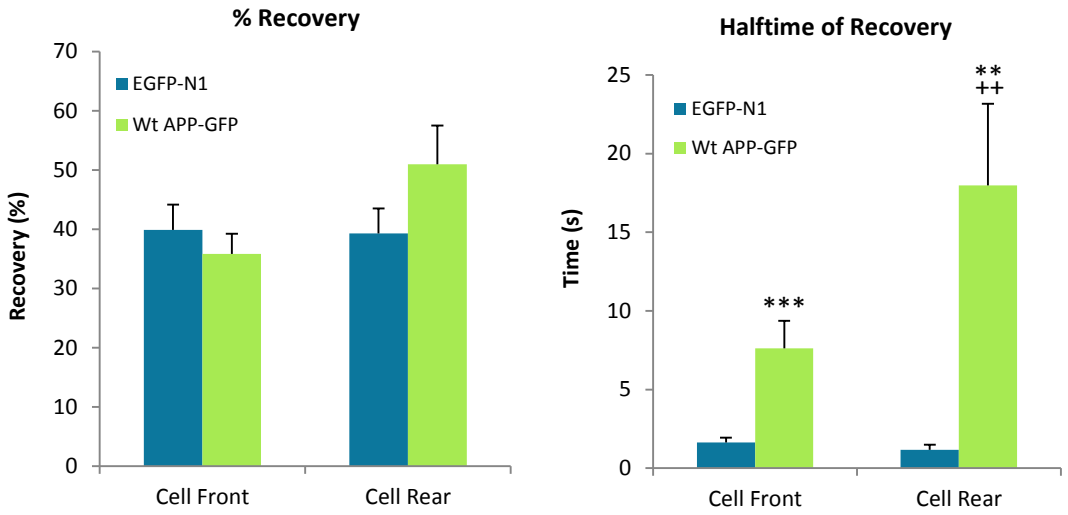


**Figure 35. Percentage and Halftime of recovery of F-actin intensities in FRAP analyses of Wt APP-GFP expressing cells.** HeLa cells were co-transfected for 20h with LifeAct-RFP and Wt APP-GFP or the control EGFP-N1 cDNAs, Upon F-actin bleaching at the cell front and rear, the intensities of the bleached area were monitored and the indicated parameters calculated. 13 EGFP1-N1 and 10 Wt APP-GFP cells were analyzed, in 42 and 28 total ROIs, respectively. The differences between the cell front or cell rear of EGFP-N1 and Wt APP-GFP cells were considered significant when using the unpaired t test, **p<0.01; ***p<0.001. The differences between the Wt APP-GFP cells front and rear were also significant when using ANOVA followed by the Tukey-Kramer test, $^{++}$p<0.01.

In what concerns the percentage of recovery, there were no noticeable differences between the cell front of Wt APP-GFP and EGFP-N1 cells, both ranging between 35-40% of initial levels. On the other hand, although not statistically significant, there seems to exist a tendency for Wt APP-GFP to increase the percentage of F-actin recovery in the cell rear. Further, while there were no differences between the percentages of recovery in the cell front and rear in EGFP-N1 cells, Wt APP-GFP cells evidenced a tendency to recover F-actin at higher extent at the cell rear than at the cell front.

The results of the halftime of recovery show evident differences between Wt APP-GFP and EGFP-N1 cells for both cell front and rear. Wt APP-GFP transfection very significantly increased the halftime of recovery for both cell front and cell rear, when compared to the EGFP-N1 empty vector. Comparing the halftime of recovery of the cell front with the one at the cell rear of cells in a given condition, EGFP-N1 cells did not shown significant differences, while the Wt APP-GFP showed a significant difference (p<0.01 when using ANOVA followed by the Tukey-Kramer test) for the Wt APP-GFP to increase the halftime of recovery in the cell rear.

### 4.4.4. Cdc42 Activation Assay

In order to investigate a potential influence of APP in Cdc42 activation, HeLa cells 24h transfected with EGFP-N1 and Wt APP-GFP were subjected to a Cdc42 Activation pull-down Assay. The protein levels of active and total Cdc42 and of exogenous APP-GFP were evaluated, in cell lysates and in active Cdc42/Rac1 pull-downs by western blot analysis (Figure 36).

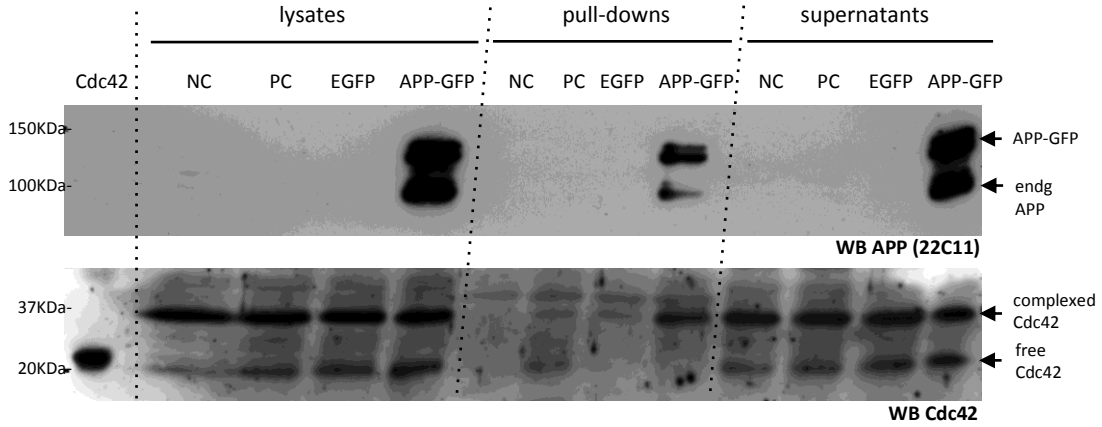


**Figure 36. Immunoblot analysis of active Cdc42/Rac1 pull-down assays performed in EGFP-N1 and Wt APP-GFP 24h transfected HeLa cells.** Active Cdc42 was pulled down with beads linked to a Cdc42 binding domain (PAK-PBD). Controls used: purified His-Cdc42 ('cdc42'); GDP-loaded non-transfected cells ('NC', negative control); GTP-loaded non-transfected cells ('PC', positive control). APP (endogenous: endg, and exogenous: APP-GFP) was probed with the anti-APP N-terminus 22C11antibody. The antibody against Cdc42 detected not only an unbound free active Cdc42 form, but also a complexed active Cdc42 form.

When analyzing the active Cdc42/Rac1 pull-downs we could observe that, in addition to the expected 22kDa Cdc42 band, the WB presented a second strong Cdc42-immunopositive protein band ('complexed Cdc42', ≈36KDa) in all lysates and supernatants, and in almost all pull downs, with the exception of the negative control pull down. Since these Cdc42-immunoreactive bands both disappear only in the negative control and appear in the positive control, this strengthens their identification as Cdc42 proteins. Further, the upper band can represent complexes or forms of the Cdc42 protein that are also recognized by the antibody, and that were not disaggregated in the Cell Lysis Buffer used. There is also a strong possibility that Cdc42 doublets are formed by incomplete denaturation since SDS is only present in the upper gel buffer of the SDS-PAGE.

Remarkably, APP-GFP not only clearly increased the amounts of total free Cdc42 in cell lysates, but also greatly increased the active form of this putatively complexed Cdc42 form. Also very interestingly and unexpected, APP itself, in both its exogenous (APP-GFP) and endogenous forms clearly appeared in the Cdc42/Rac1 pull down, raising an interesting hypothesis that APP forms complexes with active Cdc42 and/or Rac1 and other proteins.

# 5. Discussion

In the present work we aimed to unveil the roles of APP and it proteolytic fragment sAPP in cell migration, and the underlying mechanisms. Different parameters, on which the cells migration efficiency depends, were evaluated: number of migrating cells, migration distance and velocity, coordination in cellular migration, and "out-of-track" migrated distance. The effects of APP phosphorylation at S655 were also studied on some of these processes.

sAPP was already reported as presenting motogenic properties, with several effects on cell migration, such as inducing cell polarity, increasing lamellipodia and ruffle dynamics, recruiting cells for migration, enhancing their average velocity and directional persistence, and triggering chemotactic migration towards a higher concentration of sAPP [39]. The majority of these observations were made in keratinocytes and we aimed to determine if sAPP presented such a role in neuronal-like cells migration. For that, SWH assays were performed in SH-SY5Y cells, and the migration of non-transfected cells was monitored in three different experimental conditions: in the vicinity of either Wt APP-GFP or EGFP-N1 transfected cells, and in the vicinity of EGFP-N1 transfected cells upon exposure to sAPP-enriched medium (EGFP-N1+sAPP). The influence of sAPP was analyzed based on the results obtained for Wt APP-GFP and EGFP-N1+sAPP conditions, with higher sAPP media levels.

Results showed that the presence of higher sAPP levels in the Wt APP-GFP condition did not result in a higher number of migrating cells, relatively to the EGFP-N1 control condition, but rather in a different migration pattern. While control cells were initially more recruited to migrate, cells in the Wt APP-GFP condition suffered some delay in their initial migration until 2-3h of migration (Figure 20). Later, from 3-4h on, this condition presented the highest fold increases, ultimately resulting in an equal final number of migrating cells as the control. Intriguingly, non-transfected cells in the EGFP-N1+sAPP condition (with the highest sAPP levels), generally presented the lowest number of migrating cells, lower than half of the other two conditions at 8 and 24h. In terms of the migrating cells recruitment profile, EGFP-N1+sAPP presented an intermediate profile in between the EGFP-N1 and the Wt APP-GFP conditions, suggesting that sAPP is partially responsible for the higher rate of recruitment observed in Wt APP-GFP condition from 4h on.

The different sAPP levels to which non-transfected cells were exposed could explain the different results observed in Wt APP-GFP and EGFP-N1+sAPP conditions. The fact that NTf cells tend to be more recruited from 4h on in the Wt APP-GFP and EGFP-N1+sAPP conditions, suggests the presence of a later mechanism of response to sAPP in migrating cells, as for example the acquisition of a full migratory phenotype. The lower number of migrating cells in

the later condition may reflect the existence of negative feedbacks and/or an insensitization mechanism in response to a sAPP saturated environment; the presence of other soluble inhibitory molecules in this 48h enriched medium; or even a third more plausible hypothesis, where the non-transfected migrating cells had problems in defining a migratory direction. sAPP was already reported to have chemotactic effects, meaning that cells migrate towards a higher concentration of sAPP. The presence of gradually increasing sAPP levels secreted from surrounding APP-GFP transfected cells should be capable to recruit non-transfected cells for migration, due to its chemotactic effects. In the Wt APP-GFP condition, as more sAPP secreting Wt APP-GFP expressing cells enter the wound from 4h on, these may have recruited other cells to that location. In its turn, highly cumulative levels of homogeneously distributed sAPP in the medium did not reproduce this effect. As a sAPP gradient is absent in the EGFP-N1+sAPP condition, although cells may have been recruited to migrate they perform it in a more random manner, rather than in a directionally persistent way. Indeed, further results from the EGFP-N1 and EGFP-N1+sAPP "out-of-track" data support this hypothesis, with EGFP expressing cells exposed to high doses of sAPP exhibiting increased random migration.

Moreover, it was already reported that sAPP competes with APP to bind β1-integrin [67]. The constant higher sAPP levels in the EGFP-N1+sAPP condition could be thus detrimental since they may result, by competition, in very low binding of flAPP to β1-integrin. This can lead to less efficient migration, since flAPP-β1-integrin binding is reported to facilitate the formation of new adhesions (focal complexes) at the leading edge of migrating cells, to push the cell forward. In accordance with the data on the number of migrating cells, the distances migrated hourly by the leading edge of non-transfected cells in the Wt APP-GFP condition continuously increased from 4h on, surpassing the EGFP-N1 distances at 6-7h. This could be related with the previous hypothesized late response to sAPP that could be related with its competition with APP for β1-integrin when the sAPP levels reach a certain concentration. In parallel, the non-transfected leading edge in EGFP-N1+sAPP condition always migrated lower distances, reflecting the negative effect of very high doses of sAPP in a β1-integrin-mediated migratory mechanism. Further, this sAPP homogeneously distributed in the medium likely increases random migration, and not towards the center of the gap, what is reflected in its leading edge lowest migratory velocity.

Hence, we hypothesize that sAPP and APP, in interplay with β1-integrin, are necessary in correct concentrations for controlled cellular migration, with this hypothesis being further pursued in the future. Indeed, WB analysis revealed that the levels of APP and sAPP are not altered on HeLa cells migrating for 24h (Figure 32). Further, the fact that APP-GFP

overexpression in HeLa migrating cells seems to increase their β1-integrin levels (Figure 31) strengthens a combined role for APP and β1-integrin in this process.

Following, the migration efficiency of transfected cells was inferred by single-cell tracking analysis. Cell coordination in migration is described as the collective migration of cells as part of a group in a highly coordinated manner, with individual cells organized in a coherent multicellular motile structure [51,66]. When the migratory tracks of Wt APP-GFP expressing cells were analyzed, they exhibited coordinated migratory tracks with an apparent persistence in direction, within cells of a same group. This coordinated movement was absent in EGFP-N1 and EGFP-N1 expressing cells exposed to sAPP-enriched medium (EGFP-N1+sAPP), which evidenced unrelated tracks among groups of cells. These results suggest that cellular flAPP, and not medium sAPP, has a role in coordinated cell migration, but more cells are need to be analyzed to confirm these promising results. This APP effect may derive from its known role in cell-cell adhesion [68], and may be mediated by its binding to β1-integrin in the neighbor cell and/or by APP trans-homodimerization [69]. Indeed, an increase in the β1-integrin integrated intensities of both Wt APP-GFP transfected and non-transfected cells neighbor cells seemed to occur in migrating HeLa cells (Figure 31), and β1-integrin membranar patches could be observed. These results have to be triplicated, and the co-localization between APP-GFP and β1-integrin in these patches or in endocytic vesicles, potential places of β1-integrin anchorage (in new adhesions) and release, respectively [45], further analyzed.

Based on the coordinates determined for each transfected cell, the distance and velocity of these were determined. Moreover, the apparent persistence in direction of Wt APP-GFP expressing cells led us to also evaluate the “out-of-track” migrated distance. Although we have not observe differences in the total migrated distance and migration velocity of Wt APP-GFP expressing cells, compared to both EGFP-N1 and EGFP-N1+sAPP conditions, the “out-of-track” percentages evidenced that Wt APP-GFP cells migrated in a directionally persistent way, with fewer detours of the track, reflected in their best “out-of-track” percentage (122%) (Figure 28A). Since the overall rate of cell migration depends not only on the migration velocity, but also on the directional persistence, we can conclude that Wt APP-GFP cells migrated quite efficiently, with the best persistence of migration direction. In contrast, the EGFP-N1 cells exposed to sAPP-enriched medium cells migrated with the highest detours of the track, with homogenously distributed sAPP acting as an extrinsic factor that increased random migration.

Regarding S655 phosphorylation, S655E APP-GFP expressing cells seems to migrate lower distances than S655A APP-GFP cells, and with higher detours of the track. S655A APP-GFP cells behaved more similarly to Wt APP-GFP cells, with a similar “out-of-track” percentage

(133%). Hence, APP phosphorylation seems to abolish the effects of APP in directional migration and slow down migratory velocity.

Although in different cells, data obtained in HeLa transfected cells further supported a positive role for Wt APP-GFP in migration, with an observed notorious gain in Wt APP-GFP expressing cells in the wound area at 24h, relatively to EGFP-N1 expressing cells, indicating that APP overexpression is positive for cellular migration into the wound area (Figure 30). Altogether, these results lead us to propose a S655-dephosphorylation dependent role for flAPP in the coordination and directional persistence of cells migration, crucial for efficient cell migration. Nonetheless, more cells need to be analyzed, to confirm the observed behaviors.

We have next analyzed some of the possible mechanisms underlying flAPP roles in cells migration. The morphologic analysis of APP-GFP SH-SY5Y expressing cells in the wound demonstrated that APP induced cells to better acquire a more clear polarized asymmetric F-actin distribution characteristic of migrating cells, corroborating the positive role for APP in neuronal-like migration. Although not yet quantified, this was also true for migrating HeLa cells (Figure 33). Therefore, we progress to investigate a potential effect of APP on F-actin cytoskeleton dynamics at the front and rear of HeLa migrating cells. Indeed, lamellipodal protrusions at the cell front and rear release both contribute to the migration rate, and fillopodia for the cell polarization and directional migration.

APP showed a tendency to increase both the percentage of F-actin recovery and its halftime of recovery in the cell rear. While there were no differences between the recovery in the cell front and rear in EGFP-N1 cells, Wt APP-GFP cells evidenced a tendency to recover F-actin at higher extent at the cell rear than at the cell front. Moreover, APP overexpression very significantly increased the halftime of recovery also at the cell front (Figure 35). From these results, we conclude that APP increases the stability of F-actin in both the front and rear (more significantly in this later) of migrating cells, since substitution of F-actin at these locations occurs much more slowly, and APP is not impairing it, as denoted by its higher percentage of recovery at the cell rear. The stabilization effect at the cell front can be very important for efficient cell migration in at least two ways. First, stable lamellipodial protrusions allows for better directionality of migration; this stability may arise from APP-induced higher cell adhesion to the underlying substrate, and will be further confirmed by co-localization studies between β1-integrin, APP-GFP and FAK, a focal complex protein marker. Secondly, we have observed higher number or length of filopodia in APP-GFP expressing cells, in comparison to non-transfected cells, what may also help maintaining the migration directionality since filopodia guide cell migration. Further, APP also significantly increased the stability at the cell rear. This may also underline the previously observed APP-induced increase in persistent

migration, since it is known that the trailing edge of a migrating cell contributes to the maintenance of directional migration by generating contraction forces to pull the cell rear forward and limiting the formation of protrusions to maintain the orientation of migration [41]. Importantly, the stability of a front–rear axis correlates with the extent of persistent directional cell movement [41].

The high formation of filopodia in APP-GFP cells suggested increased activation of Cdc42 [45]. Furthermore and as mentioned, the Rho GTPase family member Cdc42 is a main regulator of cell polarization that influences directional migration, with Cdc42-dependent activation of the Par complex triggering polarized protrusions and directionally persistent cell migration [41]. Moreover, Cdc42 was shown to promote directional cell motility in fibroblast scratch-wound healing assays [41,50], and the activation of Cdc42 is the process that initiates a regulatory cascade leading to the formation of new adhesions [45]. When performing a pull-down assay of activated Cdc42 we not only confirmed that APP overexpression induces Cdc42 activation but also observed that APP potentially interacts with Cdc42 (or Rac1, to be further analyzed). Accordingly, we have already observed a co-localization of APP and F-actin in filopodia, and will further pursue if Cdc42 co-localizes with APP and F-actin in these structures. Further, we have also observed that APP co-localized with F-actin in intracellular round structures, and aim to unveil if APP also physically interacts with F-actin. It will be very interesting to unravel if APP is one of the actin-binding proteins observed in focal complexes and focal adhesions.

Our results lead us to hypothesize APP has a role in cell coordination and directional persistence that is, among other, mediated by Cdc42 activation and its subsequent higher number of filopodia and increased cell polarization, and by alterations in F-actin dynamics, namely its stabilization, which is also potentially related to APP-induced formation of β1-integrin-containing focal complexes that may progress to focal adhesions.

# 6. Conclusion

This work provided evidences that full-length APP plays an essential role in the coordination and directional persistence of cell migration, in an apparent S655-dephosphorylation dependent manner. Corroborating with this primary results, we observed that APP helps cells to acquire the polarized asymmetric F-actin distribution characteristic of migrating cells, and increases the stability of both front and rear F-actin of migrating cells, which may result in coordinated and directionally persistence cell migration, therefore increasing cell migration efficiency, once cell-substrate adhesion can guide the directionality of migration. Finally, we observed that APP enhances Cdc42 activation (and potentially binds this activated Cdc42 form), another mechanism by which it can determine directional migration, since Cdc42 has been reported as essential to trigger polarized protrusions and directionally persistent cell migration. Future experiments should be performed to confirm these results. Further studies on cell migration may be based on stable transfections, in order to enhance the number of transfected cells analyzed, and to include APP phosphomutants in the live-cell experiments. After this first approach on cell migration, other migration assays can be used in further studies, e.g. the Ring Assays, which uses non-injured cell cultures confined to well-defined areas easier to monitor than wounded areas. Moreover, experiments are still necessary to co-localize APP with Cdc42 and Rac1, together with F-actin, and to identify the nature of these potential complexes, to better characterize the role of APP on directional migration. In synthesis, our results helped to unveil the molecular mechanisms underlying APP role in cell migration, with potential applications in neuronal migration in in adult neurogenesis. Namely, a role played by APP in the migration of newly born neurons in the hippocampus, the first cerebral structure, affected in AD, may help to explain some of the pathogenic features observed in this disease, as impaired memory formation.

# 7. References


1. Zhou Z, Chan CH, Ma Q, Xu X, Xiao Z, Tan E-K. The roles of amyloid precursor protein (APP) in neurogenesis: Implications to pathogenesis and therapy of Alzheimer disease. Cell Adhesion & Migration. 2011 Jul 1;5(4):280–92.

2. Lazarov O, Demars MP. All in the Family: How the APPs Regulate Neurogenesis. Frontiers in neuroscience. 2012 Jan;6:81.

3. Coulson EJ, Paliga K, Beyreuther K, Masters CL. What the evolution of the amyloid protein precursor supergene family tells us about its function. Neurochem Int. 2000;

4. Ling Y, Morgan K KN. Amyloid precursor protein (APP) and the biology of proteolytic processing: relevance to Alzheimer's disease. The International Journal of Biochemistry & Cell Biology. 2003;

5. De Strooper B, Annaert W. Proteolytic processing and cell biological functions of the amyloid precursor protein. Journal of cell science. 2000 Jun;113:1857–70.

6. Da Cruz e Silva EF, Da Cruz e Silva OA. Protein phosphorylation and APP metabolism. Neurochem Res. 2003;

7. Tanaka S, Shiojiri S, Takahashi Y, Kitaguchi N, Ito H, Kameyama M, et al. Tissue-specific expression of three types of beta-protein precursor mRNA: enhancement of protease inhibitor-harboring types in Alzheimer's disease brain. Biochemical and Biophysical Research Communications. 1989;

8. Selkoe DJ. Alzheimer's Disease : Genes, Proteins, and Therapy. Physiological Reviews. 2001;81(2):741–66.

9. Hampel H, Shen Y, Walsh DM, Aisen P, Shaw LM, Zetterberg H, et al. Biological markers of amyloid beta-related mechanisms in Alzheimer's disease. Exp Neurol. 2010;

10. Suzuki T, Nakaya T. Regulation of amyloid beta-protein precursor by phosphorylation and protein interactions. The Journal of biological chemistry. 2008 Oct 31;283(44):29633–7.

11. Turner PR, O'Connor K, Tate WP, Abraham WC. Roles of amyloid precursor protein and its fragments in regulating neural activity, plasticity and memory. Progress in Neurobiology. 2003;

12. Gralle M, Ferreira ST. Structure and functions of the human amyloid precursor protein: the whole is more than the sum of its parts. Progress in Neurobiology. 2007;

13. Kong GK-W, Miles L a, Crespi G a N, Morton CJ, Ng HL, Barnham KJ, et al. Copper binding to the Alzheimer's disease amyloid precursor protein. European biophysics journal : EBJ. 2008 Mar;37(3):269–79.

14. Schmitz a, Tikkanen R, Kirfel G, Herzog V. The biological role of the Alzheimer amyloid precursor protein in epithelial cells. Histochemistry and cell biology. 2002 Mar;117(2):171–80.

15. Vieira SI, Rebelo S, Esselmann H, Wiltfang J, Lah J, Lane R, et al. Retrieval of the Alzheimer's amyloid precursor protein from the endosome to the TGN is S655 phosphorylation state-dependent and retromer-mediated. Molecular neurodegeneration. BioMed Central Ltd; 2010 Jan;5(1):40.

16. Haass C, Kaether C, Thinakaran G, Sisodia S. Trafficking and Proteolytic Processing of APP. Cold Spring Harbor perspectives in medicine. 2012 May;2(5).

17. Bayer TA, Wirths O, Majtényi K, Hartmann T, Multhaup G. Key Factors in Alzheimer ' s Disease : β-amyloid Precursor Protein Processing , Metabolism and Intraneuronal Transport. Brain Pathology. 2001;11:1–11.

18. Small SA, Gandy S. Sorting through the cell biology of Alzheimer's disease: intracellular pathways to pathogenesis. Neuron. 2006 Oct 5;52(1):15–31.

19. O'Brien RJ, Wong PC. Amyloid Precursor Protein Processing and Alzheimer's Disease. Annual review of neuroscience. 2011;1987:185–204.

20. Lee M, Kao S, Lemere CA, Xia W, Tseng H, Zhou Y, et al. APP processing is regulated by cytoplasmic phosphorylation. The Journal of cell biology. 2003 Oct 13;163(1):83–95.

21. Schettini G, Govoni S, Racchi M, Rodriguez G. Phosphorylation of APP-CTF-AICD domains and interaction with adaptor proteins: signal transduction and/or transcriptional role--relevance for Alzheimer pathology. Journal of neurochemistry. 2010 Dec;115(6):1299–308.

22. Da Cruz e Silva OA, Fardilha M, Henriques AG, Rebelo S, Vieira S, Da Cruz e Silva EF. Signal transduction therapeutics: relevance for Alzheimer's disease. J Mol Neurosci. 2004;

23. Gandy S, Czernik a J, Greengard P. Phosphorylation of Alzheimer disease amyloid precursor peptide by protein kinase C and Ca2+/calmodulin-dependent protein kinase II. Neurobiology. 1988 Aug;85(16):6218–21.

24. Isohara T, Horiuchi A, Watanabe T, Ando K, Czernik AJ, Uno I, et al. Phosphorylation of the Cytoplasmic Domain of Alzheimer's β-Amyloid Precursor Protein at Ser655 by a Novel Protein Kinase. Biochem Biophys Res Commun. 1999;

25. Vieira SI, Rebelo S, Domingues SC, Da Cruz e Silva EF, Da Cruz e Silva OAB. S655 phosphorylation enhances APP secretory traffic. Molecular and Cellular Biochemistry. 2009;

26. Liu C, Zhao X. MicroRNAs in Adult and Embryonic Neurogenesis. 2010;11(3):141–52.

27. Ming G, Song H. Adult Neurogenesis in the Mammalian Brain: Significant Answers and Significant Questions. 2012;70(4):687–702.

28. Ming G, Song H. Adult neurogenesis in the mammalian central nervous system. Annual review of neuroscience. 2005 Jan;28:223–50.

29. Altman J, Das GD. Autoradiographic and Histological Evidence of Postnatal Hippocampal Neurogenesis in Rats. The Journal of comparative neurology. 1965 Jun;124(3):319–35.

30. Paton JA, Nottebohm FN. Neurons generated in the adult brain are recruited into functional circuits. 1984;

31. Stiles J, Jernigan TL. The basics of brain development. Neuropsychology review. 2010 Dec;20(4):327–48.

32. Cayre M, Canoll P, Goldman JE. Cell migration in the normal and pathological postnatal mammalian brain. 2010;88(1):41–63.

33. Hsieh J. Orchestrating transcriptional control of adult neurogenesis. 2012;1010–21.

34. Young-Pearse TL, Bai J, Chang R, Zheng JB, LoTurco JJ, Selkoe DJ. A critical function for beta-amyloid precursor protein in neuronal migration revealed by in utero RNA interference. The Journal of Neuroscience. 2007;27(52):14459–69.

35. Young-Pearse TL, Suth S, S. Luth E, Sawa A, J. Selkoe D. Biochemical and functional interaction of DISC1 and APP regulates neuronal migration during mammalian cortical development. The Journal of Neuroscience. 2011;30(31):10431–40.

36. Rice HC, Townsend M, Bai J, Suth S, Cavanaugh W, Selkoe DJ, et al. Pancortins interact with amyloid precursor protein and modulate cortical cell migration. Development. 2012 Nov;139(21):3986–96.

37. Caillé I, Allinquant B, Dupont E, Bouillot C, Langer A, Müller U, et al. Soluble form of amyloid precursor protein regulates proliferation of progenitors in the adult subventricular zone. Development (Cambridge, England). 2004 May;131(9):2173–81.

38. Mu Y, Gage FH. Adult hippocampal neurogenesis and its role in Alzheimer's disease. Molecular neurodegeneration. BioMed Central Ltd; 2011 Jan;6(1):85.

39. Kirfel G, Borm B, Rigort A, Herzog V. The secretory beta-amyloid precursor protein is a motogen for human epidermal keratinocytes. European journal of cell biology. 2002 Dec;81(12):664–76.

40. Muller T, Concannon CG, Ward MW, Walsh CM, Tirniceriu AL, Tribl F, et al. Modulation of Gene Expression and Cytoskeletal Dynamics by the Amyloid Precursor Protein Intracellular Domain ( AICD ) □. Molecular Biology of the Cell. 2007;18(January):201–10.

41. Petrie R, Doyle A, Yamada K. Random versus directionally persistent cell migration. Nat Rev Mol Cell Biol. 2009;10(8):538–49.

42. Ciobanasu C, Faivre B, Le Clainche C. Actin dynamics associated with focal adhesions. International journal of cell biology. 2012 Jan;2012:941292.

43. Friedl P, Wolf K. Plasticity of cell migration: a multiscale tuning model. The Journal of cell biology. 2010 Jan 11;188(1):11–9.

44. Friedl P, Wolf K, Lammerding J. Nuclear mechanics during cell migration. Curr Opin Cell Biol. 2011;23(1):55–64.

45. Lauffenburger D a, Horwitz a F. Cell migration: a physically integrated molecular process. Cell. 1996 Mar 9;84(3):359–69.

46. Vicente-Manzanares M, Webb DJ, Horwitz a R. Cell migration at a glance. Journal of cell science. 2005 Dec 1;118(Pt 21):4917–9.

47. Clainche CLE, Carlier M. Regulation of Actin Assembly Associated With Protrusion and Adhesion in Cell Migration. Physiological Reviews. 2008;489–513.

48. Ballestrem C, Wehrle-Haller B, Imhof B a. Actin dynamics in living mammalian cells. Journal of cell science. 1998 Jul;111:1649–58.

49. Parent CA, Devreotes PN. A Cell's Sense of Direction. Science. 1999 Apr 30;284(5415):765–70.

50. Gomes E, Jani S, Gundersen G. Nuclear movement regulated by Cdc42, MRCK, myosin, and actin flow establishes MTOC polarization in migrating cells. Cell. 2005;

51. Emery G, Ramel D. Cell coordination of collective migration by Rab11 and Moesin. 2013;(August):1–3.

52. Sabo SL, Ikin a F, Buxbaum JD, Greengard P. The Alzheimer amyloid precursor protein (APP) and FE65, an APP-binding protein, regulate cell movement. The Journal of cell biology. 2001 Jul 25;153(7):1403–14.

53. Sabo SL, Lanier LM, Ikin a F, Khorkova O, Sahasrabudhe S, Greengard P, et al. Regulation of beta-amyloid secretion by FE65, an amyloid protein precursor-binding protein. The Journal of biological chemistry. 1999 Mar 19;274(12):7952–7.

54. Bear JE, Loureiro JJ, Libova I, Fässler R, Wehland J, Gertler FB. Negative regulation of fibroblast motility by Ena/VASP proteins. Cell. 2000 Jun 23;101(7):717–28.

55. Bashaw GJ, Kidd T, Murray D, Pawson T, Goodman CS. Repulsive axon guidance: Abelson and Enabled play opposing roles downstream of the roundabout receptor. Cell. 2000 Jun 23;101(7):703–15.

56. Da Cruz e Silva OAB, Iverfeldt K, Oltersdorf T, Sinha S, Lieberburg I, Ramabhadran T., et al. Regulated cleavage of alzheimer β-amyloid precursor protein in the absence of the cytoplasmic tail. Neuroscience. 1993;

57. Riedl J, Crevenna AH, Kessenbrock K, Yu JH, Bista M, Bradke F, et al. Lifeact: a versatile marker to visualize F-actin. Nat. Methods. 2008;5(7):1–8.

58. Ferreira R, Santos T, Cortes L, Cochauda S, Agassea F, Silva AP, et al. Neuropeptide Y inhibits interleukin-1 beta (IL-1β)-induced microglia motility. p. 1–29.

59. Decaestecker C, Debeir O, Van Ham P, Kiss R. Can anti-migratory drugs be screened in vitro? A review of 2D and 3D assays for the quantitative analysis of cell migration. Medicinal research reviews. 2007 Mar;27(2):149–76.

60. Romero-Calvo I, Ocón B, Martínez-Moya P, Suárez MD, Zarzuelo A, Martínez-Augustin O, et al. Reversible Ponceau staining as a loading control alternative to actin in Western blots. Analytical Biochemistry. 2010;

61. A Video Tour of Cell Motility [Internet]. 2013. Available from: http://cellix.imba.oeaw.ac.at/7-actin-can-push/

62. Schröder J. Fluorescence Recovery after Photobleaching (FRAP) & its offspring [Internet]. Leica Microsystems, Wetzlar, Germany. 2011. Available from: http://www.leica-microsystems.com/science-lab/fluorescence-recovery-after-photobleaching-frap-and-its-offspring/

63. Borlinghaus RT. Leica Microsystems [Internet]. Quantitative Fluorescence - An Overview. 2012. Available from: http://www.leica-microsystems.com/science-lab/quantitative-fluorescence/

64. Zhang H, Ma Q, Zhang Y, Xu H. Proteolytic processing of Alzheimer's β-amyloid precursor protein. Journal of neurochemistry. 2012;120:9–21.

65. Lu DC, Rabizadeh S, Chandra S, Shayya RF, Ellerby LM, Ye X, Salvesen GS, Koo EH BD. A second cytotoxic proteolytic peptide derived from amyloid beta-protein precursor. Nature Medicine. 2000;

66. Ng MR, Besser A, Danuser G, Brugge JS. Substrate stiffness regulates cadherin-dependent collective migration through myosin-II contractility. The Journal of cell biology. 2012 Oct 29;199(3):545–63.

67. Young-Pearse TL, Chen AC, Chang R, Marquez C, Selkoe DJ. Secreted APP regulates the function of full-length APP in neurite outgrowth through interaction with integrin beta1. Neural development. 2008 Jan;3(June):15.

68. Müller UC, Zheng H. Physiological Functions of APP Family Proteins. Cold Spring Harbor perspectives in medicine. 2012 Mar;2(2).

69. Soba P, Eggert S, Wagner K, Zentgraf H, Siehl K, Kreger S, et al. Homo- and heterodimerization of APP family members promotes intercellular adhesion. The EMBO journal. 2005 Oct 19;24(20):3624–34.

# Appendix

## cDNA amplification and purification solutions

- **Luria-Bertani (LB) growth medium with Ampicillin**

For a final volume of 1 L, dissolve 25 g of LB (Merck) in deionized water ($dH_2O$). Adjust the volume up to 1 L of $dH_2O$ and autoclave the solution (the LB will mix during autoclaving). Let the medium cool down to 60$^oC$ and add 1 mL of ampicillin of a 50 mg/mL stock solution.

- **Super Optimal broth with Catabolite repression (SOC) medium**

For a final volume of 1 L, dissolve 25,5 g of SOB broth (Sigma-Aldrich) in $dH_2O$. Shake until the solute is dissolved, add 10 mL of 250 mM KCL solution, adjust the pH to 7.0 with 5 N of sodium hydroxide and adjust the final volume up to 1 L with $dH_2O$. Sterilize by autoclaving, cool it down to about 60$^oC$ and add 20 mL of a sterile 1M glucose solution.

- **Cell Resuspension Solution**

  - 50 mM of Tris-HCl (pH 7,5)
  - 10 mM of EDTA
  - 100 µg/mL of RNase A

- **Cell Lysis Solution**

  - 0.2 M of sodium hydroxide
  - 1% of SDS

- **Neutralization Solution**

  - 1.32 M of potassium acetate (pH 4.8)

- **Neutralization Solution**

  - 80 mM of potassium acetate
  - 8.3 mM of Tris-HCl (pH 7.5)
  - 40 µM of EDTA
  - 55% of ethanol

- **PBS (1x)**

For a final volume of 500 ml, dissolve one pack of BupH Modified Dulbecco's Phosphate Buffered Saline Pack (Pierce) in deionized $H_2O$. Final composition:

- 8 mM Sodium Phosphate
- 2 mM Potassium Phosphate
- 140 mM Sodium Chloride
- 10 mM Potassim Chloride

Sterilize by filtering through a 0.2 µm filter and store at 4$^{o}$C.

- **10% FBS MEM:F12 (1:1)**

| | |
|---|---|
| MEM (Gibco, Invitrogen) | 4,805 g |
| F12 (Gibco, Invitrogen) | 5,315 g |
| NaHCO3 (Sigma) | 1,5 g |
| Sodium pyruvate (Sigma) | 0,055 g |
| 1% antibiotic/antimycotic (AA) mix (Gibco, Invitrogen) | 10 mL |
| 10% FBS (Gibco, Invitrogen) | 100 mL |
| L-glutamine (200 mM stock solution) | 2,5 mL |

Dissolve in $dH_2O$;

Adjust the pH to 7.2/ 7.3;

Adjust the volume to 1000 mL with $dH_2O$.

- **Freezing medium**

| | |
|---|---|
| Growth medium (MEM:F12) | 7 mL |
| FBS (10-20%) | 2 mL |
| Glycerol (10-15%) or DMSO (5-20%) | 1 mL |

- **4% Paraformaldehyde**

For a final volume of 100 mL, add 4g of paraformaldehyde to 25 mL deionized $H_2O$. Dissolve by heating the mixture at 58ºC while stirring. Add 1-2 drops of 1 M NaOH to clarify the solution and filter (0.2 µm filter). Add 50 mL of 2X PBS and adjust the volume to 100 mL with deionized $H_2O$.

## SDS-PAGE and Immunoblotting Solutions

- **LGB (Lower gel buffer) (4x)**

  To 900 ml of deionized $H_2O$ add:

  | | |
  |---|---|
  | Tris | 181.65 g |
  | SDS | 4 g |

  Mix until the solutes have dissolved. Adjust the pH to 8.9 and adjust the volume to 1L with deionized $H_2O$.

- **UGB (Upper gel buffer) (5x)**

  To 900 ml of deionized H2O add:

  | | |
  |---|---|
  | - Tris | 75.69 g |

  Mix until the solute has dissolved. Adjust the pH to 6.8 and adjust the volume to 1 L with deionized H2O.

- **30% Acrylamide/0.8% Bisacrylamide**

  To 70 ml of deionized H2O add:

  | | |
  |---|---|
  | Acrylamide | 29.2 g |
  | Bisacrylamide | 0.8 g |

  Mix until the solute has dissolved. Adjust the volume to 100 ml with deionized water. Filter through a 0.2 µm filter and store at 4$^{o}$C.

- **10% APS (ammonium persulfate)**

  In 10 ml of deionized H2O dissolve 1 g of APS. Note: prepare fresh before use.

- **10% SDS (sodium dodecilsulfate)**

  In 10 ml of deionized H2O dissolve 1 g of SDS.

- **Loading Gel Buffer (4x)**

  | | |
  |---|---|
  | 1 M Tris solution (pH 6.8) | 2.5 mL (250 mM) |
  | SDS | 0.8 g (8%) |
  | Glicerol | 4 ml (40%) |

| | |
|---|---|
| β-Mercaptoetanol | 2 ml (2%) |
| Bromofenol blue | 1 mg (0.01%) |

Adjust the volume to 10 ml with $dH_2O$. Store in darkness at room temperature.

- **1 M Tris (pH 6.8) solution**

  To 150 ml of deionized H2O add:

| | |
|---|---|
| Tris base | 30.3 g |

  Adjust the pH to 6.8 and adjust the final volume to 250 ml.

- **10x Running Buffer**

| | |
|---|---|
| Tris | 30.3 g (250 mM) |
| Glycine | 144.2 g (2.5 M) |
| SDS | 10 g (1%) |

  Dissolve in $dH_2O$, adjust the pH to 8.3 and adjust the volume to 1 L.

- **Resolving (lower) gel solution** (60 ml)

| | **7.5%** | or | **10%** |
|---|---|---|---|
| $H_2O$ | 29,25 ml | | 25,2 ml |
| 30% Acryl/0.8% Bisacryl solution | 15 ml | | 19,8 ml |
| LGB (4x) | 15 ml | | 15 ml |
| 10% APS | 300 µL | | 300 µL |
| TEMED | 30 µL | | 30 µL |

- **Resolving (lower) gel solution for gradient gels** (60 ml)

| | **5%** | and | **20%** |
|---|---|---|---|
| $H_2O$ | 17.4 ml | | 2.2 ml |
| 30% Acryl/0.8% Bisacryl solution | 5 ml | | 20 ml |
| LGB (4x) | 7.5 ml | | 7.5 ml |
| 10% APS | 150 µL | | 150 µL |
| TEMED | 15 µL | | 15 µL |

- **Stacking (upper) gel solution** (20 ml)

| | **3.5%** |
|---|---|
| $H_2O$ | 13.2 ml |
| 30% Acryl/0.8% Bisacryl solution | 2.4 ml |
| UGB (5x) | 4.0 ml |
| 10% APS | 200 µL |
| 10% SDS | 200 µL |
| TEMED | 20 µL |

- **1x Transfer Buffer**

| | |
|---|---|
| Tris | 3.03 g (25 mM) |
| Glycine | 14.41 g (192 mM) |

Mix until solutes dissolution. Adjust the pH to 8.3 with HCl and adjust the volume to 800 ml with deionized $H_2O$. Just prior to use add 200 ml of methanol (20%).

- **10x TBS (Tris buffered saline)**

| | |
|---|---|
| Tris | 12.11 g (10 mM) |
| NaCl | 87.66 g (150 mM) |

Adjust the pH to 8.0 with HCl and adjust the volume to 1L with deionized $H_2O$.

- **10x TBS-T (TBS+Tween)**

| | |
|---|---|
| Tris | 12.11 g (10 mM) |
| NaCl | 87.66 g (150 mM) |
| Tween | 20 5 ml (0.05%) |

Adjust the pH to 8.0 with HCl and adjust the volume to 1L with deionized $H_2O$.

- **Membranes Stripping Solution** (500 ml)

| | |
|---|---|
| Tris-HCl (pH 6.7) | 3.76 g (62.5 mM) |
| SDS | 10 g (2%) |
| β-mercaptoetanol | 3.5 ml (100 mM) |

Dissolve Tris and SDS in $dH_2O$ and adjust with HCl to pH 6.7. Add the mercaptoethanol and adjust volume to 500 ml.